# Heat2Control

OCTOBER 5&6

# COMBURA

NVV 2016

## Book of Abstracts

NVV KIVI NIRIA STW connecting innovators

# PROGRAMME

## PARALLEL SESSION 1 — Industrial and residential combustion systems

- Recent combustor developments for the OP16 gas turbine to extend the fuel flexibility
  **Th. Bouten** — READ
- Challenges on the combustion of pyrolysis oil in residential heating systems
  **R.T.E. Hermanns, A. Frassoldati, S. Feldhoff, D. Möntmann, T. Rütten.** — READ
- Highly efficient RANS and manifold based modeling for the simulation of industrial combustion processes
  **J.E. Anker, L. Romagnosi, K. Claramunt, J. Vanherzeele, C. Hirsch** — READ
- Combustion simulation methodology for swirl burners based on PANS+FGM
  **B. Basara, F. Tap** — READ

## PARALLEL SESSION 2 — Measurement and modeling

- Modeling of mass evaporation behavior of single and multicomponent fuels under combustion conditions in pool fires
  **P.H. Saptogino, M. Grote, R.T.E. Hermanns, D. Diarra** — READ
- LES modeling of lifted jet-in-hot-coflow flames using FGM
  **A. Vasavan, J.A. van Oijen** — READ
- Experimental and numerical study of MILD combustion in a lab-scale furnace
  **X. Huang, M. Tummers, D.J.E.M. Roekaerts** — READ
- Capturing curvature effects using MuSt-FGM in a non-premixed auto-igniting flame
  **M.U. Göktolga, L.P.H. de Goey, J.A. van Oijen** — READ

## PARALLEL SESSION 3 — Combustion spectroscopy

- Development of simultaneous hyperspectral coherent Raman imaging for advancing reduced emission combustion technology
  **A. Bohlin** — READ
- The role of toluene in PAH formation: Raman spectroscopy
  **R. Doddema** — READ
- Comparison of normal spectral emittance of sulfates and carbonates - significant mineral classes of ashes under oxy-fuel conditions
  **J. Gorewoda, V. Scherer** — READ

## PARALLEL SESSION 4 — Turbulence-chemistry-interaction modeling

- Recent improvements of the Heat Flux setup to determine laminar burning velocities of liquid fuels
  **S. Feldhoff, R.T.E. Hermanns** — READ
- Temperature effect on flame induced ionization current for oxidized Langmuir probes
  **D. Raj, J.A. van Oijen, N.A. Beishuizen** — READ
- Assessing radiation losses by temperature measurements in laminar flat flames
  **S. Van Damme** — READ

# POSTER PRESENTATIONS

- Biomass Gasification in a novel 50kW$^{th}$ Indirectly Heated Bubbling Fluidized Bed Steam Reformer
  **Mara Del Grosso, Wiebren de Jong** — READ

- Effect of dilution in an inter-turbine Flameless combustor
  **A.A.V. Perpignan, A.G. Rao** — READ

- High-Resolution True-Color Imaging of Reacting Sprays
  **P.C. Bakker, Robin Doddema, Noud Maes and Nico Dam** — READ

- Unraveling the Obscurities of Soot Reduction by Post Injections
  **R. Dreezen, J. Vervaet, P.C. Bakker & R.C. Willems** — READ

- Alternative Use of FTIR for the Analysis of Industrial Gases Emission
  **I. V. Dyakov, B. Bergmans, S. Petitjean, F. Idczak** — READ

- Numerical modeling of multi-component viscous fuels combustion
  **A.H. Mahmoudi, A.K. Pozarlik, E. van der Weide, S.R.A. Kersten, S. Luding, G. Brem** — READ

- Heat2Control, Modeling of Split-injection Spray-A Case from ECN with FGM in OpenFOAM
  **B. Akkurt, L.M.T. Somers, N.G. Deen** — READ

- Numerical Study on Diesel Spray Combustion Characteristics: LES of Spray-A using Flamelet Generated Manifold
  **H.Y. Akargun, L.M.T. Somers, N.G. Deen** — READ

- Validation of Standard and Extended Eddy Dissipation Concept Model for the Delft Jet-in Hot Coflow (DJHC) Flame
  **H. Bao, X. Huang, D.J.E.M. Roekaerts** — READ

- Investigating the effects of a heat exchanger on the thermoacoustics in a Rijke tube
  **Naseh Hosseini, Viktor Kornilov, O.J. Teerling, Ines Lopez Arteaga, L. P. H. de Goey** — READ

# POSTER PRESENTATIONS

- Comparative study of RANS-EDC, LES-CSE and LES-FGM simulations of Delft jet-in-hot-coflow (DJHC) natural gas flames
  **D.J.E.M. Roekaerts, H. Bao, X. Huang, A. Vasavan, J.A. van Oijen, J. Labahn, C. Devaud**

READ

- FGM with additional chemically reactive dimensions
  **D.V. Efimov, J.A. van Oijen**

READ

- Angle-dependent light scattering study of soot aggregate growth in 1-D premixed rich ethylene/air flames
  **P.N. Langenkamp, H.B. Levinsky, A.V. Mokhov**

READ

- The Three Power Crossover (3PX) concept. Utilizing a plug-in hybrid electric car as a micro-CHP
  **B.F.W. Vermeltfoort**

READ

- Plasma Assisted Combustion: Interaction of a Flat Flame with a Nanosecond Dielectric Barrier Discharge Plasma
  **Ahmed Elkholy, Jeroen van Oijen, Philip de Goey**

READ

- A study of flame stabilization and blow-off phenomenon for laminar premixed methane flames with hydrogen addition
  **F.H. Vance, Y. Shoshyn, J.A. van Oijen, L.P.H. de Goey**

READ

# RECENT COMBUSTOR DEVELOPMENTS FOR THE OP16 GAS TURBINE TO EXTEND THE FUEL FLEXIBILITY

**Thijs Bouten and Lars-Uno Axelsson**
OPRA Turbines International B.V.
Hengelo, The Netherlands
Email: t.bouten@opra.nl

## INTRODUCTION

OPRA Turbines develops, manufactures, markets and maintains generator sets using the OP16 series of gas turbines, which is rated at 1.85 MWe. The gas turbine generator set comes in a containerized package that includes the OP16 gas turbine, fuel systems, generator, control system, air intake and ventilation system. The OP16 gas turbine, shown in Figure 1 is of an all-radial design, which provides robustness, reliability and highest efficiency in its class. A key feature of the OP16 gas turbine is the ability to utilize a wide range of fuels. Natural gas and fuel oils are commonly used as gas turbine fuel. However, the potential range of gas turbine fuels is much wider. The wish to find alternatives for fossil fuels has led to an increasing interest to operate gas turbines on fuels originating from waste and renewable resources.

## OPRA'S COMBUSTION TECHNOLOGY

Depending on the application and requirements, the appropriate combustion system will be mounted on the OP16 gas turbines. The 3A combustor is a conventional, diffusion type, combustor capable of operating on a wide range of gaseous and liquid fuels, including heavily contaminated and sour well-head gases. The 3B combustor is a dry low-emissions combustor specifically designed for low emission operation on natural gas. To meet the increasing demand to utilize alternative fuels, OPRA Turbines has initiated a research program to develop combustion technologies that will enable the use of low calorific fuels in the OP16 gas turbine. Based on this research, a new combustor (3C) has been developed [1]. This combustor is able to handle low calorific liquid and gaseous fuels efficiently.

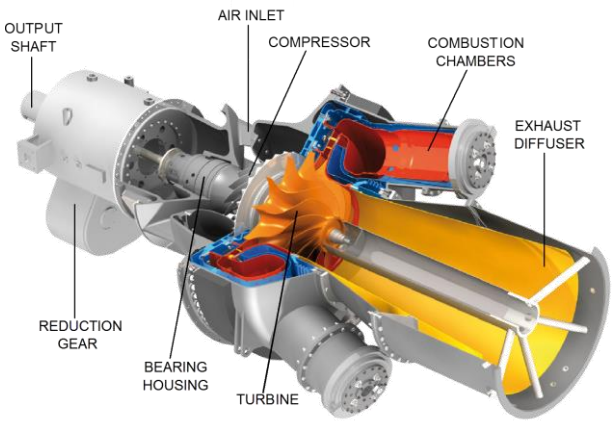


**Figure 1. The OP16 gas turbine**

The volume of the 3C combustor is significantly larger than for the conventional combustion systems. This ensures sufficient burnout time for carbon monoxide in low calorific gaseous fuels and carbon content in liquid fuels such as residual and pyrolysis oil. The increase of the combustor volume can be achieved relatively easy in the OP16 gas turbine due to the reverse-flow mounting of the can combustors.

OPRA's OP16-3C gas turbine can handle gaseous fuels with a lower heating value (LHV) down to 7 MJ/kg. A lower LHV down to 5 MJ/kg, or even lower, might be allowed when sufficient hydrogen is present in the fuel. The 3C combustor is specifically designed for low calorific fuels but high calorific fuels (e.g. diesel and natural gas) can be used as backup fuels.

## TEST FACILITIES

OPRA Turbines has access to various in-house test facilities, which includes an engine test cell for full-scale engine testing, a package test area for the whole gas turbine generator set and an atmospheric combustor test rig for combustor development tests.

The atmospheric combustor test rig is shown in Figure 2. The main components of the rig are the air compressor, air pre-heater and combustion chamber. The air is sucked from the surroundings by the air compressor and it is heated up to the same temperature as the combustor inlet temperature of the OP16 gas turbine. The pre-heated air is injected into the combustor module and the exhaust gases are emitted through an exhaust stack. The gaseous fuel is supplied by a gas mixing station, which can supply gas mixtures consisting of up to five different components from gas cylinders. These components include methane or propane, hydrogen, carbon monoxide, nitrogen and carbon dioxide. Five mass flow controllers continuously measure and regulate the gas flow of the different components. Various liquid fuels can be stored in liquid fuel tanks for supply to the combustor. The thermal input of the atmospheric combustor test rig can be varied from 0 to 300 kW for gas mixtures in the range of 5-70 MJ/kg and a large variety of liquid fuels. Pressures, temperatures and exhaust gas emissions are measured in the atmospheric combustor test rig. Furthermore, temperature profiles of combustor hardware can be evaluated with the use of thermochromic paint. The flame chemiluminescence can be evaluated through the combustor outlet (e.g. discussed in [2]).

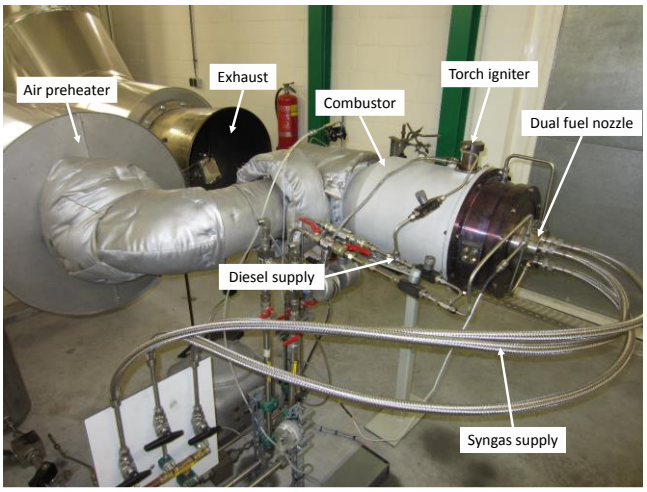


**Figure 2. OPRA's atmospheric combustor test rig**

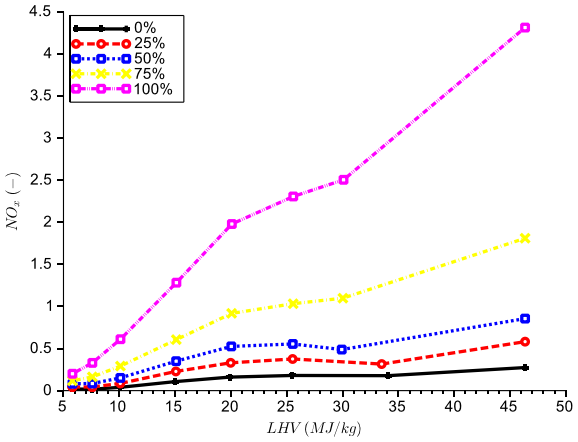


**Figure 3. Normalized $NO_x$ emissions for gaseous fuels with various heating values at different combustor loads in the 3C combustor.**

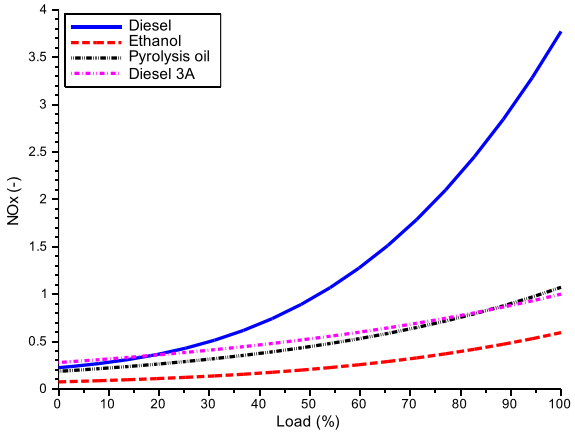


**Figure 4. Normalized $NO_x$ emissions for various liquid fuels at different combustor loads in the 3C combustor.**

## TEST RESULTS

The 3C combustor has been tested successfully in OPRA's test rig on several (ultra)-low calorific gases and liquid fuels, including syngas, pyrolysis oil and ethanol. More details of gaseous fuel combustion have been discussed in [3] and liquid fuel combustion in [4].

The LHV of a fuel has a strong influence on the $NO_x$ emissions from the combustion process, as can be seen in Figure 3. The formation of $NO_x$ is strongly dependent on the temperature of the flame, whereby less thermal $NO_x$ is formed for a lower flame temperature. Fuels with a lower LHV, have a lower flame temperature due to the presence of e.g. dilutants in the fuel. This effect can also be seen for liquid fuels (Figure 4), where both ethanol and diesel are found to have lower emissions than diesel. It has to be noted that the wood based pyrolysis oil contains 0.1 wt% bounded nitrogen, therefore about 60% of the nitric oxides comes from the fuel itself [4].

The volume of the low-calorific fuel combustor is significantly larger than for a conventional combustor. Therefore, the residence time of the gases at high temperature is longer for the low-calorific fuel combustor. The residence time strongly influences the formation of $NO_x$ in the combustor [5]. By providing a longer residence time at high temperature, thermal $NO_x$ has more time to be formed. This effect can clearly be seen in Figure 4 where the diesel emissions for a conventional combustor (3A) are significantly lower than for the 3C combustor. However, high-calorific fuels are only used for back-up in the 3C combustor and higher emissions during a shorter period is permitted.

## CONCLUSION

To meet the growing demand for utilization of low-calorific fuels OPRA Turbines has developed a new combustor for the OP16 gas turbine fleet. The low-calorific fuel combustor has successfully been tested on various (low calorific) gaseous and liquid fuels

## REFERENCES

[1] M. Beran, M. Koranek and L.-U. Axelsson, "Low calorific fuel combustor for gas turbine". Patent US 8844260 B2, 30 September 2014.

[2] J. L. Sallevelt, A. K. Pozarlik, M. Beran, L.-U. Axelsson and G. Brem, "Bioethanol Combustion in an Industrial Gas Turbine Combustor: Simulations and Experiments," *Journal of Engineering for Gas Turbines and Power*, vol. 136, no. 7, p. 071501, 2014.

[3] T. Bouten, M. Beran and L.-U. Axelsson, "Experimental Investigation of Fuel Composition Effects on Syngas Combustion," in *Proceedings of ASME Turbo Expo 2015*, Montréal, 2015.

[4] M. Beran and L.-U. Axelsson, "Development and Experimental Investigation of a Tubular Combustor for Pyrolysis Oil Burning," *Journal of Engineering for Gas Turbines and Power*, vol. 137, no. 3, p. 031508, 2015.

[5] A. H. Lefebvre and D. R. Ballal, Gas Turbine Combustion Alternative Fuels and Emissions, 3rd ed., CRC Press, 2010.

# Challenges on the combustion of pyrolysis oil in residential heating systems

R.T.E. Hermanns[1,a] , S. Feldhoff[1], D. Möntmann[1], A. Frassoldati[2], P. Massoli[3], T. Rütten[4]
[1]*OWI Oel-Waerme-Institut gGmbH, Germany*
[2] *Politecnico di Milano, Italy*
[3]*Istituto Motori, Italy*
[3]*MEKU Energie Systeme GmbH & CO. KG, Germany*

**Key words:** Pyrolysis oil, FPBO, combustion

## INTRODUCTION

Residue2Heat is a H2020 Research and Innovation Action initiated by 9 partners from 5 countries which aims at developing a concept for renewable residential heating using fast pyrolysis bio-oil. Alternative sustainable fuels for residential heating are needed in the household sector to reduce greenhouse gas emissions. There is a particular need to improve efficiency of low emission biomass heating systems while widening the feedstock base. This means that new flexible and robust residential-scale low emission boilers for heat applications need to be developed which can run on a wider range of sustainable feedstock with high ash contents.

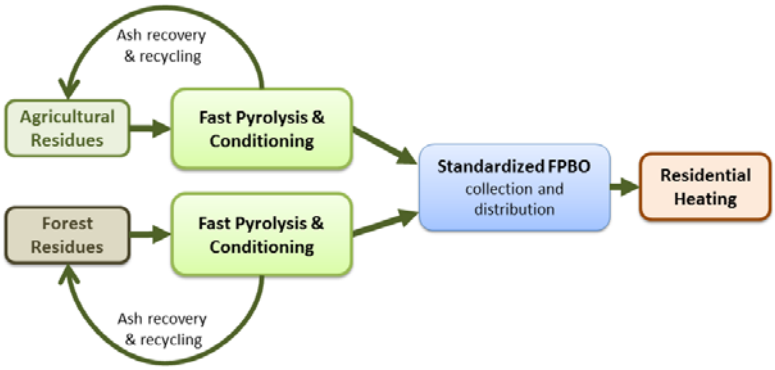


*Figure 1: The overall concept of the EU research project "Residue2Heat" focusses on the development of a standardized pyrolysis oil from biomass residues, which can be used as fuel in the residential heating market.*

## OVERALL CONCEPT

The overall concept of Residue2Heat is to use various streams of biomass waste for residential heat generation (Figure 1). The aim is, by means of a liquid fuel produced in a sustainable manner from agricultural and forestry biomass residues, to considerably reduce the $CO_2$ emissions compared to fossil fuels. This 2nd generation bio-fuel is being produced employing a fast pyrolysis process in which organic material is heated in the absence of oxygen to about 500 °C within a few seconds. Under these conditions organic and aqueous vapours, pyrolysis gas and charcoal arise. The vapours are rapidly cooled and condensed into a highly viscous liquid, so-called pyrolysis oil or Fast Pyrolysis Bio-Oil

[a] *Corresponding author*
*E-Mail: r.hermanns@owi-aachen.de*

(FPBO). The FPBO has about 70% of the energy content of the biomass and about half of the heating value of a conventional fuel oil. The fuel is to be used for efficient heat generation in residential heating systems in the power range from 20 to 200 kW. Additionally, the valuable by-products (charcoal (10-15%) and low calorific gases (15-20%)) can be recycled.

## CHALLENGES ON THE COMBUSTION OF PYROLYSIS OIL

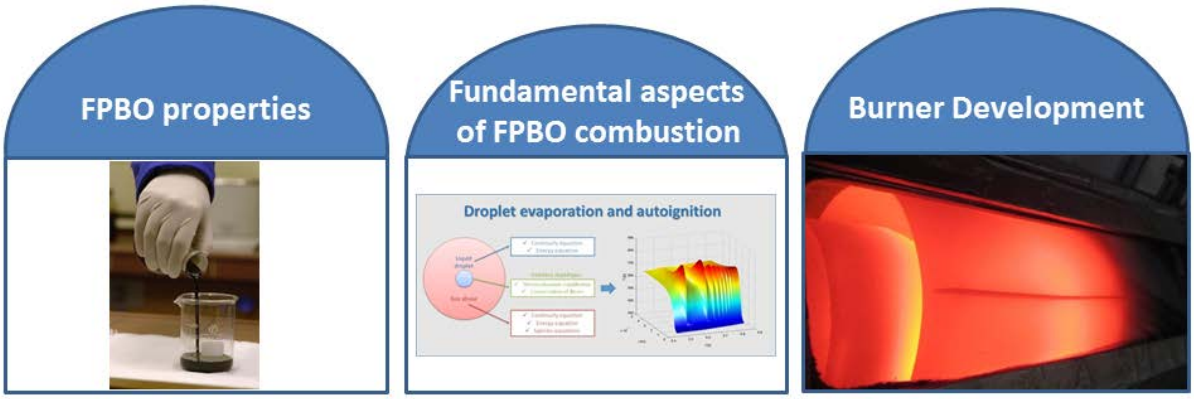


The first challenge in this project is to produce FPBO despite its wide range of possible biogenic raw materials with a consistently high quality and highly standardized physical-chemical properties. The second central challenge is the fundamental aspects of FPBO combustion since the FPBO properties differ from those of conventional fuels. In order to control and improve a burner system a better understanding of FPBO combustion and spray parameters is essential. Particularly, in Residue2Heat the focus of development is on the mixture preparation, which is responsible for an efficient and low-emission operation of the burner. The third central challenge is the technical adaptation of a highly efficient condensing heating system for the use of FPBO. The applied burner concept is based on a so called blue flame type leading to low emissions compared to standard yellow flame type burners.

## SUMMARY AND OUTLOOK

The overall ambition in Residue2Heat is to address all technical and non-technical challenges associated with the use of residual biomass for sustainable residential heating. Advances beyond the state of the art include the production of high quality, standardized FPBO from high ash biomass residues as intermediate energy carrier, and optimizing the atomization and combustion of this dedicated biofuel. It results in the development of an integrated FPBO fired heating system -consisting of a blue-flame burner and condensing boiler unit- meeting all operational and environmental demands at a competitive price.

## ACKNOWLEDGEMENT

The *Residue2Heat* project has received funding from the European Union's Horizon 2020 Research and Innovation programme under Grant Agreement No. 654650

More information is available at: www.residue2heat.eu

# Highly Efficient RANS and Manifold Based Modeling for the Simulation of Industrial Combustion Processes

J. E. Anker, L. Romagnosi, K. Claramunt, Ch. Hirsch*
NUMECA Int., Chaussée de la Hulpe/Terhulpsesteenweg 189,
BE-1170 Brussels, Belgium, www.numeca.com
*charles.hirsch@numeca.be

## Synopsis

**The Flamelet Generated Manifolds (FGM) method has been implemented into the unstructured simulation system FINE™/Open with OpenLabs™ for the computation of industrial combustion processes. Although LES simulations for combustion are gaining larger acceptance in industry, design considerations still require rapid turnovers implying the need of RANS solutions. The RANS solver of FINE™/Open contains efficient and optimized algorithms for table look-ups and convergence acceleration methods based on the CPU-Booster™ technology. A critical step in bringing the FGM method to industrial maturity was the development of the table generation tool TabGen/Chemistry to generate FGM tables in an automated, reliable, and efficient manner. Results from the simulation of various test cases ranging from elementary flames to practical configurations like furnaces and combustors are used to demonstrate the strength of the RANS-FGM method.**

## Numerical Modeling and Convergence Acceleration

The software environment FINE™/Open is used for solving the governing system of equations for flow, turbulence and combustion on unstructured, hexa-dominant grids. The fully integrated CFD software package consists of HEXPRESS™/Hybrid for the generation of unstructured, hexahedral or mixed element meshes, FINE/Open for solving the flow equations, and CFView for postprocessing and visualization. In addition, the software package contains OpenLabs™, which gives the user the possibility to add, modify as well as develop new models using a user-friendly meta-language. The flow solver applies a cell-centered finite volume method. All transport equations are advanced in time by means of an explicit 4-stage Runge-Kutta scheme. Since the density is modeled as being dependent on the combustion transport variables, but not on the pressure, an artificial compressibility approach is employed. For convergence acceleration a local time-stepping procedure, parallelization and agglomeration multigrid method are used. In addition, a novel CPU-Booster™ technique has been implemented, which speeds up combustion simulations significantly. The effect of the CPU-Booster™ on the convergence rate of the simulation of TU Darmstadt's Generic Gas Turbine combustor [1], which is operated at an elevated pressure and fuelled with methane, is shown in Fig. 1. The CPUBooster™ leads to a significant convergence acceleration and reduces the CPU-time needed for convergence by a factor of three.

## Combustion Modeling and Table Generation Method

In the current work, the Flamelet Generated Manifolds (FGM) method is used to model the combustion processes. This method is also known as the Flamelet Prolongated ILDM and was first introduced by van Oijen and de Goey [2] and Gicquel et al. [3]. As both names suggest, the idea of the method is to construct a manifold based on a set of flamelets. In the current work, the FGM tables have been generated using TabGen/Chemistry, which is a combustion table generation tool based on TU Eindhoven's 1D-chemistry code Chem1D [4]. The FGMs are created from a library of non-premixed flamelets completely filling up the state-space between the mixing and the equilibrium lines by mapping the flamelets onto a two-dimensional grid spanned by the mixture fraction and the progress variable. The FGM table generation method offered in TabGen/Chemistry is completely automated and is so robust that it can be used reliably for the simulation of industrial applications with complex fuels.

The FGM tables are generated in a preprocessing step in dependence of the boundary conditions of the fuel and oxidizer streams and the chemistry calculations can be kept outside of the flow solver. In the FGM approach, only a transport equation for the progress variable, the mixture fraction, and the mixture fraction variance are solved in addition to the RANS equations, which makes this model computationally efficient. The dependent thermochemical properties as well as the reaction source term are retrieved from the FGM table.

## Verification and Validation

The combustion models have been verified and validated on a large series of elementary configuration and flames. The mixture fraction method has been verified on an inert propane jet of the International Workshop for Measurement and Computation of Turbulent Non-premixed Flames (TNF) [5], a flat diffusive plate, and a convective wave, whereas the progress variable framework has been verified on an analytical Bunsen and a 1D premixed flame. The FGM model has been validated on TNF's Flame D, TU Darmstadt's stratified burner, DLR Flame A, Gould's premixed combustor, premixed TECFLAM burner, TNF's Cabra flame, BERL combustor, among other test cases.

## The FGM Method for the Simulation of Industrial Combustion Processes

To assess the performance of the FGM method for the simulation of industrial combustion processes, various furnaces and gas turbine combustors have been simulated. As examples for an industrial furnace simulation, the results of the computation of the reactive flow in the NG7 furnace [6] of IFRF will be shown. This furnace is a prototype for glass melting furnaces and in the simulations not only the combustion process, but also the radiative and conjugate heat transfer, as well the soot production was accounted for. To compute the radiative heat transfer the Finite-Volume-Method (similar to the Discrete-Ordinate-Method) was used. Figure 2 shows the temperature contour in the mid-plane of the combustor and Fig. 3 shows the convergence of the mass flow with and without the use of the CPU-Booster™ technique. Obviously, the use of the CPU-Booster™ method greatly enhances the convergence rate of the mass flows and drastically reduces the computational time.

As an example from the propulsion sector, results from the simulation of the KJ66 micro aero-engine [7], which is fuelled with pre-evaporized kerosene, will be shown. Finally, computational results for the lean Cooretec gas turbine combustor of Siemens [8] will be presented. Figure 4 shows the simulated temperature in the combustor. The numerical results will then be compared against available data from Raman spectroscopy measurements. Overall, the industrial examples will demonstrate that the FGM method offered in FINE™/Open with Openlabs™ is able to predict the reactive flow field reliably in complex industrial applications.

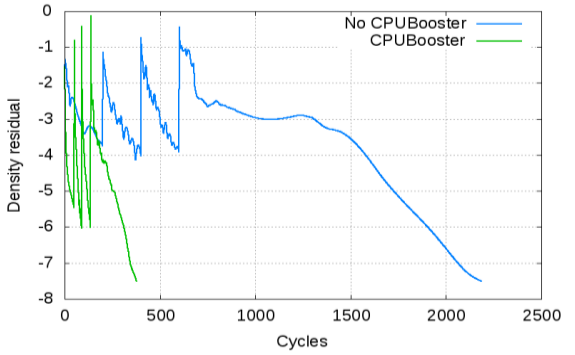


**Fig. 1:** Convergence rate with and without the CPU-Booster™ for a generic gas turbine combustor

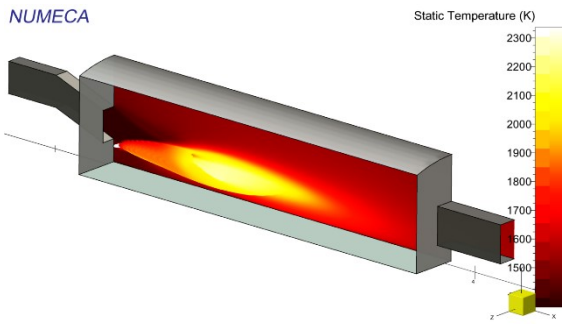


**Fig. 2:** Computed temperature contours in IFRF's glass melting furnace (NG7)

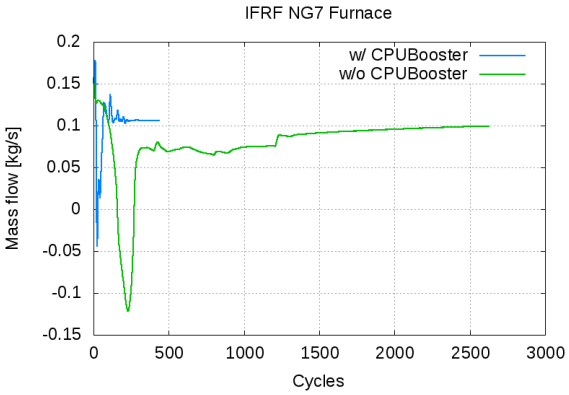


**Fig. 3:** Convergence of the mass flow rates with and without the CPU-Booster™ for IFRF's glass melting furnace (NG7)

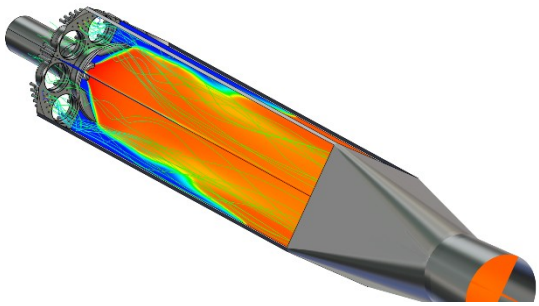

**Fig. 4:** Simulated temperature contour in Siemens' combustor

## References


[1] Janus, B., Dreizler, A., Janicka, J., 2004, Experimental Study on Stabilization of Lifted Swirl Flames in a Model GT Combustor, Flow. Turb. and Combust., 75, pp. 293-315.
[2] Van Oijen, J. A., de Goey, L. P. H., 2000, Combustion Science and Technology, 161(1), pp. 113-137
[3] Gicquel, O., Darabiha, N., Thevenin, D., 2000, Proc. Combust. Inst., 28, pp. 1901-1908
[4] Somers, B., 1994, PhD-thesis, TU Eindhoven
[5] International Workshop on Measurement and Computation of Turbulent Non-premixed Flames (TNF Workshop), Sandia National Laboratories, CA, www.ca.sandia.gov/TNF.
[6] Nakamura, T., van de Kamp, W.L., Smart, J.P., 1991, "Further studies on high temperature natural gas combustion in glass furnaces", Technical report IFRF Doc. No. f90/y/7, IFRF, Ijmuiden, The Netherlands
[7] Ling, J., Wong, K.C., Armfield. S., 2006, Numerical Investigation of a Small Gas Turbine Compressor, School of Aerospace, Mechanical, and Mechatronic Engineering, University of Sydney, NSW, Australia
[8] Lückerath, R., Lammel, O., Stöhr, M., Boxx, I., Stopper, U., Meier, W., Janus, B., and Wegner, B., 2011, "Experimental Investigations of Flame Stabilisation of a Gas Turbine Combustor", ASME Paper GT2011-45790

# Combustion simulation methodology development for swirl burners based on URANS/PANS+FGM

B. Basara and Z. Pavlovic - *AVL List GmbH, Graz, AT*
C. Meijer and F.A. Tap* - *AVL Dacolt BV, Maastricht, NL*
**Corresponding author: ferry.tap@avl.com*

## Introduction

The Partially-Averaged Navier-Stokes (PANS) method [1] belongs to so called bridging or seamless variable resolution methods. This approach adjusts seamlessly between Reynolds-Averaged Navier-Stokes (RANS) and Direct Numerical Simulation (DNS). The PANS method is derived from the RANS model equations. It inevitably improves results when compared with its corresponding RANS model if more scales of motions are resolved. The turbulence model adopted in the present PANS variant [2] is the four-equation k-ε-ζ-f formulation [3] which is the variant of more known v2-f model based on the elliptic relaxation concept. As this model represents a practical and accurate RANS choice for a wide range of industrial applications, especially when used in conjunction with the universal wall approach, its PANS variant therefore guarantees that the proper near-wall model is used for any mesh resolution near the wall. Therefore, the primary goal of this study is to assess URANS k-ε-ζ-f and PANS k-ε-ζ-f cold flow predictions for the DLR gas turbine model combustor [4] using AVL FIRE™. Secondary, reacting flow simulations are performed using FGM [5] to describe the turbulent flame front. This work builds on previous work with URANS and DES [6] as well as LES [7,8,9].

## Model gas turbine combustor

The gas turbine model combustor investigated in this study is schematically depicted in Figure 1.

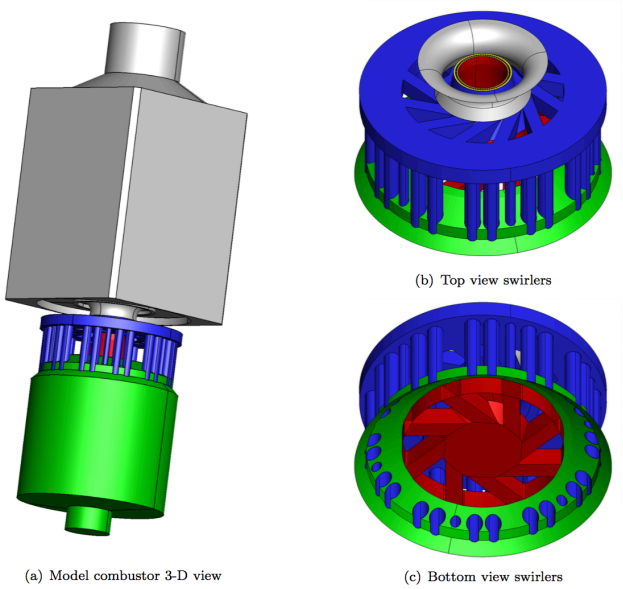


**Figure 1: Gas turbine model combustor geometry**

The air enters the plenum, depicted in green in figure 1(a). The air feeds into two concentric radial swirlers. The inner swirler is depicted in red in figure 1(c); it feeds to the combustion chamber through the central nozzle. The outer swirler (depicted in blue in figure 1(b)) is supplied with air from the plenum through twelve channels, and has a nozzle with a double-curved outer wall connected to the combustion chamber. Methane is injected into the combustion chamber through an annular ring of 72 small fuel tubes, depicted in yellow in the top view in figure 1(b). The combustion chamber has a square cross-section measuring 85 x 85 mm, and a height of 110 mm. All walls in the geometry are treated as being adiabatic walls. The air plenum is included in this study, and assures a natural mass flow split between inner and outer swirler.

Simulation set-up

The cold flow condition for Flame A from [1] is investigated. Polyhedral mesh topology was used (Fig. 2), containing approx. 5.6 million cells. The cell size is ranging from approx. 0.05 mm in the fuel nozzles and 0.1 mm on the double-curved nozzle wall, via approx. 0.75-1.0 mm in the swirlers and flame zone to approx. 5.0 mm in the downstream region of the combustion chamber.

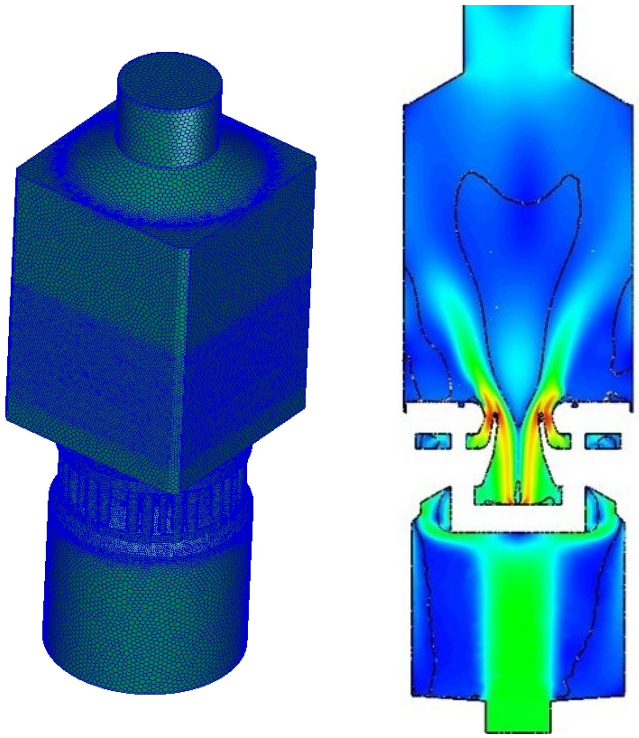

**Figure 2: left: computational mesh, right: predicted velocity field**

Simulation results

The measured flow field [4] is very well reproduced by the URANS k-ε-ζ-f simulation, see Fig. 3. The predicted velocity components for one measured plane (H = 5 mm) are shown in Fig. 3. All components are well captured. However, turbulent kinetic energy is under-predicted (not shown here) and in general, the PANS method is expected to improve the prediction of turbulent fluctuations.

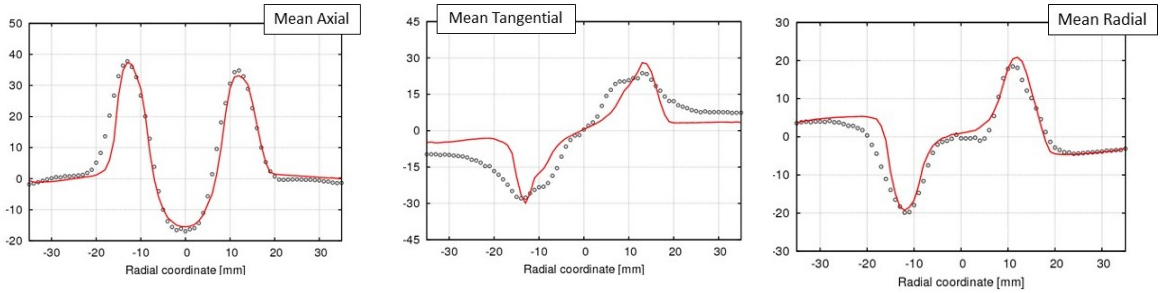


**Figure 3: Predicted velocity components at the measured plane H=5mm.**

References


1. S. Girimaji, Partially-Averaged Navier-Stokes Model for Turbulence: A Rynolds-Averaged Navier-Stokes to Direct Numerical Simulation Bridging Method, J. of Applied Mechanics, 73, pp. 413-421, (2006).
2. B. Basara, S. Krajnovic, S. Girimaji, and Z. Pavlovic, Near-wall formulation of the Partially-Averaged Navier-Stokes Turbulence Model," AIAA J., 49, pp. 2627-2636, (2011).
3. K. Hanjalic, M. Popovac, M., and M. Hadziabdic, A robust near-wall elliptic-relaxation eddy-viscosity turbulence model for CFD, Int. J. Heat and Fluid Flow, 25(6), pp. 1047-1051 (2004).
4. P. Weigand, W. Meier, X.R. Duan, W. Stricker and M. Aigner, Investigation of Swirl Flames in a Gas Turbine Model Combustor 1: Flow-field, structures, temperature and species distributions, Combust. Flame 144, pp. 205–224 (2006).
5. J.A. van Oijen and L.P.H. de Goey, Combust. Sci. Technol. 161 (2000), pp. 113–137.
6. M. Wankhede, F. Tap, P. Schapotschnikow and W. Ramaekers, Numerical Study of Unsteady Flow- Field and Flame Dynamics in a Gas Turbine Model Combustor, GT2014-25784, Proc. ASME Turbo Expo 2014 (2014).
7. W.J.S. Ramakers et al., submitted to Flow, Turbulence and Combustion (2016)
8. Y.C. See and M. Ihme, Large Eddy Simulation of a Gas Turbine Model Combustor, AIAA 2013-0172 (2013).
9. Y.C. See and M. Ihme, LES Investigation of Flow Field Sensitivity in a Gas Turbine Model Com- bustor, AIAA 2014-0621 (2014)

# MODELING OF MASS EVAPORATION BEHAVIOUR OF SINGLE AND MULTI-COMPONENT FUELS UNDER COMBUSTION CONDITIONS IN POOL FIRES

**P.H.Saptogino*, M.Grote, R.T.E.Hermanns and D.Diarra**

*OWI Oel-Waerme-Institut gGmbH, Kaiserstraße 100, D-52134 Herzogenrath, Germany*
**E-Mail: habib.saptogino@owi-aachen.de*

**Key words:** Pool fire, burning rate, evaporation rate, multicomponent fuel

## INTRODUCTION

Fire accidents are a major concern for the safety of refineries, power plants, petrochemical and offshore facilities. Accidental fires in industrial facilities are often in form of pool fires, which occur when accidently released flammable liquids accumulate and ignite. Fire safety analysis of pool fires are generally carried out using computational fluid dynamics (CFD) simulations, which require mass burning rates or fuel evaporation rates as boundary condition. This boundary condition is generally prescribed using experimental data or empirical correlations [1]. However, limited data is available in literature for determining the boundary conditions. Hence, the development of a model to predict the mass evaporation rate which can deliver the required boundary condition for CFD simulations is of highly relevance.

In this work, a model based on a theoretical analysis of the time-dependent mass evaporation rate of liquid pool fires is used. The model is extended to be able to calculate multicomponent fuels. As reference fuels heptane, ethanol and their mixtures are used for the analysis. Implementation of the model is done in MATLAB®. For validation, the model predictions are compared with the results of laboratory experiments.

## MODEL DESCRIPTION

The model is based on the one-dimensional energy flux balance on the surface of the liquid pool, given by:

$$\frac{\partial T}{\partial t} = \frac{\lambda_L}{\rho_L c_{pL}} \frac{\partial^2 T}{\partial z^2} + \frac{1}{\rho_L c_{pL} \Delta z} \left[ \dot{q}''_{rad} + \dot{q}''_{conv} - \dot{q}''_{vap} - \dot{q}''_{rerad} \right]. \quad (1)$$

Where $T$ denotes Temperature, $t$ represents the time, $\lambda_L$ is the thermal conduction, $c_{pL}$ is the liquid heat capacity, $\rho_L$ is the density and $\dot{q}''$ the heat fluxes on the liquid surface. The liquid domain is spatially discretized using 50 cells, where $\Delta z$ represents the height of the cell. The input heat source from the flame to the liquid surface consists of radiation and convection. The heat loss from the liquid surface consists of the energy needed to vaporize the liquid and the emitted radiation. After balancing, the remaining heat is used to heat up the rest of the liquid underneath the surface, given by the first term on the right side in Equation (1). The evaporation rate is calculated according to the film theory with consideration of the bulk-flow effect [2]. The gas phase and the chemical reactions are represented by a heat source. The heat feedback from the flame is calculated through correlations in form of radiation [3] and convection [4]. For multicomponent fuels, the mass evaporation rate of each species is calculated separately while the liquid properties are calculated as a mixture. The liquid mixture is assumed to be constantly ideal mixed.

## EXPERIMENTAL SETUP

The experimental setup consists of a small stainless steel pan of 50.5 mm inside diameter and 11 mm depth filled with fuel. After Ignition, the mass decrements over time are measured by an electric scale with uncertainty of 0.01 gram. A wooden plate as isolator is inserted between the pan and the scale. The experiment is done inside an experiment box to eliminate environmental influences.

## RESULTS

Fig. 1(a) shows the results of the calculated and experimental obtained mass evaporation rate of a heptane pool fire. From the experimental results the progress of the mass evaporation rate can be divided into five stages: 1) initial start-up, 2) preheating, 3) transition, 4) steady state boiling and 5) decay. Similar progress has been observed in the literature [5]. Overall, a qualitative agreement of the mass evaporation rate can be seen, especially at the steady state stage near the end, with discrepancy around 10%. During the preheating stage the calculated values show the largest differences. The total burn out time is predicted about 12% faster in comparison to the experimental results. Using the analysis of the energy balance it can be concluded that the source of the raise in mass evaporation rate during the different stages is the heat requirement to heat up the liquid beneath the fuel surface. After the liquid surface reached the boiling temperature, the mass evaporation rate stays constant. During this time the liquid below the surface is still heated. After the bottom of the liquid

begins to increase in temperature, the mass evaporation rate begins to increase. This is because the heat used for heating the liquid is at this point less than at the beginning. The remaining energy is used to vaporize more fuel until the maximum evaporation rate is reached when all of the fuel reached the end temperature.

The results of the calculated and experimental obtained mass evaporation rate of an ethanol pool fire are presented in Fig. 1(b). Deviating from the heptane pool fire, the mass evaporating rate in the experimental results shows no distinct change during the preheating, transition and steady state phase. This can be attributed to the higher evaporation heat of ethanol. The overall modelled mass evaporation rate agrees qualitatively with the experimental results. The initial start-up and preheating stage shows the largest discrepancy with lower predicted values.

As an example for calculating fuels with multicomponent compositions, a mixture of 80 vol% heptane and 20 vol% ethanol is used as fuel. The results are presented in Fig. 1(c). Observing the experimental results, the mass evaporation rate first progresses to the steady rate of ethanol. Since the saturation pressure of ethanol is lower than heptane it will deplete first. After ethanol is burned out, the mass evaporation rate of the mixture raises to the rate of heptane. The evaporation model predicts a higher mass evaporation rate of the mixture and captures the burning out behaviour of the first component.

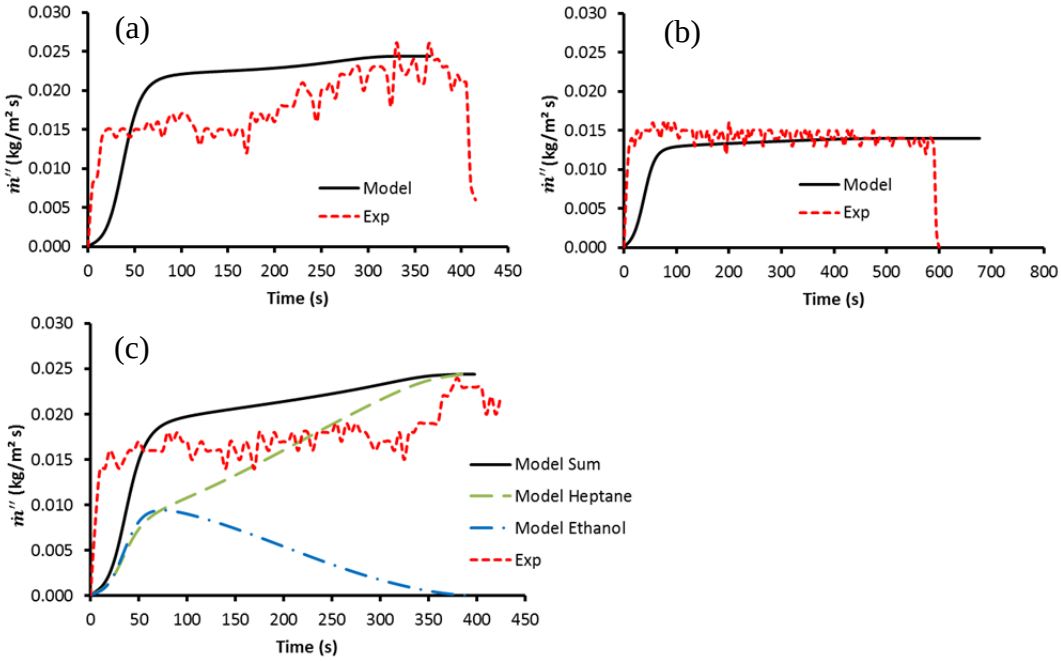


*Figure 1 :* Comparisons of predicted mass evaporation rate of (a) heptane, (b) ethanol and (c) mixture 80 vol% heptane and 20 vol% ethanol pool fire with experimental results.

## SUMMARY AND OUTLOOK

From the above obtained results and comparisons it can be concluded that the model is capable of predicting first order approximation of the transient mass evaporation rate of small-scale pool fires for single and multicomponent fuels. The suitability of the model for larger pool fires need to be verified in further studies. In combination of the evaporation model with a CFD fire code the predicted mass evaporation rate can be used as an input for the fuel inlet boundary condition.

## REFERENCE


[1] C.-j. Wang, Y.-m. Ding and S.-x. Lu, "Large Eddy Simulation of Ethanol-gasoline Fire," *Procedia Engineering*, vol. 71, pp. 421-426, 2014.

[2] E. J. Henley, J. D. Seader and D. K. Roper, Separation process principles, 3rd ed., Wiley, 2011.

[3] J. R. Howell, R. Siegel and M. P. Menguc, Thermal radiation heat transfer, CRC press, 2010.

[4] B. T. Rhodes and J. G. Quintiere, "Burning rate and flame heat flux for PMMA in a cone calorimeter," *Fire Safety Journal*, vol. 26, no. 3, pp. 221-240, 1996.

[5] H. Hayasaka, "Unsteady burning rates of small pool fires," *Fire Safety Science*, vol. 5, pp. 499-510, 1997.

# LES modeling for lifted Delft jet-in-hot-coflow flames using the FGM approach

A. Vasavan, J.A. van Oijen

*Multiphase & Reactive Flow, Mechanical Engineering, Eindhoven University of Technology*

*a.vasavan@tue.nl*

The Delft jet-in-hot-coflow (DJHC) experiments conducted by Oldenhof et al. have revealed many essential characteristics of lifted turbulent diffusion flames [1,2]. Unlike several well-known experiments on JHC flames, the DJHC burner has a significant influence of heat loss on the ignition and stabilization of the lifted flames. In the current study, the DJHC-I flame for DNG as a fuel is modeled using the FGM approach in LES [3]. The effects of heat loss on the flame chemistry are modeled by using igniting mixing layer (IML) flamelets [4] for a range of oxidizer temperatures. The measured temperatures of the coflow boundary are the basis for the range of oxidizer temperatures. A transport equation for enthalpy is solved in the LES besides the mixture fraction and progress variable.

From the preliminary 1D flamelet studies it is observed that the oxidizer temperature is of paramount importance when it comes to the prediction of ignition delay. A variation of oxygen concentration within the range of 9 to 6% does not show a strong influence on the ignition delay of the laminar mixing layer. Hence the current study assumes a constant oxygen concentration across the entire coflow, whereas temperature of the oxidizer varies along the radial direction. Temperature fluctuations are not included at the inlet boundary.

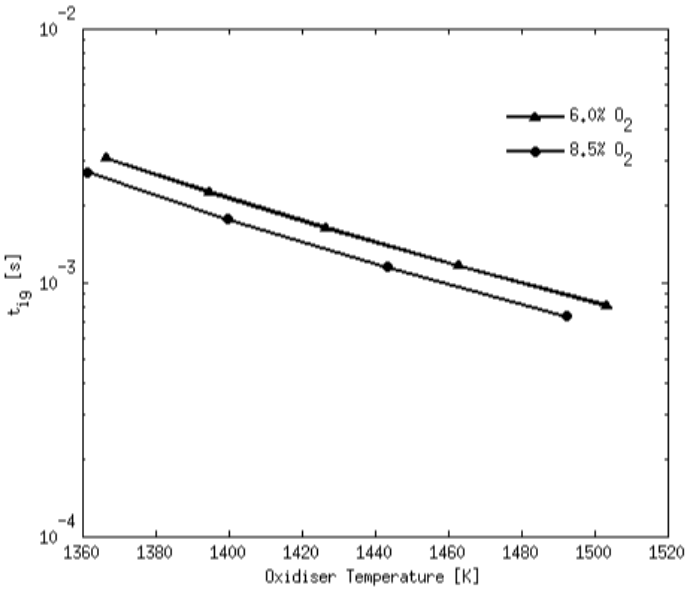


Figure 1: The ignition delay vs oxidiser temperature at different of $O_2$ levels

The turbulence chemistry interaction is modeled using the beta PDF assumption for mixture fraction and progress variable and are investigated in separate simulations. The variances are estimated using an algebraic model.

In the early LES studies, neglecting the heat loss in the coflow has led to an attached flame. The inclusion of heat loss tells a different story. As observed from the 1D studies, there is an exponential rise in the ignition delay on reducing the oxidiser temperature. Taking the heat loss into account, it captures the entrainment of hotter oxidiser into the fuel jet leading to sudden ignition. Whereas the inner region in the coflow with lower temperatures does not.

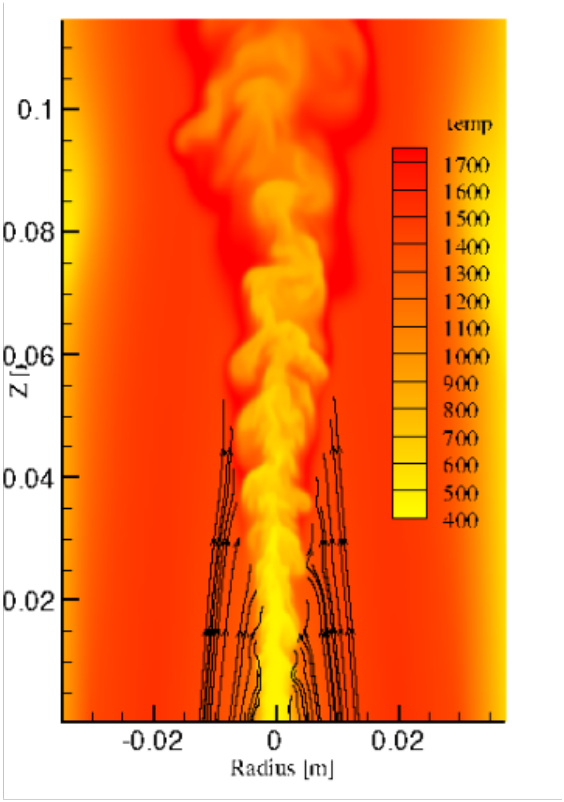

Figure 2: Instantaneous temperature contours for DJHC-I with DNG, with streamlines showing entrainment of coflow

An investigation of the influence the fuel jet Reynolds number confirms this phenomenon. At higher Re, the jet entrains the higher temperature zone in the coflow at an early point. This brings down the point of first ignition, reducing the flame lift off height.

In comparison with the experimental measurements, the velocity field shows a good agreement. The simulated temperature field shows a more intense burning than in the experiments, the reasons for which is an open problem at the moment.

**References**

[1] E. Oldenhof et al., Combustion and Flame, 2010, 157 (6), 1167 -1178

[2] E. Oldenhof et al., Combustion and Flame, 2011, 158 (8), 1553-1563

[3] A. W. Vreman et al., Flow Turbulence Combust, 2009, 82, 511-535

[4] E. Abtahizadeh et al., Combustion and Flame, 2015,

# Experimental and numerical study of MILD combustion in a lab-scale furnace

X. Huang *[1], M.J. Tummers[1], and D.J.E.M. Roekaerts[1]

[1] *Section of Fluid Mechanics, Department of Process and Energy, Delft University of Technology, The Netherlands*

## Abstract

Moderate or Intense Low-oxygen Dilution (MILD) combustion has been proven to be a clean and efficient combustion technology in industrial process furnaces due to its capability of combining low NOx emission and air preheating. Jet in hot coflow burners[1,2] were used to mimic the dilution of air by recirculation of combustion products in furnaces. Semi-industrial furnace[3] work in similar way as industrial furnaces, and represent almost all their features, but it is very difficult to make detailed measurements in it. Lab-scale furnaces[4–6] offer the best opportunities for studying, experimentally and numerically, MILD combustion processes in the presence of significant recirculation and heat transfer.

The inner dimensions of the furnace are $320mm \times 320mm$ with a height of $630mm$, operating with a recuperative Flame-FLOX burner. To heat up the furnace the burner first works in flame mode, with premixed flames stabilised on the nozzles that subsequently when the burner operates in MILD mode are used as air nozzles. The switch to MILD mode is made when the furnace temperature reaches $850°\mathrm{C}$. Then natural gas and air are injected through the central fuel nozzle ($\phi 4.5mm$) and four air nozzles ($4 \times \phi 8.6mm$), respectively. Flue gas is introduced into the recuperator to preheat the combustion air. The top wall of the combustion chamber is air cooled and can act as a heat sink. Quartz windows provide full optical access to the interior of the furnace to enable laser diagnostics.

The furnace was fired with Dutch natural gas (DNG) at $10kW$, equivalence ratio 0.8 with one vertical window ($105mm \times 600mm$) and without top plate cooling. The OH* chemiluminescence originates only from the reaction zone so that it yields information about the position and size of the reaction zone[7]. To find out the location of reaction zone, the OH* chemiluminescence images were collected at different heights with an intensified high-speed camera, equipped with a UV lens and a bandpass UV filter centred at 308 nm with a bandwidth of 20 nm. In chemiluminescence measurements, 4000 single instantaneous images were recorded and averaged, and then reconstructed. The reconstructed OH* chemiluminescence image as shown in figure 1 covers the region from $165mm$ to $525mm$ above the nozzle and shows reactions start from $300mm$ above the nozzle and intensity is relatively uniformly distributed around the fuel jet axis.

Although Eddy Dissipation Concept (EDC) model shows its power in MILD combustion modeling in furnace, it is too computational expensive when incorporating with detailed chemistry mechanism. Flamelet Generated Manifold (FGM) approach is more attractive in this sense. The challenge of modelling combustion in furnace with FGM approach is the dilution effect of internal recirculated flue gas. FGM approach has been extended to consider the flue gas as a dilution stream[8–10]. In the extended approach, an additional independent variable, in addition to mixture fraction, progress variable and enthalpy is introduced, namely a dilution variable $Y_d$. It describes the dilution by recirculation and entrainment of flue gas. Local gas mixture is consider as a mixture of fuel, air and diluent, and local mixture fraction $Z$ is written as: $Z = (1-\alpha)Z_0 + \alpha Z_d$, where $Z_0, Z_d$ and $\alpha$ denote the mixture fraction of fresh fuel and air, mixture fraction of flue gas and flue gas mass fraction, respectively. $\alpha$ is calculated as the ratio between local dilution variable ($Y_d$) and dilution variable in flue gas ($Y_d^{dil}$).

However, using flue gas as dilution is not appropriate when furnaces are working at lean condition. On the one hand, the excess air left in the flue gas also takes part in reactions, especially it reacts with fuel immediately when entrained by fuel jet. On the other hand, the local dilution variable is larger than that in flue gas when local mixture fraction $Z_0$ of fuel and air is at stoichiometric mixture fraction $Z_0 = Z_{st}$,

*Xu Huang: x.huang-2@tudelft.nl

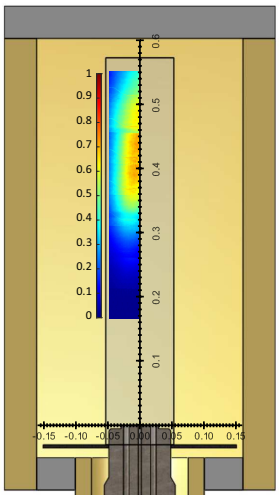

Figure 1: OH* chemiluminescence

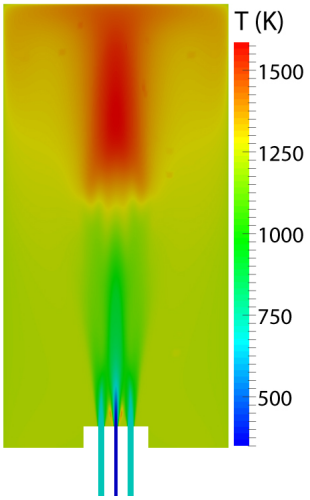


Figure 2: Predicted temperature on the mid-plane

resulting in mass fraction $\alpha > 1$ which is not physical. How to define the dilution stream determines the model is physical or not. To use combustion products at stoichiometric condition as the diluent is proposed. Flue gas is treated as a mixture of excess air and diluent. The local mixture fraction $Z$ is then expressed as: $Z = (1-\alpha)Z_0 + \alpha Z_{st}$. Now, $Z_0, Z_{st}$ and $\alpha$ denote the mixture fraction of fuel and air (excess air is included), mixture fraction of diluent and diluent mass fraction. The newly introduced dilution variable is solved by its transport equation with a source term $\dot{\omega}_{Y_d}$ which transfer the products to diluent at local condition when reaction is complete, that is progress variable equals to 1.

Numerical simulations are made based on the extended FGM approach including also the effects of radiation. Influence of turbulence on local flame structure is taken into account by presuming $\beta$-shape PDF for mixture fraction and progress variable. Control parameters in this approach are mixture fraction, mixture fraction variance, progress variable, progress variable variance, enthalpy loss parameter and dilution variable. The 6 dimensional tables are pre-calculated. Modeling results show the high temperature zone (figure 2) is consistent with the reaction zone indicated by OH* chemiluminescence measurements. The reactions between fresh fuel and air left in flue gas are predicted when fuel enters the furnace. Radiation significantly influences the heat transfer inside the furnace.

## References


[1] E. Oldenhof, M. J. Tummers, E. H. van Veen, and D. J. E. M. Roekaerts. *Combustion and Flame*, 157(6):1167–1178, 2010.

[2] P. R. Medwell, P.A.M. Kalt, and B.B. Dally. *Combustion and Flame*, 148(1-2):48–61, 2007.

[3] E.S. Cho, D. Shin, J. Lu, W. de Jong, and D.J.E.M. Roekaerts. *Applied Energy*, 107:25–32, 2013.

[4] P.J. Coelho and N. Peters. *Combustion and Flame*, 124:503518, 2001.

[5] G.G. Szegö, B.B. Dally, and G.J. Nathan. *Combustion and Flame*, 154:281–295, 2008.

[6] A.S. Verissimo, A.M.A. Rocha, and M. Costa. *Energy and Fuels*, 25:2469–2480, 2011.

[7] J. G. Lee and D. A. Santavicca. *Journal of Propulsion and Power*, 19(5):735–750, 2003.

[8] J. Lamouroux, M. Ihme, B. Fiorina, and O. Gicquel. *Combustion and Flame*, 161(8):2120–2136, 2014.

[9] C. Locci, O. Colin, and J.B. Michel. *Flow, Turbulence and Combustion*, 93(2):305–347, 2014.

[10] O. Colin and J.B. Michel. *Flow, Turbulence and Combustion*, pages 1–32, 2016.

# Capturing curvature effects using MuSt-FGM in a non-premixed auto-igniting flame

M. Ugur Göktolga, Jeroen van Oijen, Philip de Goey

Mechanical Engineering, Eindhoven University of Technology

Contact: m.u.goktolga@tue.nl j.a.v.oijen@tue.nl l.p.h.d.goey@tue.nl

In non-premixed flames where preferential diffusion is present, curvature can play a crucial role by strengthening or weakening the preferential diffusion depending on the direction of the curvature and Lewis numbers of fuel and oxidizer [1]. Since almost all the practical flames are curved, the effects of curvature must be taken into account whenever the preferential diffusion effects are of importance. Therefore, suitable computational models must be developed to capture curvature effects.

In terms of flamelet-based approaches, there are studies in the literature which modify the classical flamelet approach to take curvature terms into account [2, 3]. However, to our knowledge, there are no studies which try to model curvature effects for non-premixed systems using flamelet-based chemistry tabulation methods. This motivated us to extend flamelet generated manifold (FGM) method to model curved non-premixed flames.

Firstly, 1D detailed simulations of strained and curved counter-flow flames were performed. The conditions were taken from the experiments of Dally et al. [4]. The fuel is composed of hydrogen and methane of equal volumes, and the oxidizer is hot and diluted so that the combustion is in MILD regime [5], and the mixture auto-ignites. The strain rate has been fixed at 300 $s^{-1}$ and the curvature radius has been changed from -1 $mm^{-1}$ to 1 $mm^{-1}$. How the initial mass fraction of hydrogen in mixture fraction space and the ignition delay of the flame change with curvature is shown in Figure 1.

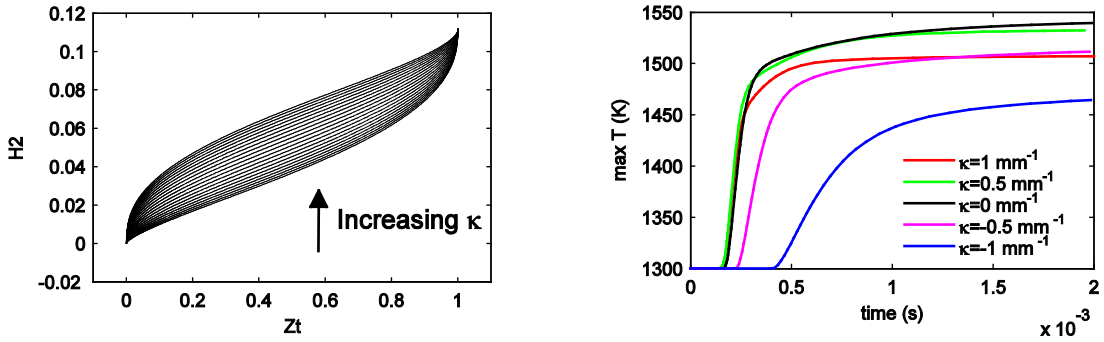


Figure 1. Effect of curvature on some variables: Initial mass fraction of hydrogen (left), maximum temperature of the flame (right).

As can be seen from Figure 1, positive curvature (concave to the fuel) strengthens the effect of preferential diffusion, whereas negative curvature weakens it. As a result, ignition is considerably delayed when the flame is negatively curved. It should be noted that the situation would be reversed if the Lewis number of hydrogen were more than unity.

Curvature increases the dimension of the manifold; hence it should be modeled using an extra control variable that can represent the effects of curvature properly. The obvious choice would be to use curvature itself as the control variable. However, this way the unsteady effects due to the change in curvature cannot be captured. We have decided to use a passive scalar that has the same diffusivity as hydrogen. This new variable can be considered as a new mixture fraction, and was named as “ZH” accordingly. The transported mixture fraction was used as the main mixture fraction instead of Bilger’s definition in order to make two mixture fractions (Zt and ZH) independent of each other.

In order to capture both the pre-ignition and oxidation stages of the combustion, we used the multi-stage (MuSt) FGM approach as in our previous study [6]. $HO_2$ and $H_2O$ were used as the first and second progress variables,

respectively. Using the detailed simulations, a 3D FGM table was created using Zt, ZH, and progress variables as control variables. For comparison purposes, a 2D FGM table without ZH as a control variable was created as well, using the detailed simulation for 0 curvature. Simulations with MuSt-FGM were performed for different curvature values. Evolution of the maximum of progress variables for $\kappa = -1\ mm^{-1}$ are shown in Figure 2.

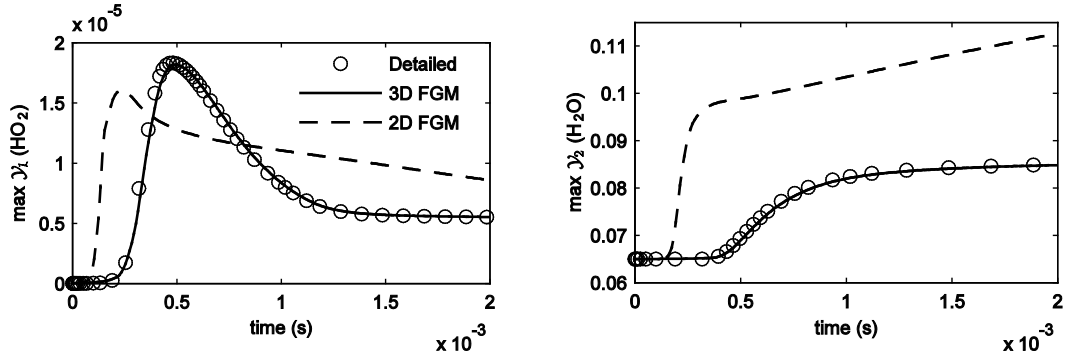


Figure 2. Change of maximum of PV1 (left) and PV2 (right) for $\kappa = -1\ mm^{-1}$

It is clearly seen that the simulation with 2D FGM, which ignores the effects of curvature, cannot capture the ignition delay and miscalculates progress variables. On the other hand, the simulation with 3D FGM can predict all the pre-ignition, autoignition, and oxidation stages perfectly. To further assess the capability of this approach, a case with varying curvature was tested. The mixture was initialized without any curvature, and a curvature of -1 $mm^{-1}$ was applied during the simulation. Again the maxima of progress variables are shown in Figure 3.

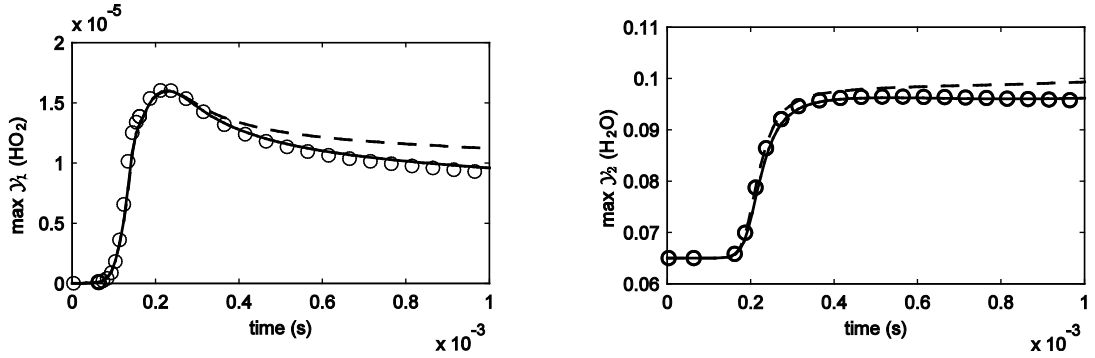


Figure 3. Change of maximum of PV1 (left) and PV2 (right) for $\kappa = 0\ to\ -1\ mm^{-1}$

For this case, 2D FGM performs well for the beginning as well, because the initial condition of 0 curvature dominates in that region. However, as time progresses, 2D FGM fails to capture the change in curvature from 0 to -1 $mm^{-1}$. The 3D FGM is again successful throughout the entire simulation.

We have shown that curvature can be modeled using MuSt-FGM by increasing the dimension of the manifold by 1, and using a mixture fraction with the diffusivity of that of the main fuel component. In the future, we will test this method in simulations of a multidimensional flame.

**References**

[1] P. Wang, S. Hu, R.W. Pitz, Prog. Proc. Combust. Inst. 31 (2007) 989–96.

[2] Y. Xuan, G. Blanquart, M.E. Mueller, Combust. Flame 161 (2014) 1294–1309.

[3] A. Scholtissek, R.W. Pitz, C. Hasse, Proc. Combust. Inst., In Press.

[4] B. B. Dally, A. Karpetis, R. S. Barlow, Proc. Combust. Inst. 29 (2002) 1147–54.

[5] A. Cavaliere, M. de Joannon, Prog. Energy and Combust. Sci. 30 (2004) 329–66.

[6] M.U. Goktolga, J.A. van Oijen, L.P.H. de Goey, Proc. Combust. Inst., In Press.

# Development of simultaneous hyperspectral coherent Raman imaging for advancing reduced emission combustion technology

Alexis Bohlin, Ph.D.
AWEP Department, Faculty of Aerospace Engineering, Delft University of Technology
g.a.bohlin@tudelft.nl

***Overall aim and key objectives***

Advances in optical imaging techniques over the past decades have revolutionized our ability to study chemically reactive flows encountered in air-breathing combustion systems. Emerging technology for unravelling clean- and efficient heat release is needed for advancing new reduced emission technology, and is on the central agenda for a wide variety of energy production- and transport industry. Combustion of fossil fuels remains our largest source of energy production in the world, and global concerns regarding energy security, environmental pollution, and anthropogenic climate change have motivated a large body of research devoted to the experimental measurement and numerical simulation of combustion systems. Clean combustion engineering is the search for improved efficiency by means of strengthen the systems fuel-economy and lowering the emission of NOx, particulates, CO and unburned hydrocarbons (incomplete combustion). New reduced emission technology, greatly rely upon the ability to control the heat release and the exhaust produced by the exothermic reactions between the fuel and the oxidizer in the chemically reactive flow. For the engineering system design, it exist a significant need to inform on the flame-physics involved based on direct observation of the combustion reaction progress and interaction, which is a demanding task for any measurement technique. Chemically reactive flows are inherently multiscale, fully characterized in three-dimensional space and evolving on rapid time-scales. The combustion environment imposes a significant challenge for diagnostics, where it needs to be collected complete information ideally with correlated-field multi-parameter measurement capabilities, exhibiting high spatial and temporal resolution and provided within a snap-shot to freeze the fast dynamics involved. Concurrent detection of major- and minor molecular species (multiplexing) and determining the three most important scalars; the temperature, the flow-field, and the mixture fraction, is vitally important in studies of the reactive flow. The temperature marks the evolution of heat release and energy transfer, while species concentration gradients provide critical information on mixing and chemical reaction.

Optical imaging techniques have the advantage of being non-invasive, which means that the studied process is not significantly perturbed by the measurement technique, and allowing for the acquisition of statistics *in-situ*. Spectroscopy offer intrinsic chemical specificity, in that different classes of molecules have specific spectral signatures serving as unique fingerprints for their identification. Laser-based diagnostics may in general provide measurements with exceptionally high spatial- and temporal resolution, which is important in producing reliable and accurate experimental data. Coherent anti-Stokes Raman spectroscopy (CARS) is one such versatile technique, which has had a profound impact on a wide variety of fields. It was pioneered in composition- and temperature measurements almost 40 years ago, and is referred to as authoritative with the level of accuracy and precision it may provide. A limitation still, has been its main applicability as a single point-measurement technique, where the experimenter needs to raster-scan the measurement samples assembling the spatial image. Because many complex systems can be fully characterized in multidimensional space, there is a large motivation for the advancement of multidimensional CARS imaging techniques.

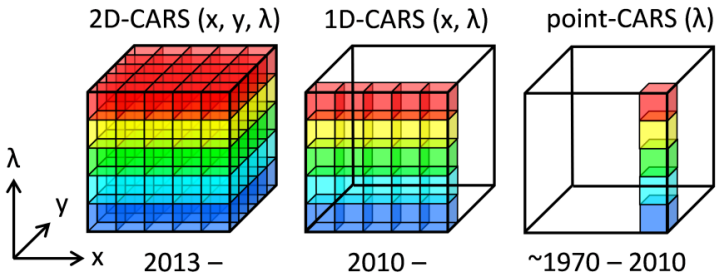


The history development of gas-phase simultaneous CARS imaging. The first 2D-CARS imaging technique was demonstrated in 2013, by me and Sandia researcher Christopher J. Kliewer. The hyperspectral 3D data cube (λ,y,x) is retrieved in a snap-shot (non-scanning) procedure.

***CARS imaging of ignition-kernels and flame propagation in vitiated flows***

Flameless Combustion (FC) has emerged as one interesting option to be investigated for future gas-turbine operation, inspired by the progress obtained in furnaces- and fluidized-bed combustion applications (see for example [1]). FC is characterized by fuel oxidation at lower peak temperatures and with non-visible flames for the naked eye, where the combustion process occur in a more distributed reaction zone. The FC mode has demonstrated low emissions of NOx, particulates, CO and unburned hydrocarbons, and would be very beneficial for gas-turbines because of the more uniform temperature profile leading to lower combustor pattern factor, and reduced perturbation from thermo-acoustics in comparison with conventional combustors. To implement the FC

mode in aero-engines and gas-turbines used for power production is not straightforward, however; the implications related to the different physical scales relative a combustion furnace, makes it a difficult technical challenge and more insight is needed to mature this promising technology. The gas-turbine combustors need to be contained in a restricted volume, and requiring a broad operational range obtained with high stability and with low overall pressure losses.

We will carry out the realization experiment of this new combustion mode in a fuel-flexible FC combustor (~250kW), with access to compressed air provided at a maximum mass-flow rate of ~250g/s up to 5 bar. The combustor prototype will be operated with different fuels (methane and/or hydrogen) in mixtures with air and dilution gases ($N_2$ and $CO_2$) at variable mass-flow rates and thermal inputs. The air and dilution gases are pre-heated prior to the injection with the utility of exploring a range of input temperatures using an electric heater (maximum power of ~50 kW, ~900K). The flexibility will enable the attainment of FC and to acquire quantitative data on this combustion mode with its boundaries. The examination provided by the current multi-parameter diagnostics platform is unique, since the *in-situ* information on temperature and its fluctuations is particularly important for understanding the thermal NO formation process, which is the predominant one in gas-turbine combustion with a residence time ranging from 10 to 30 ms. CARS multiplexing across the entrance to the exit section of the combustor, will be able to provide information on the complete oxidation of the reactants, the air-entrainment- and the exhaust-gas-recirculation processes as a consequence of the complex fluid-dynamics involved. The realization experiment will serve as the primary input developing computational codes (CFD) on FC, which will be performed in direct connection to the experiment. The CARS system is built from the <35 fs output of a high-power femtosecond regenerative amplifier with a pulse energy of ~7mJ provided at a 1kHz repetition-rate. The setup is implemented with the two-beam femtosecond/picosecond phase-matching scheme, recently utilized for multi-parameter spatio-thermochemical probing of flame-wall interactions [2] (displayed in the figure below), with an efficient coherent excitation bandwidth spanning the pure-rotational manifold of all Raman active species. The narrowband ps-duration probe-beam centered at 400nm, is efficiently produced by the principles of second-harmonic bandwidth compression [3], originating from a portion of the fs laser output being repetition-wise synchronized with the fs pump/Stokes-beam, and automatically phase-locked to the impulsive excitation pulse at the experiment with an arbitrary time-arrival. This ultrafast coherent Raman imaging is offering a well-benchmarked ~1% relative standard-deviation in single-shot precision thermometry. The new utility of image post-processing available from the spatially correlated measurements will improve the precision of the flame-data even further. In this way, the direct imaging will bring new possibilities for noise reduction with robust performance, and the claimed stability of the FC mode which is still an open question, can now uniquely be assessed at each the measurement locations in the combustor chamber. Statistics on single ignition-kernels is a goal and to watch the flame propagation from these events.

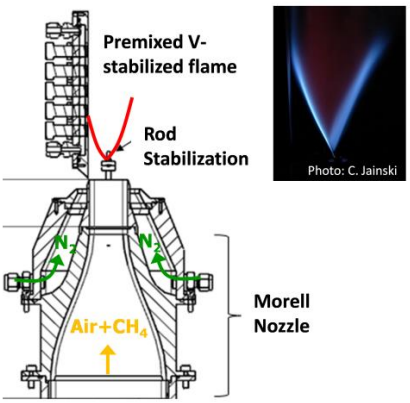


*Burner design (Dreizler group, TU Darmstadt)*

Flame-wall interaction plays a key role in the formation of pollutants in a combustion chamber, such as unburned hydrocarbons or carbon monoxide.

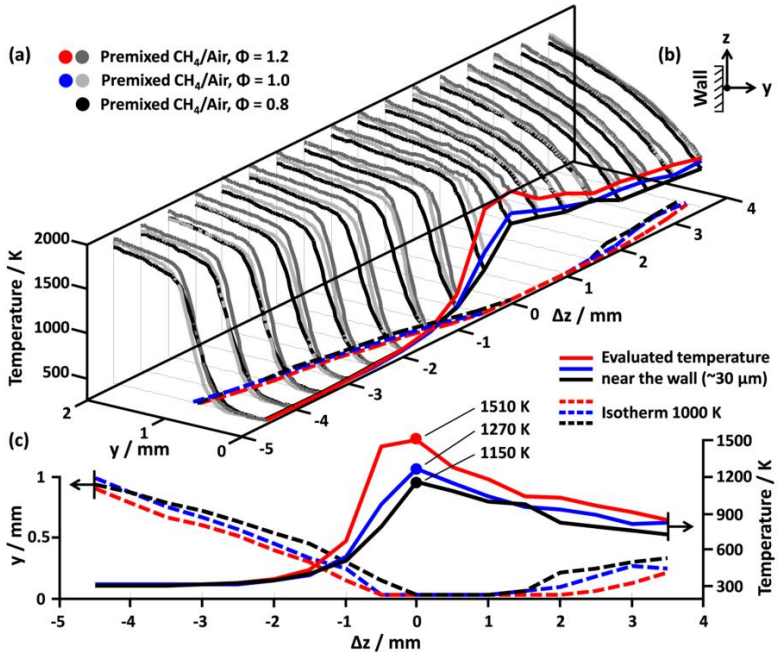


***References***


[1] B. Danon, E.S. Cho, W.- de Jong, D.J.E.M. Roekaerts, *Appl. Therm. Eng.*, 31, 3885–3896 (2011)

[2] A. Bohlin, C. Jainski, B.D. Patterson, A. Dreizler, and C.J. Kliewer, Multiparameter spatio-thermochemical probing of flame–wall interactions advanced with coherent Raman imaging, *Proceedings of the Combustion Institute* (2016), http://dx.doi.org/10.1016/j.proci.2016.07.062

[3] S. P. Kearney, *Combust. Flame* 162, 1748 (2015)

# The role of Toluene in PAH formation: Raman Spectroscopy

R. Doddema*, N.J. Dam, N.G. Deen
Multiphase & Reactive flows, Eindhoven University of Technology, Eindhoven, the Netherlands
*Corresponding author. email: r.doddema@tue.nl

## Introduction

Harmful exhaust emissions of diesel engines in the automotive sector received a lot of media attention lately, as a result of fraudulent practices by large OEMs, involving mainly exhaust NOx levels. Besides NOx, diesel engines are also infamous for producing soot particles, making fuel-rich diffusion-type flames a research topic during the last decades. All kinds of different hydrocarbon fuels have been studied to determine their sooting tendency, in-flame soot levels are measured and quantified in terms of soot volume fractions, soot particle structure and composition have been investigated with electron microscopes, etc. The list of applied techniques and used combustion devices is endless; soot is complex matter. The topic of this study is the perceived higher sooting tendency of aromatic hydrocarbon fuels in diffusion flames, with emphasis on the transition of fuel to poly-cyclic aromatic hydrocarbons (PAHs), which act as precursors in the soot formation process. Current understanding of the PAH formation process attributes an important role to acetylene [1]. Mokhov et al [2] have shown that quantitative measurements of acetylene are possible using Raman scattering in a methane-air diffusion flame. Trying to extend this work, a spontaneous Raman scattering setup is built in order to identify major species along the central axis of a sooting heptane-toluene diffusion flame.
The research is still ongoing, but the experimental approach will be explained and some preliminary results are shown.

## Experimental setup

In this work a tube-in-tube co-flow burner is used, capable of burning vaporized liquid fuels. Via a heated line, the inner tube is fed with a vaporized $95\%_{vol}$ heptane - $5\%_{vol}$ toluene fuel mixture plus nitrogen carrier gas. The outer tube introduces an air co-flow. The burner is situated in a closed vessel with optical access to prevent flow perturbations by external factors. The liquid fuel is vaporized in a Bronkhorst CEM and flows are controlled by Bronkhorst mass flow controllers.
Spontaneous Raman measurements are performed using a Nd:YLF laser (Photonics Industries DM20-527) with an average power of 20W at a repetition rate of 1 kHz, wavelength of 527 nm and a pulse duration of 170 ns. Polarization of the laser beam is controlled by a half-wave plate in combination with a polarizing beam-splitter. The laser beam is focused down to a 'line focus' using a spherical $f$ = 1000 mm lens, enters the burner vessel via the flue-gas exit and is directed downwards into the fuel tube of the burner. The positive lens is placed such, that the 'line focus' of the laser beam is positioned along the central axis of the diffusion flame, enabling spectral information as a function of height-above-burner (HAB), see figure 1. The laser beam is dumped inside the burner at the bottom-end of the fuel line. Optical breakdown is prevented by the relatively long pulse duration of 170 ns.

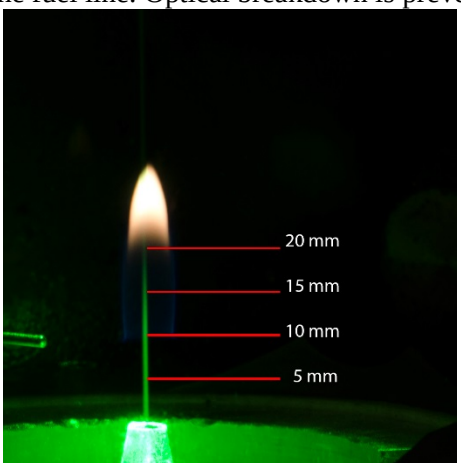


*Figure 1: Picture of the diffusion flame and exciting laser beam (green). Relevant heights above burner have been indicated.*

The Raman scattered signal is collected by an $f$ = 150 mm, $f$/2,5 fixed focal length objective fitted with an Edmund Optics OD4 532 nm notch filter and is dispersed in an $f$/5.6 Acton SpectraPro 500i spectrograph with 300 g/mm grating (blazed at 500 nm). The spectrograph is oriented such that its entrance slit is aligned parallel to the line focus of the laser beam. A Princeton Instruments PI-MAX 3 ICCD camera, with filmless Unigen II intensifier, is used as detector. Synchronization of laser and camera intensifier is accomplished through a BNC Berkeley Model 555 pulse/delay generator. Each recorded spectrum is a result of 100,000 gates per exposure, and with the image intensifier keeping up with the laser repetition rate of 1 kHz, a measurement time of 100 seconds.
Combining the equipment results in a field-of-view (vertical) of about 6 mm, a spatial resolution of 51 pixels per mm and a spectral resolution of 0.083 nm/pixel. The spectrograph was lifted and lowered to capture the entire of 0-20 mm HAB.

**Preliminary results**
Right above the tip of the burner a clear Raman spectrum of the fuel mixture is observed, as can be seen in figure 2 below. When moving up along the central axis of the flame, the peaks originating from the fuel mixture disappear, peaks corresponding to $CO_2$ (~1300 $cm^{-1}$) and $H_2O$ (~3625 $cm^{-1}$) arise and broadband laser induced soot incandescence appears. Unfortunately, no distinguishable Raman signal of acetylene (~1950 $cm^{-1}$) has been observed in the recorded spectra.

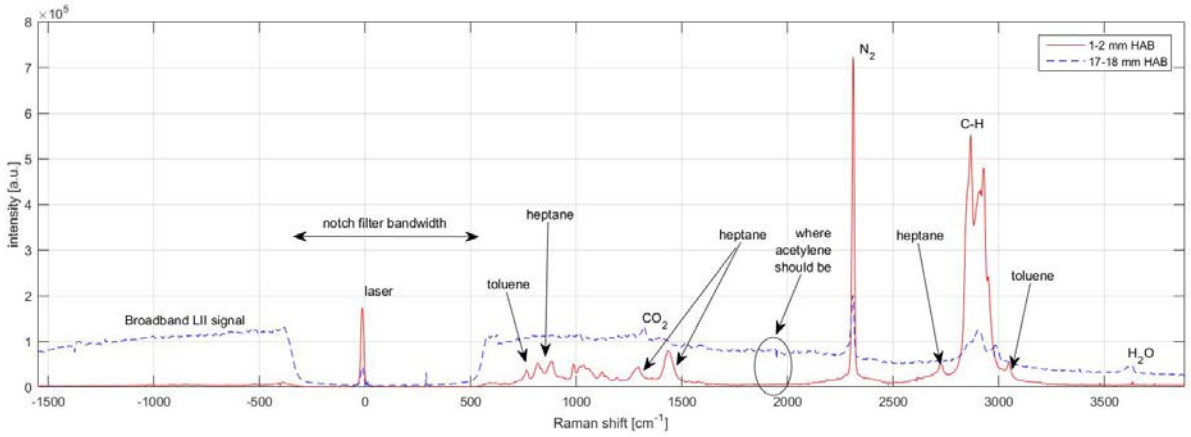


*Figure 2: Example Raman spectrum at 1-2 mm HAB (red solid line) and 17-18 mm HAB (blue dashed line), showing intensity [a.u.] as a function of Raman shift [$cm^{-1}$]. Spectrum is obtained by binning 51 pixels (1 mm) and gluing multiple spectra (stepping of the grating).*

**Future steps**
Longer measurement times will be employed, focusing on the detection of acetylene at 1950 $cm^{-1}$. Beam steering in the hot flue gases causes the focused light beam to oscillate around the flame center axis, moving out of the field of view. This decreases the already low efficiency of the spontaneous Raman scattering technique even further. To solve this, the laser beam will be introduced into the burner vessel from below, via a window under Brewster's angle at the bottom end of the fuel tube.

**References**
[1] Bockhorn, H, 'Soot Formation in Combustion – Mechanisms and Models', *Springer Series in Chemical Physics*. Berlin: 1994.
[2] Mokhov, AV, Bennett, BAV, Levinsky, HB & Smooke, MD. 2007, 'Experimental and computational study of $C_2H_2$ and CO in a laminar axisymmetric methane-air diffusion flame' *Proceedings of the Combustion Institute*, vol 31 I, pp. 997-1004.

# Comparison of normal spectral emittance of sulfates and carbonates - significant mineral classes of ashes under oxy-fuel conditions

*Jeanette Gorewoda[1]*, Viktor Scherer[1]*

Corresponding author: *gorewoda@leat.rub.de, +49-234-32 26323

[1]Department of Energy Plant Technology, Faculty of Mechanical Engineering, Ruhr-University of Bochum, Universitätsstr. 150, 44801 Bochum, Germany

Ashes of solid fuels form deposits of on heat exchanger surface in boilers. These deposits influence the heat transfer from the flame to the heating surfaces. Especially in the furnace of the boilers were radiation dominates the emittance characteristics of ash layer are of great importance. The emittance is influenced by physical structure of the surface (mean particle size, roughness of the layer) and by the mineral composition of the ashes. Oxy-fuel firing system - compared to air fired system – have significantly higher $CO_2$ concentration in the combustion zone but also show an increased concentration of minor species like $SO_2$ due to the intensive flue gas recirculation. Therefore, oxy-fuel ashes might contain more carbonates and sulfates than ashes from air-fired systems. The statements in literature whether carbonates or sulfates dominate are contradictory. Scheffknecht et al. [1] did find an increased amount of sulfates, especially $CaSO_4$ in the ash deposits under oxy-fuel conditions, whereas Kull et al. [2] propose an enhanced presence of carbonates.

Therefore, we examined the spectral characteristics of the emittance of typical carbonates and sulfates contained in coal ashes. Due to the size limit of the current contribution, we concentrate on $CaCO_3$ and $CaSO_4$, because Ca is typically contained in large amount in coal ashes and forms carbonates and sulfates. As a comparison we added $K_2SO_4$. Note that we have made a very detailed study on the emittance of Ca-, Mg- and Sr-carbonates as pure substances and mixed with $SiO_2$ which can be found in [3].

The minerals $CaCO_3$, $CaSO_4$, and $K_2SO_4$ were prepared in powder form and sieved to defined particle size fractions. For $CaCO_3$, $CaSO_4$ we show results for a size fraction of $125 < x < 160$ µm and for $K_2SO_4$ additionally for a size fraction of $x < 32$ µm). The comparability of the particle size distribution has been checked by laser diffraction. The measurements of the heat radiation are carried out in a facility where samples can be heated up to a temperature between 500 °C and 1000 °C. The test rig consists of a Fourier transform infrared (FT-IR) spectrometer and an electrical heating unit that includes both, the sample holder as well as the reference radiator, a black body. Radiation of the heated sample (22 mm diameter, 2 mm thickness) and the black body is guided to a FT-IR spectrometer via a gold coated off-axis parabolic mirror. Thermal radiation is detected in the range from 1.6 µm to 12 µm. The sample surface temperature is determined by two thermocouples (type K, 0.25 mm diameter). They are installed 1 and 2 mm below the sample surface (in the central axis of the disk shaped sample). The sample surface temperature is calculated by assuming a linear temperature profile across the sample height. In order to obtain the spectral emittance (see Eq. (1)) the sample radiation $S_{sample}(\lambda, T)$ is compared with the radiation of a black body $S_{BB}(\lambda, T)$:

$$\varepsilon(\lambda, T) = \frac{S_{sample}(\lambda, T)}{S_{BB}(\lambda, T)} \quad (1)$$

As examples, for carbonates and sulfates, the spectral emittances of $CaCO_3$, $CaSO_4$ and $K_2SO_4$ are shown in Figure 1 – 3 for selected temperatures. The general trend of the spectral emittances is similar and typical for minerals, i.e. also for coal ashes. The spectral emittance is small at low temperatures and increases with wavelength to values in the order of 0.8 to 0.9 above 10 microns. This spectral dependence is important for boiler lay-out. Coal ashes are strongly non-grey which has to be considered in spectrally resolved CFD simulations, or if non-spectrally resolved radiation balances are carried out, appropriate averaging of the spectral emittance has to be accounted for (e.g. a weighted averaging procedure using Planck's law as weighting function, see [1]).

Figure 1 presents the spectral emittance for $CaCO_3$ for the particle size fraction $125 < x < 160$ µm. Spectral bands of the characteristic $CO_3$ group are shaded in grey. Thermodynamic calculation carried out with FactSage predict a decomposition at 775 °C for $CaCO_3$ to CaO. Thus, $CaCO_3$ is completely decomposed at 976 °C as evidenced by X-ray diffraction measurements. The phase change from $CaCO_3$ to CaO can be clearly seen in Figure 1, emittance reduces during phase transformation. The characteristic spectral peaks present for $CaCO_3$ are vanished at 976 °C. When comparing Figure 1 and 2 it is obvious that for calcium the spectral emittance of the corresponding carbonate (Figure 1) is higher than the spectral emittance of the corresponding sulfate (Figure 2), up to a value of approximately 4.5 µm. Above 4.5 µm, the spectral emittances of $CaCO_3$ and $CaSO_4$ are similar in the order of 0.9. Also $CaSO_4$ (Figure 2) shows characteristics bands which occur in different ranges of wavelengths compared to $CaCO_3$. Note that $CaSO_4$ is stable at typical temperatures of coals ashes in boilers, indicating that the S-O bands can also been detected in real coals ashes which have seen very high temperatures. $K_2SO_4$ (Figure 3) shows the characteristics S-O bands as well. Also $K_2SO_4$ shows no phase transformation even at elevated temperature.

Figure 3 clearly indicates that higher particle sizes lead to higher emittance, a well-known effect [3]. This indicates that very fine ash layers (with low particle sizes) can effectively reflect thermal radiation in a boiler, un unwanted effect, whereas powders with larger particles sizes, i.e. rough ash layer surface can absorb heat to a larger extend. Note that the bands around 3 microns in Figure 1 to 3 are to the presence of $CO_2$ in the sample surrounding air.

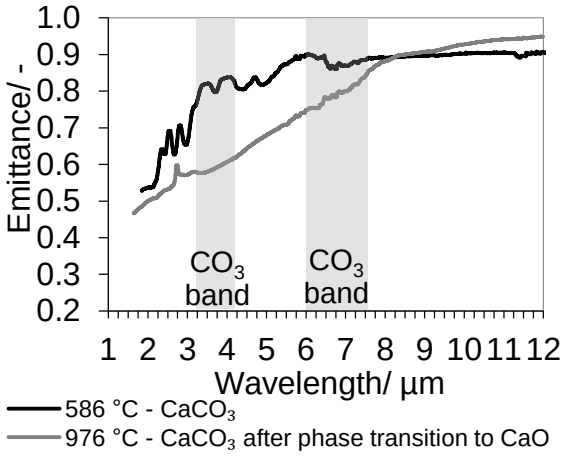


Figure 1. Spectral emittance of $CaCO_3$, particle size fraction $125 < x < 160$ µm.

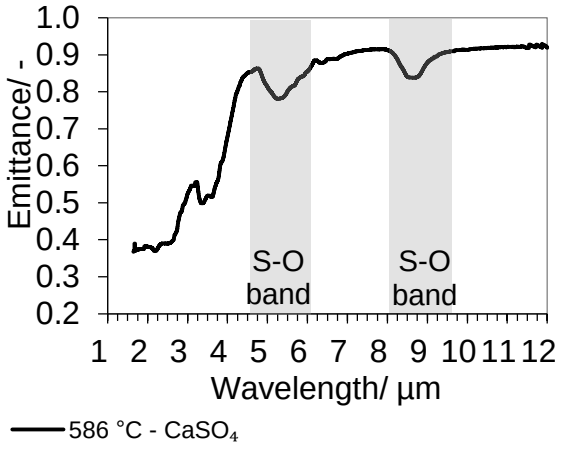


Figure 2. Spectral emittance of $CaSO_4$, particle size fraction $125 < x < 160$ µm.

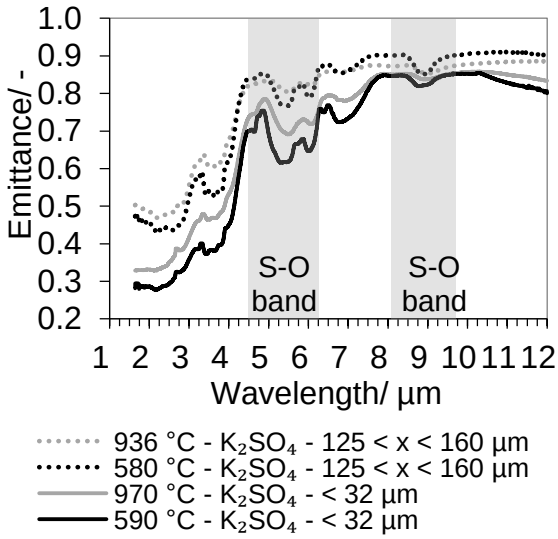


Figure 3. Spectral emittance of $K_2SO_4$, particle size fraction $x < 32$ µm and $125 < x < 160$ µm.

ACKNOWLEDGMENT

This work has been funded by the German Science Foundation (DFG) within the Sonderforschungsbereich/Transregio TR 129 "Development of methods and models to describe solid fuel reactions within an oxy-fuel atmosphere".

LITERATURE

[1] G. Scheffknecht, L. Al-Makhadmeh, U. Schnell, J. Maier, Oxy-fuel coal combustion—A review of the current state-of-the-art, Int. J. Greenh. Gas Control. 5 (2011) S16–S35. doi:10.1016/j.ijggc.2011.05.020.

[2] R. Kull, G. Stein-Brzozowoska, J. Maeyer, G. Scheffknecht, Corrosion of superheater materials under oxy-fuel conditions, in: 1st Oxyfuel Combust. Conf., Cottbus (2009).

[3] J. Gorewoda, V. Scherer, The influence of carbonate decomposition on normal spectral radiative emittance in the context of oxy-fuel combustion, accepted for publication in Energy & Fuels (2016).

# Recent improvements of the Heat Flux setup to determine laminar burning velocities of liquid fuels

S. Feldhoff[1,a], R.T.E. Hermanns[1]
[1]*OWI Oel-Waerme-Institut gGmbH, Germany*

**Key words:** laminar flames, burning velocity, combustion

## INTRODUCTION

The adiabatic burning velocity is an important parameter governing the properties of combustion. It can for example be used to validate reaction mechanisms. This is the reason that research has focused on the adiabatic burning velocity of several types of fuel-oxidizer mixtures. However, the adiabatic burning velocity is not easily measured. The heat flux method is one of the methods to measure the adiabatic burning velocity, developed by de Goey and van Maaren [1]. The heat flux burner consists of a thin, brass burner plate with a hexagonal pattern of holes. The burner plate is heated in such way that the premixed mixture flowing though the burner plate is heated. Now the heat gained by the unburnt mixture compensates the heat loss of the flame. The advantage is that mixture velocities higher and lower than the adiabatic burning velocity can be stabilized on this burner. In contrast to other methods, it is possible to determine the laminar burning velocity at a state of a nearly adiabatic stretchless flame by means of interpolation, rather than extrapolation. This has as advantage that the uncertainties due to extrapolation are circumvented.

## HEAT FLUX BURNER DESIGN AND RECENT IMPROVEMENTS

The original burner head consists of a brass burner plate which is glued onto the heating jacket assembly. Our previous heat flux setup had a burner plate with a hole pattern with holes of 0.5 mm diameter and a pitch of 0.7 mm. This configuration had a couple of shortcomings. Firstly, because the brass burner plate is glued onto the heating jacket assembly and heat conduction between the burner plate and the heating jacket is not efficient. Insufficient conduction between heating jacket and burner plate causes measurement inaccuracies, because in a situation where the observed temperature profile is flat, heat still might be transferred from the burner plate to the heating jacket, when the average plate temperature is higher than the heating jacket temperature

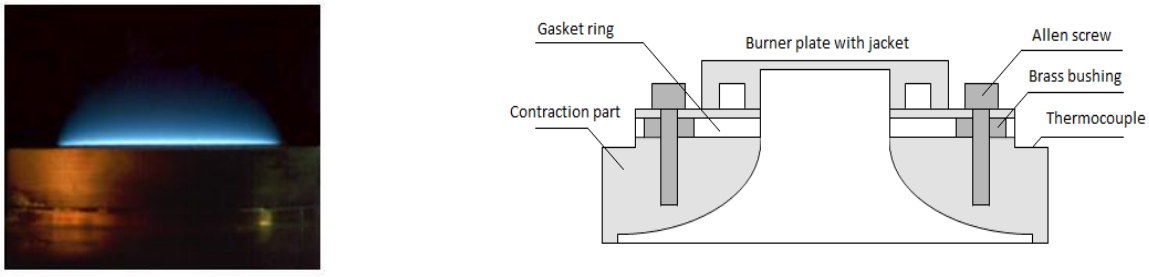


*Figure 1: A flat plate/heat flux burner (left) and schematic section view of the new burner head (right).*

Secondly, a hole diameter of 0.5 mm in combination with a pitch of 0.7 mm limits the velocity range of the unburnt mixture to around 60 cm/s. A smaller hole diameter permits higher unburnt mixture velocities before curvature effects become significant. The new burner head differs from the old one in the sense that it does not use a separate burner plate anymore (see Figure 1).

[a] *Corresponding author*
*E-Mail: s.feldhoff@owi-aachen.de*

The heating jacket and burner plate are made out of one single piece of brass, increasing the conductivity between the heating jacket and the burner plate. This means that the temperature of the burner plate at the outer edges should reach the heating jacket temperature. Ideally, when a flat temperature profile is observed, the temperature should be roughly equal to the heating jacket temperature. This indicates there is no heat transfer between burner plate and the jacket, thus representing an adiabatic flame. Furthermore, the diameter of the burner plate holes is 0.4 mm, with a pitch of 0.47 mm for the new plate, permitting higher unburnt mixture velocities. Also, the number of thermocouples has been increased from 8 to 15 for the new burner head.

## RESULTS

In Figure 2 preliminary results of a stoichiometric ethanol-air flame are shown. The results show that the temperature at the edge of the burner plate reached the temperature of the heating jacket of approximately 110 °C, indicating that the heat conduction is significantly improved. Furthermore, the estimated laminar burning velocity of 44.43 cm/s is comparable to literature data (Figure 2 - right).

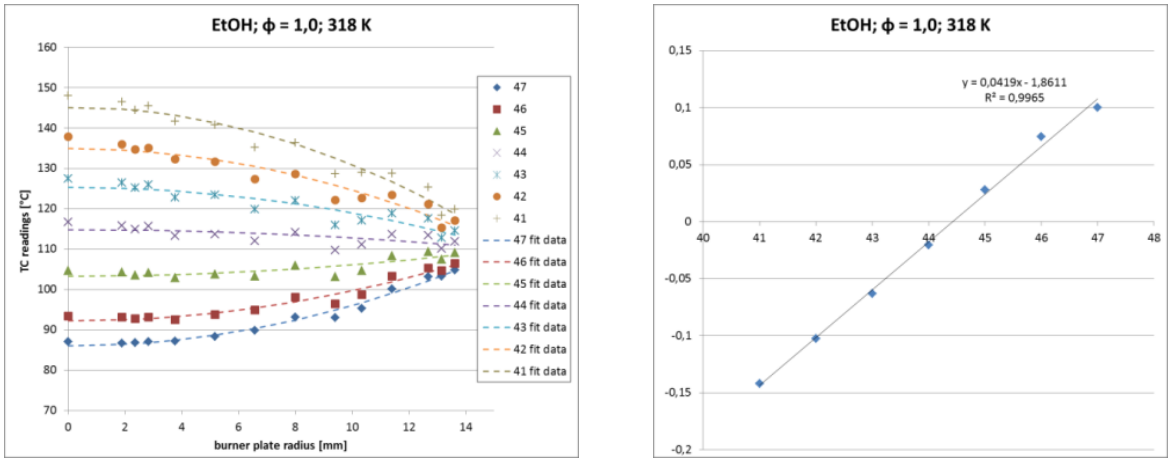


*Figure 2: thermocouple readings in the burner plate at various gas velocities (41 – 47 cm/s) including parabolic fit curves (left) and plot of the parabolic coefficients (right).*

## SUMMARY AND OUTLOOK

The heat flux experimental setup at OWI has been further improved to provide more accurate measurement data of the laminar burning velocity. The new burner head is a significant improvement. The heat conduction between heating jacket and burner plate has been improved and the thermocouple scatter has been reduced. A reduced hole diameter and pitch permits a larger range of unburnt gas velocities. Currently, commissioning tests are running and up-to-date results with special focus on liquid fuels such as ethanol and gasoline will be available within short notice.

## ACKNOWLEDGEMENT

The improvement of the heat flux experimental setup at OWI is part of a research project which has received funding from the Federal Ministry of Food and Agriculture by decision of the German Bundestag through the FNR.

## REFERENCES

[1] L.P.H. de Goey, A. van Maaren and R.M. Quax: *Stabilization of adiabatic premixed laminar flames on a flat flame burner*, Combustion Science Technology, Volume 92, pages 201–207.

# Temperature Effect on Flame Induced Ionization Current for Oxidized Langmuir Probes

D. Raj [a] [1] J.A. van Oijen [a] L.P.H. de Goey [a] N. Beishuizen [b]

[a] Multiphase and Reactive Flows, Eindhoven University of Technology, Eindhoven, The Netherlands.
[b] Bosch Thermotechniek B.V., Deventer, The Netherlands.

**Abstract :** The temperature dependent electrical properties of the oxide layer formed on the ionization pin placed at the flame front are investigated experimentally. All the necessary fundamental principles related to combustion, ionization current, electric fields, oxide layer formation and their electrical properties are explained. Simulations of the internally cooled probe are used to determine the specifications of the setup and set-points for temperature control of the ionization probe. An experimental setup was built, and detailed description on setup calibration is provided to have accurate and reproducible setup conditions. Error sources are identified and quantified. Finally, correlations and physical explanations are provided to support the measurement results. The measured data is compared with literature. A look-up table is generated from the measured data with a linear interpolation scheme and the accuracy is validated. Conclusions from this study are drawn and recommendations are made for future research.

**Keywords :** Ionization current, Langmuir probe, Oxide layer resistance, Kanthal APM.

**Introduction :** Bosch employs Kanthal APM ionization pins to measure the ionization current produced in the flame, for feedback control in its Combustion Management System (CMS) [1]. Probes are placed directly at the flame front, and are thus oxidized forming an oxide layer of primarily alumina ($Al_2O_3$) on the surface. Alumina has excellent thermal properties, effectively protecting the alloy from spallation, increasing the lifetime of the probe significantly. However, with increased oxidation (aging) there is a drop in ionization current for the probe. This effect of aging on ionization current is analyzed in this study to detect, analyze and quantify the parameters that cause the drop in ionization current.

**Setup Description :** The setup is divided into four sections as shown in Figure 1. A burner setup [2] to produce a well defined laminar flat flame [3,4]; ionization current and temperature measurement setup; air and water cooling setup. Dimensions of probe samples were determined from simulations which were also used to validate the surface temperature of the cooled probe. Probe samples are oxidized in an electric oven at a constant temperature of $1473K$ for 10-600 hours in order to produce a homogeneous oxide layer of $\alpha - alumina$. Calibration of the burner is done to have a correlation with the previous research [5,6,7] and to have reproducible set of measurements. Error sources are identified and determined to analyze the accuracy of the setup.

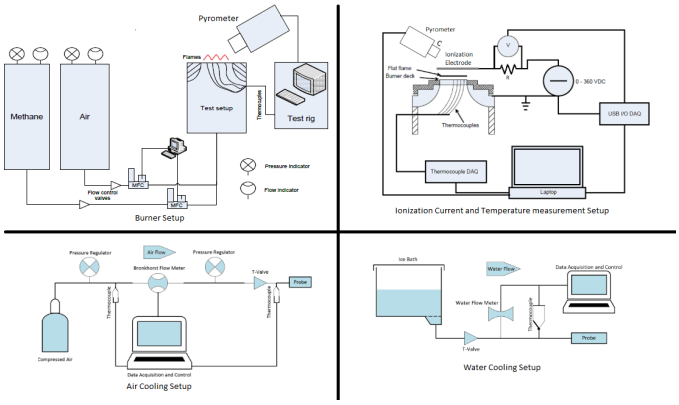


Figure 1 : Setup Schematics

**Results :** The resistance of the oxide layer is determined by correcting the stabilized ionization current curves of the oxidized samples with the IV-curve for an unoxidized sample. This resistance contains a part which is dependent on the concentration of electrons in the flame and a part which is the physical resistance of the oxide layer. Thus, in this study it is referred as the

[1] Corresponding author, email d.raj@student.tue.nl

dynamic electric resistance of the oxide layer. It is dependent on the applied voltage (Fig.2,3,4), oxidation level (aging) (Fig. 2), equivalence ratio of the mixture (Fig. 3), and surface temperature of the probe (Fig. 4).

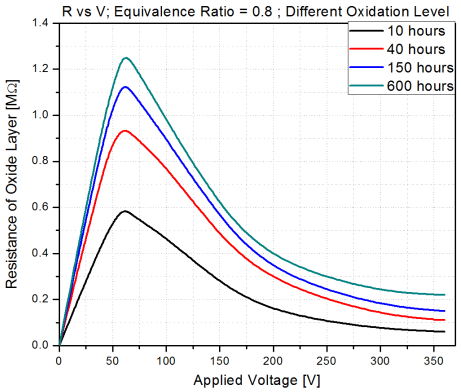


Figure 2 : Effect of oxidation time

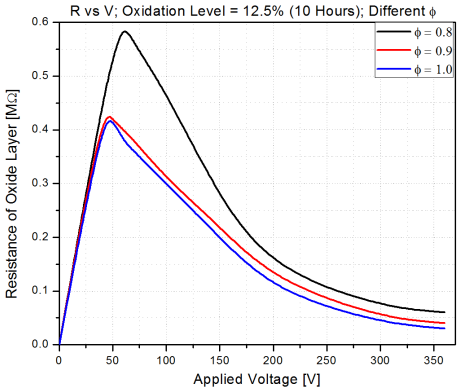


Figure 3 : Effect of equivalence ratio

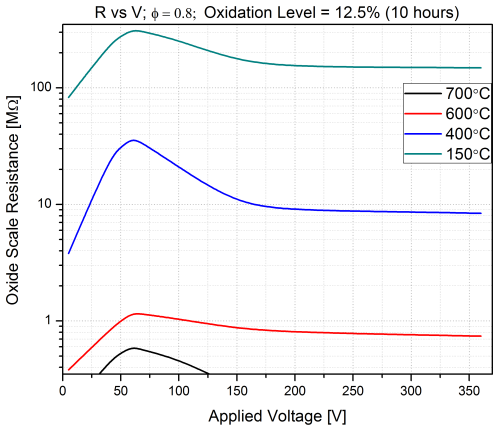


Figure 4 : Effect of probe's surface temperature

Electric resistance for the oxide layer is smaller then the electric resistance for pure aluminium oxide [8] as shown in Fig. 5. This is because, impurities in the oxide layer decreases resistance. The impurities are mainly chromium and iron oxide.

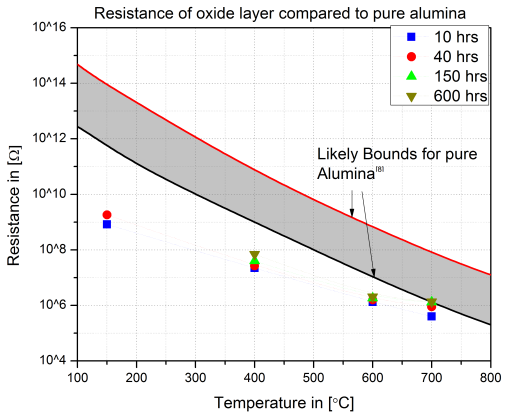


Figure 5 : Oxide layer and alumina resistances.

**Conclusion :** The effect of parameters on the ionization current is analyzed. Dynamic resistance is determined which can be used to calculate ionization current for any specific values of voltage, equivalence ratio, oxidation time, surface temperature of probe. Physical resistance can be used to determine the composition of impurities in the oxide layer.

**Acknowledgment :** This study was done as part of a MSc Mechanical Engineering program at Technical University of Eindhoven and was supported by Bosch Thermotechnology and NVV (Nederlandse Vereniging voor Vlamonderzoek)

**References :**

[1] M. Kiefer, *Combustion management system.* MSc Thesis, University of Karlsruhe, March 2010.

[2] H. Gupta, *Prototype design of a burner with low emissions and high modularity*, MSc Thesis, University of Twente, 2013.

[3] L.P.H. de Goey, K.J. Bosschaart, *Detailed analysis of the heat flux method for measuring burning velocities*, Combustion and Flame 132, 170-180, 2003.

[4] L.P.H. de Goey, J.A. van Oijen, V.N. Kornilov, and J.H.M. ten Thije Boonkkamp. *Propagation, dynamics and control of laminar premixed flames.* Proceedings of the Combustion Institute, 33(1):863 886, 2011.

[5] Y.C.Bruinsma, *Experimental investigation of flame ionization currents and electrode oxidation effects in static and alternating electric fields*, MSc Thesis, University of Eindhoven, 2015.

[6] A. Hiemstra, *Oxidation behaviour of the flame ionization sensor-utilized in fuel quality adaptive heating appliances*, MSc Thesis, University of Twente, 2012.

[7] L.B.W. Peerlings. *Flame saturation current as a measure of the flame thermo-acoustic behavior.* MSc Thesis, University of Eindhoven, August 2012.

[8] P. Auerkari, *Mechanical and physical properties of engineering alumina ceramics*, VTT, Technical research centre of Finland Espoo, 1996.

# Assessing radiation losses by temperature measurements in laminar flat flames

Stefanie Van Damme[a,b,c], Véronique Dias[c], Hervé Jeanmart[c], Francesco Contino[a,b]
[a]Thermodynamics and Fluid dynamics research group, Mechanical Engineering (MECH), Vrije Universiteit Brussel (VUB)
[b]BURN, Joint Research Group, Vrije Universiteit Brussel (VUB) and Université Libre de Bruxelle (ULB)
[c]Thermodynamics and Fluid mechanics (TFL) Institute of Mechanics, Materials and Civil engineering (iMMC) Université catholique de Louvain (UCL)

## Abstract
The temperature profile of a laminar flat flame is required to run simulations. If the temperature of the flame is measured by a thermocouple, correction for radiation losses is needed. However applying the Electrical Compensation Method (ECM) is not always possible, since the required rise of the temperature by the Joule effect in the flame can increase the risk of breaking the thermocouple.
A solution to avoid ECM is to use a simple heat transfer model over the thermocouple wire that can predict the radiation losses based on the properties of the used thermocouple and the characteristics of the assessed flame.
In this presentation the effect of changing the equivalence ratio and the argon dilution on the radiation losses in ethylene flames is assessed, both experimentally and by modelling.
The model focused on predicting a correct value for the convection heat transfer coefficient, h, for the different assessed flames, since the radiation losses are most sensitive to this unknown parameter.
By the ethylene flame experiments a value for h ranging from 63 to 200 W/m² K over a temperature interval of 600 to 1200K is found. From the model the h values ranges from 116 to 258 W/m² K, which is the same order of magnitude as found experimentally. Also the effect of changing the equivalence ratio and the argon dilution is predicted correctly.

## Introduction
To measure the temperature of flames, different methods can be used. The options can be divided into invasive and non-invasive methods. Thermocouples are an invasive method, which means that they can change the nature of the flame they are emerged in, leading to a difference between the measured values and reality. However they are cheaper and easier to use than the non-invasive methods based on laser induced changes in vibrational state and energy level of the molecules in the flame that are currently used [1].
For this work a type B thermocouple is used, composed of PtRh6% and PtRh30% with a diameter of 0.1 mm. A coating of 7%BeO-93%$Y_2O_3$ of 0.02 mm is applied to avoid radical reaction on the thermocouple surface. This type of thermocouple can be used continuously at a temperature of 1600°C and intermittently to 1800°C. It is therefore suitable for flame temperature measurements. The welding point of the Pt alloy is the actual thermocouple and is placed in parallel to the flame as shown in Figure 1.

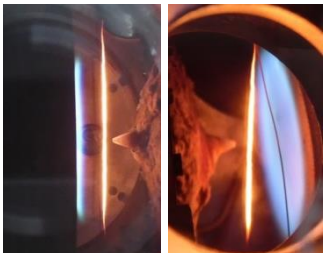

**Figure 1: The thermocouple is placed parallel to the flame.**

## Electrical compensation method
As can be seen in Figure 1, the thermocouple radiates an unneglectable amount of the received heat of the flame, implying that the measured temperature ($T_c$) is lower than the actual temperature ($T_g$) of the flame. Next to radiation losses, convection of the burning gas stream to the thermocouple increases the measured temperature. Losses by conduction are not accounted for. If the gain by convection and the losses by radiation are in steady state, the power balance over the wire can be written as Eq. 1

$$\pi h d\left(T_g - T_c\right) = \pi d \epsilon \sigma \left(T_c^{\,4} - T_0^{\,4}\right) \qquad (1)$$

Where $T_0$ is the temperature of the surroundings, d is the diameter of the thermocouple, $\epsilon$ is the emissivity of the thermocouple, $\sigma$ the Stefan-Boltzmann constant and h is the heat transfer coefficient for convection.
With the ECM the real temperature of the gas can be found experimentally in two steps [2]. The first step is defining the characteristic curve of the thermocouple in vacuum. Only radiation plays a role in vacuum and the convection term in Eq. 1 is zero. The temperature of the thermocouple is increased by the Joule effect and the power balance over the wire in steady state contains now a term for the radiation losses and the current to the second power ($I^2$) multiplied with the resistance of the wire (R) as a second term for the Joule effect (Eq. 2).

$$R\, I^2 = \pi d \epsilon \sigma \left(T_c^{\,4} - T_0^{\,4}\right) \qquad (2)$$

Secondly, the flame of interest, where convection is present, is assessed with the Joule effect measurements. The power balance over the wire now contains a Joule effect, a convection and a radiation term (Eq. 3).

$$R\, I^2 + \pi h d(T_g - T_c) = \pi d \epsilon \sigma \left(T_c^{\,4} - T_0^{\,4}\right) \qquad (3)$$

Correspondent author: stefvdam@vub.ac.be

At the intersection of Eq. 2 and 3 the measured temperature ($T_c$) equals the real temperature of the flame ($T_g$). So if the characteristic curve and the parallel curves obtained by Eq. 3 for different $T_c$ values are plotted, the correction for radiation losses can be found visually. $T_c$ is the temperature where the Joule effect term is zero ($I^2=0$) on the parallels from Eq. 3, and $T_g$ is the temperature found at the intersection of the parallels with the characteristic curve.
Experimental results for the ECM for different ethylene flames are shown in Figure 1. The default value for the argon dilution is set to 70.8 mole%, while the equivalence ratio ranges from 1.00 to 1.43. In addition, an ethylene flame with an equivalence ratio of 1.43 and an argon dilution of 59.2 mole% is also investigated. The characteristic curve is the same for every flame. However for different compositions of the flames, the slopes of the obtained parallel curves by Eq. 3 are different, indicating that the radiation losses between the flames differ. If the flame with an equivalence ratio of 1.43 and an argon dilution of 70.8 mole% is set as reference, an increase of 40K for the radiation losses at a measured temperature of 1167K is found if the equivalence ratio is decreased to 1.00. The opposite effect is found when the argon dilution is decreased, than the radiation losses decrease with 28K (Figure 2).

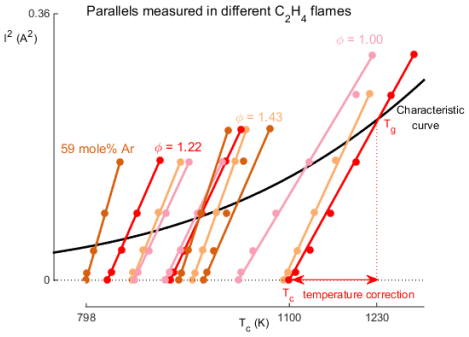


**Figure 2: When ECM is applied on ethylene flames with different composition, parallel curves with different slopes are found, indicating that the value for h and the radiation losses differ between the flames.**

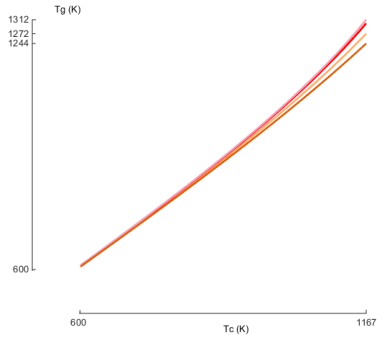


**Figure 3: Changing the composition of a flame can affect the radiation correction. Decreasing the equivalence ratio seems to increase the radiation losses, while decreasing the argon dilution seems to decrease the losses.**

The ECM method can not be used in flames where the starting temperature is already high, like for new types of biofuels, to avoid deterioration of the thermocouple. Therefore we suggest to solve the rate of heat transfer (Eq.1) expressed in the following form:

$$T_g = T_c + \frac{\epsilon\sigma\left(T_c^{\,4} - T_0^{\,4}\right)}{h} \qquad (4)$$

Three parameters, h, $\epsilon$ and $T_0$ from Eq. 4 are unknown. The $\epsilon$ of the thermocouple can be derived from the characteristic curve, while for $T_0$ a value of 320K is assumed. Finding a plausible value for h is more complex, since convection over a wire is depending on the composition of the gas stream, the diameter of the thermocouple, the pressure, the temperature and the velocity of the stream.
To assess the sensitivity of h to the parameters it is depending on, the ethylene flames with varying compositions mentioned before were assessed, focusing on finding the same value for h experimentally and by simulation. The experimental h values found for the different compositions, ranges between 63 and 200 W/m² K (Figure 4). By simulations values ranging from 116 to 258 W/m² K are found (Figure 5), which is the same order of magnitude as experimentally. Also the same effect of changing the composition is found. To improve the fit, further investigation is needed, focusing on the sensitivity of h for the different input parameters and uncertainties of the model.

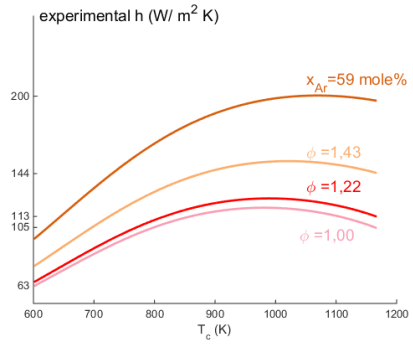


**Figure 4: h values found experimentally ranges from 63 to 200 W/m² K**

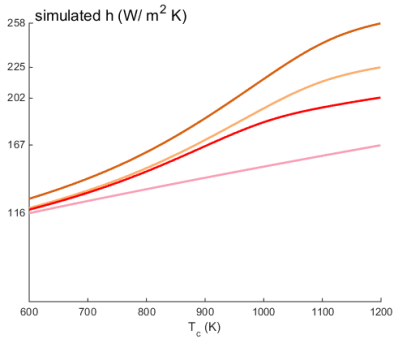


**Figure 5: By simulations higher values for h are found. Further investigation of the model is needed to improve the fit.**

**Acknowledgements**
The authors thank the Service Public de Wallonia (Belgium) for the financial support (Convention n°1250393). This project is also part of the IEA (International Energy Agency) Implementing Agreement for Energy Conservation and Emission Reduction in Combustion.

[1] P. Childs et al., "Review of temperature measurement", Rev. Sci Instrum. 71, 2959 (2000)
[2] U. Bonne et al.,"Messungen in der Reaktionzone von wasserstoff-sauerstoff und methane-sauerstoff Flammen," Z. Phys. Chem., 26, 93–110 (1960)

Correspondent author: stefvdam@vub.ac.be

# Biomass Gasification in a novel 50kW$_{th}$ Indirectly Heated Bubbling Fluidized Bed Steam Reformer

**Mara Del Grosso[a,b], Wiebren de Jong[a]**
[a]Technical University of Delft. Process and Energy Department. Leeghwaterstraat 39. 2628 CB Delft. The Netherlands
[b]M.delGrosso@tudelft.nl

In the global chase towards sustainability and cleaner ways of generating power, the utilization of biomass for clean energy conversion process has become increasingly interesting as biomass is potentially a $CO_2$-neutral energy source. Among the processes known to produce power, gasification represents an attractive and versatile technology to convert wide variety of biomass into product gas mainly composed by CO, $H_2$, $CO_2$, $H_2O$ and $CH_4$, that can be used for (combined) heat and power (CHP) production, transportation fuels and chemicals. For small to medium scale biomass gasification, fluidized bed technology is attractive: the process takes place in a bed of small particles fluidised by a suitable gasification medium and the very good gas-solid mixing ensures temperature uniformity through the bed and leads to an excellent mass and heat transfer.
In indirectly heated gasification, also known as second generation or allothermal gasification, the heat needed for the desired reactions is provided by ex-situ oxidation reactions and this leads to a higher quality product.

The project, which started in May 2016, is a four years Doctoral research project carried out at the Delft University of Technology (TUD), in the Netherlands and it is in cooperation with the company Petrogas Gas-Systems, based in Gouda. In particular, Petrogas Gas-Systems and the TU Delft Process & Energy section are designing, engineering, and commissioning a small 50 kW$_{th}$ Indirectly Heated Bubbling Fluidized Bed Steam Reformer (IHBFBSR) heated by two radiant tube burners placed vertically inside the reactor.

The aim of the work is to study how the use of this new concept of indirectly heating based on combustion, biomasses with different characteristics, various operating conditions and bed with different particle size affects the product gas yield and composition, the cold gas efficiency and, in particular, the carbon conversion.

During the work, an experimental study on the heat transfer of radiant tube burners as well as an experimental gasification campaign will be carried out. Moreover, a process modelling by using the flow sheeting software package Aspen Plus™ and a model of the heat transfer inside the radiant tube burners and the reactor by using the computational fluid dynamics software package Fluent™ will also be developed.

**Acknowledgments**
The authors would like to acknowledge Petrogas Gas-Systems for co-financing the project.

# Effect of dilution in an inter-turbine Flameless combustor

A.A.V. Perpignan and A.G. Rao

*Faculty of Aerospace Engineering, Delft University of Technology, The Netherlands*

A.A.V.Perpignan@tudelft.nl / A.GangoliRao@tudelft.nl

Alternatives to combustion in aircraft engines are not expected to become feasible in the decades to come. As the aviation traffic increases and regulations become more stringent, reduction in pollutant emissions are needed. The Flameless Combustion (FC) regime has been one of the promising candidates to achieve lower emissions in gas turbine engines. This combustion regime is characterized by well-distributed reactions, with low peak temperatures, resulting in lower emissions and acoustic oscillations. However, the attainment of the FC regime is not straight forward considering the conditions and requirements of gas turbines. Most of the previous combustor design attempts failed to provide broad operational range, high combustion efficiency, or were difficult to integrate in an engine.

Along with a novel aircraft concept, the European project AHEAD (Advanced Hybrid Engines for Aircraft Development) resulted in the conceptual design of a gas turbine engine with two sequential combustion chambers[1]. As the aircraft concept allows the use of cryogenic fuels, the first combustion chamber was designed to operate with hydrogen or natural gas. The second is the inter-turbine combustor herein studied, which would operate under the FC regime burning conventional fuels.

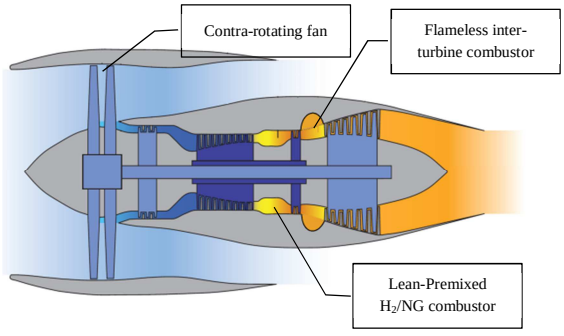


Figure 1 – Engine concept proposed along the AHEAD project[1].

As the incoming oxidizer in the inter-turbine combustor is the exhaust of the first combustor, temperatures would be high and oxygen concentration lower, helping the attainment of the FC regime. Furthermore, the power split between the two combustors would enhance the operational range.

After the conceptual design was accomplished[2], a scaled and simplified experimental combustor was built to assess the design and allow improvements. Instead of the full annular combustor, a 18 degree wedge was adopted, containing three fuel ports (Fig. 2). The fuel employed was methane, to simplify operation and subsequent computational simulations. Data on emissions was acquired for several levels of oxidizer dilution with nitrogen. Air and nitrogen were mixed and preheated to temperatures around 580 K.

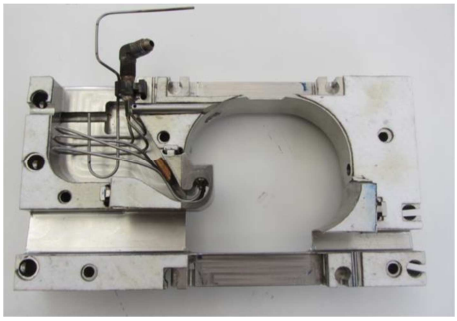

Figure 2 – Section of the proposed annular combustor used during the experiments.

The simulations here presented were performed in order to assess the use of CFD to improve the design of the combustor in relation to pollutant emissions. More specifically, the use of FGM (Flamelet Generate Manifolds)[3] along with RANS was investigated, since its computational cost is considerably lower than other models (as the Eddy Dissipation Concept and the Conditional Source Term Estimation). ANSYS Fluent® was employed while combustion was modelled using both adiabatic and non-adiabatic FGM. The manifolds were generated using the GRI 3.0 mechanism. FGM's progress variable was defined in function of $CO_2$ and CO mass fractions. Attempts using $H_2O$ did not provide better results. The $k$-$\varepsilon$ turbulence model was employed as tests using $k$-$\omega$ SST and Reynolds Stress turbulence models did not significantly change the results in terms of emissions. Along with the non-adiabatic approach, radiation was

taken into account using the Discrete Ordinates model. In some simulations, heat conduction through the walls was included by imposing an estimated outer wall temperature, as well as their thicknesses and thermal properties. The NOx emissions were predicted using transport equations for the mass fraction of NO, $N_2O$, $NH_3$ and HCN, with their source terms calculated via Thermal and Prompt NOx mechanisms.

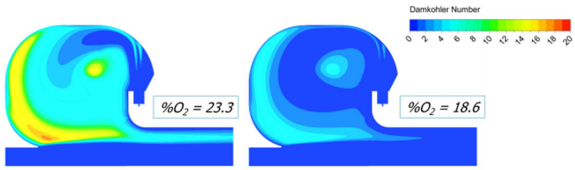


Figure 3 – Damköhler number contours in the mid-plane of the combustor for two different oxidizer compositions. Simulations including radiation modelling.

The computational mesh was refined until no relevant difference was spotted in the emissions and mid-plane fields results. The employed mesh was fully hexahedral and had 5.6 million nodes.

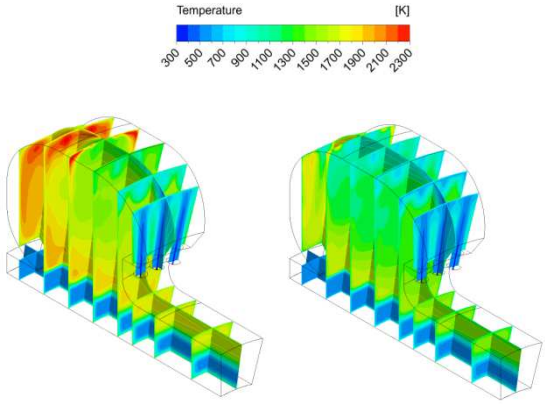


Figure 4 – Temperature contours for the case without nitrogen dilution (left) and with 100 l/min nitrogen addition to the oxidizer stream (right). Simulations including radiation modelling.

The cases simulated had different levels of $N_2$ dilution. The air (230 $l_n$/min) and fuel flows were constant. The case with no $N_2$ addition had global equivalence ratio of 0.2, taking into account both the dilution air and the combustion air that enters the chamber along with the fuel (in coflows).

Analysing Figs. 3 and 4, it is noticeable that dilution possibly shifts combustion to the FC regime, as temperature and Damköhler number drop. Interestingly, 60 $l_n$/min of $N_2$ addition (right hand side of Fig. 3) results in very low NOx emissions and further dilution is not advantageous (Fig. 5).

The computational modelling was able to predict the trend in both NOx and CO emissions with increasing amount of $N_2$ in the oxidizer stream. NOx emissions were very sensitive to the inclusion of radiation, especially for cases without $N_2$ or with little dilution. The peak temperatures in the combustor drop significantly with radiation.

Although the trend was captured, CO emissions were overpredicted. Possibly, such limitation could be overcome using a multi-stage FGM approach, as suggested by Göktolga et al.[4]. Using more than one progress variable could be the solution to have more accurate predictions.

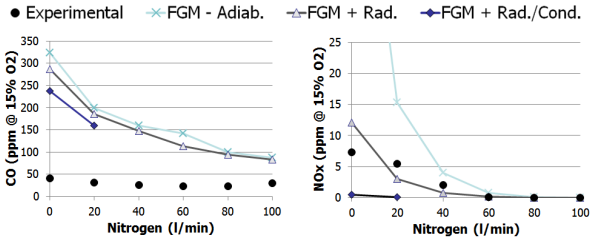


Figure 5 –CO and NOx emissions as function of nitrogen addition in the oxidizer stream.

When heat conduction through the walls was included, the predicted NOx emissions were too low. The discrepancy is attributed to the uncertainty in the estimated wall temperatures. No measurements were performed and the chosen values could be wrong.

Analysing the overall results, one can conclude that the set of models can be used to evaluate modifications and possible improvements in the inter-turbine combustion. However, this should be done carefully, as only the qualitative behaviour is replicated. The flow field analysis shows most of the reactions happen close to the combustor walls. Therefore, the large recirculation region designed to accommodate the highly distributed reactions is not performing as expected. Different fuel injection positions and directions shall be tested, as well as modified cavity geometries.

**References**

[1] Rao, A.G.; Yin, F.; van Buijtenen, J.P. *A hybrid engine concept for multi-fuel blended wing body.* Aircraft Engineering and Aerospace Technology: An International Journal 86 n. 6, 483-493, 2014.

[2] Levy, Y.; Erenburg, V.; Sherbaum, V.; Gaissinski, I. *Flameless oxidation combustor development for a sequential combustion hybrid turbofan engine.* Proceedings of ASME Turbo Expo, 2016.

[3] van Oijen, J.A.; de Goey, L.P.H. *Modelling of premixed laminar flames using Flamelet-Generated Manifolds.* Combustion Science and Technology 161, 113-137, 2000.

[4] Göktolga, M.U.; van Oijen, J.A.; de Goey, L.P.H. *Modeling MILD combustion using a novel multistage FGM method.* Proceedings of the Combustion Institute, 2016.

# High-Resolution True-Color Imaging of Reacting Sprays

*P.C. Bakker, Robin Doddema, Noud Maes and Nico Dam*
*Department of Mechanical Engineering, P.O. Box 513, 5600 MB Eindhoven*

The development of dedicated, scientific cameras has been primarily focused on fast response times, high sensitivity and well-known spectral sensitivity. The downside of these cameras is that they come at a high price tag, producing often gray-scale (intensity) image data and, when compared to modern day consumer cameras, their resolution (~1 megapixel) is rather low.

Consumer cameras offer true-color (RGB) images at high-resolution (~20 megapixel) at a low price (in the order of 1 k€, compared to around 50 k€ for scientific camera systems). Downside of these cameras is the long insertion delay (54 ms for the Nikon D7000 camera used), high jitter (0.5 ms) and limited minimum exposure time (0.125 ms).

Here, the goal is to create high-resolution true-color images of burning fuel sprays in the available optical setups.

A wired remote is adapted to create a trigger box that enables TTL control of a Nikon DSLR camera. With the internal delay of the camera known, the camera can be synchronized with repetitive processes, to take pictures at a pre-selected time. Two combustion events will be imaged: burning Diesel sprays in an optical engine and the pre-burn and subsequent Diesel spray in a constant volume vessel. We present four images for each system.

## Optical engine

This single cylinder, heavy-duty engine, with dimensions mimicking DAF production engines, is fitted with a quartz piston crown to allow optical accessibility of the combustion chamber. Fuel is introduced into the cylinder via an 8-hole injector using a double injection scheme, which explains the characteristic pattern in the images (A through D) in Figure 1 below.

- A: *Ignition of the pilot injection*. Short injection pulse just before top-dead-center, fuel ignites after the pilot injection has ended. Combustion remains within the piston bowl region.
- B: Spray-driven phase '*quasi-steady flame thrower*' of the main injection pulse, fuel is burning while injection is still ongoing.
- C: *End-of-injection combustion recession* is captured. Injection has ended, the tail of the fuel spray loses momentum and the flame progresses towards the injector nozzle.
- D: *burn-out phase*. After the end of the main injection, fuel remnants are burned and most of the formed soot will be oxidized.

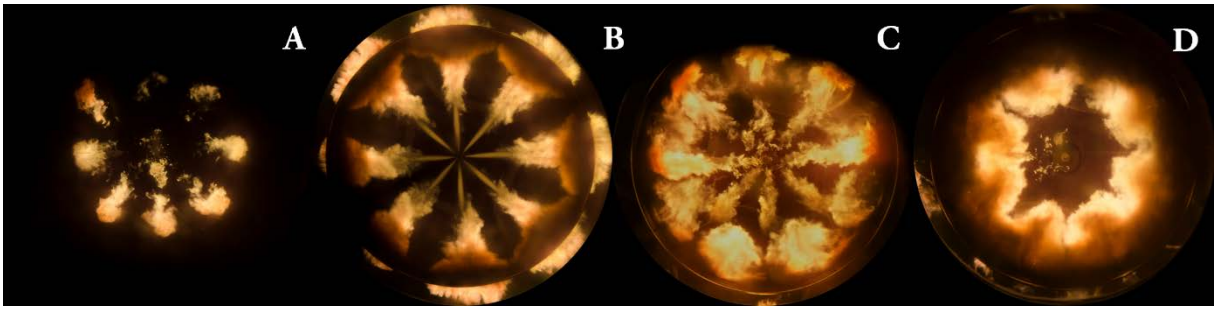


*Figure 1. Four example snapshots of a Diesel combustion event.*

## Eindhoven High-Pressure Cell

A constant-volume high-pressure spray vessel with a single-hole injector mounted to study (non-)reacting fuel sprays under engine-like conditions, without interference of moving parts or neighboring sprays. The desired thermodynamic conditions are created using a pre-burn approach, and after a relatively long cool-down period, a Diesel-like fuel is introduced into the vessel. Figure 2 depicts two snapshots capturing the pre-burn event and two shots visualizing the (igniting) Diesel spray.

- 1: Flame propagation in an acetylene/$O_2$/$N_2$ mixture during the early stage of the pre-burn event.
- 2: Soot formation during the final stage of the pre-burn (at high-pressure and high-temperature).
- 3: Ignition of the isolated fuel spray under engine-like pressure and temperature conditions (~60 bar and ~900 K, respectively).
- 4: "quasi-steady" matured Diesel spray.

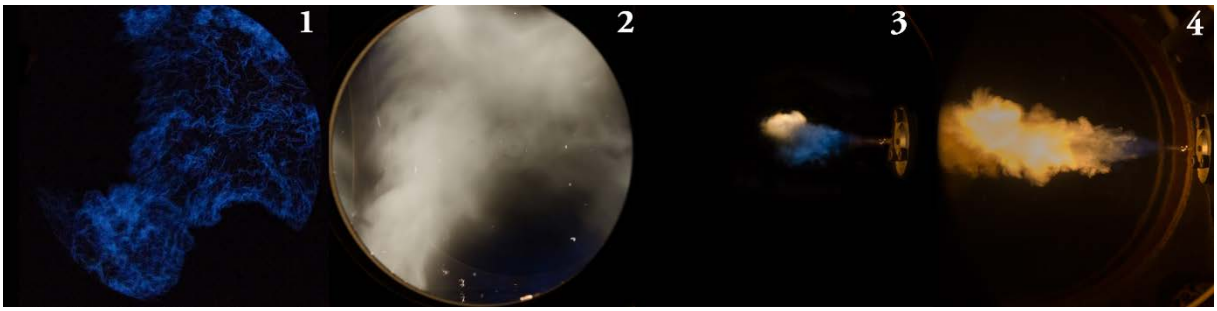


*Figure 2. Four photographs of the combustion event(s) in the Eindhoven High-Pressure Cell. Exposure and ISO were adjusted to capture the faint chemiluminescence (no. 1 and 3).*

**Unraveling the Obscurities of Soot Reduction by Post Injections**

*R. Dreezen, J. Vervaet, P.C. Bakker & R.C. Willems*

To comply with ever more stringent emission standards, new methods for emission reduction in conventional diesel combustion are being examined. A promising technique to reduce pollutant emission and potentially increase efficiency is the use of a post-injection, which is a relatively short injection pulse after the main injection. A substantial amount of research has already been conducted on this topic, however results are often contradictory and fundamental understanding of the effects of a post-injection is still lacking. The most pronounced effect of a post-injection, described in previous work, is the reduction of engine-out soot. O'Connor and Musculus [1] give three frequently used explanations:

- Enhanced mixing within the cylinder influencing the formation an oxidation process of soot
- Enhanced oxidation of soot by increased temperature
- Interruption in fuel-rich combustion, allowing oxidation of soot

### Metal engine approach

In the current work research on a heavy duty metal test engine is combined with efforts on an optically accessible engine to get a better insight in the effects of a post-injection.
The work on the metal engine focuses on engine-out emissions and efficiency over a variety of operating conditions and post-injection timing and quantity. Design of Experiments (DOE) is used to test a wide variety of operating points in a structured and efficient way. As a proof of concept concerning use of DOE and to set a baseline case, single injection tests where carried out were the response of emissions and efficiency to Start of Actuation (SOA), rail pressure, boost pressure and EGR rate were examined. This yielded models to predict emission and efficiency over a variety of operating conditions. An example is shown in Figure 1.

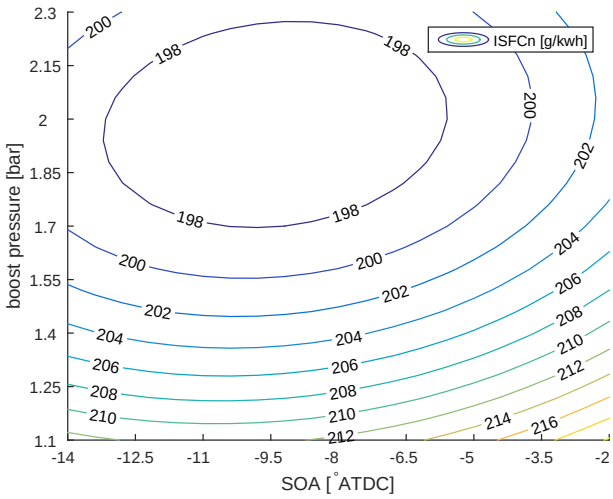


**Figure 1:** *ISFCn as function of boost pressure and SOA*

### Optical engine approach

Aside from the full metal engine experiments measurements on an optical engine are also performed. Optical measurement techniques such as Laser-Induced Incandescence (LII) have the main advantage of being able to measure *in situ*. Previous research validated the feasibility of high-speed LII [2]. However, the strong temperature dependencies of the LII signal ($\sim T^{14}$) complicates decent interpretation of the signal without any temperature information. Therefore, LII is combined with

the well-understood method of two color pyrometry. The ratio of the collected light at two distinct wavelengths can be related to a temperature. This is achieved by calculating a theoretical ratio for every temperature using both Planck's law and the detection equipment's transmission curve.
The engine used for these experiments is an optically accessible Ricardo Proteus single cylinder. Using a quartz piston crown and a 45° mirror allows for in-cylinder imaging. An image doubler projects the two differently filtered signals on a single chip to allow simultaneous collection of both wavelengths. A simplified overview of the detection setup can be seen in Figure 2 below.

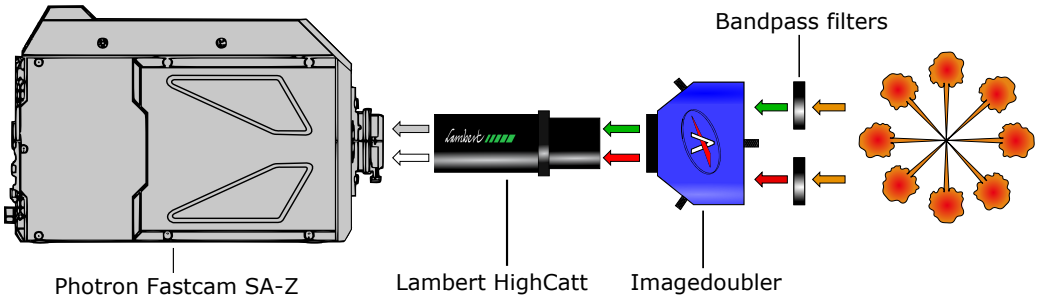


**Figure 2:** *Schematic overview of image detection setup.*

The collected images are matched spatially and a 2D temperature field is found and used to correct the signal. So far only natural luminosity experiments have been performed. From these experiments the bias of the signal towards higher temperatures becomes evident as can be seen in Figure 3. This figure shows one of the eight sprays at 9 [CAD] after top dead center.

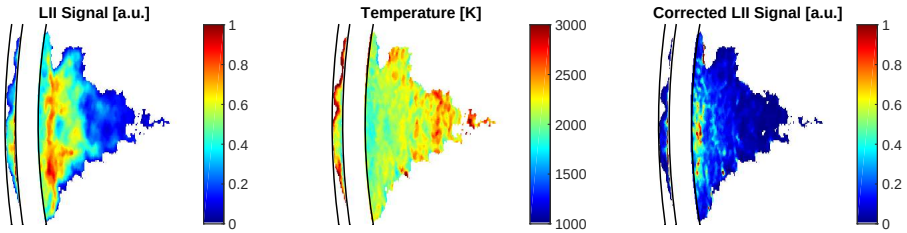


**Figure 3:** *Natural luminosity with the found temperature and the corrected signal.*

Although the preliminary results look promising for volume fraction estimation, it has to be noted that chemiluminescence and line of sight effects might influence the calculation [3]. During LII experiments these issues are bypassed and should therefore give more conclusive evidence.

## References

[1] J. O'Connor and M. Musculus. Post Injections for Soot Reduction in Diesel Engines: A Review of Current Understanding. *SAE International*, 2013.

[2] R. C. Willems. Shedding light on soot burnout in conventional diesel combustion by high-speed laser-induced incandescence imaging. Master's thesis, 2016.

[3] C. Mueller and G. Martin. Effects of oxygenated compounds on combustion and soot evolution in a di diesel engine:broadband natural luminosity imaging. *SAE International*, 2002.

# Alternative Use of FTIR for the Analysis of Industrial Gases Emission

I. V. Dyakov, B. Bergmans, S. Petitjean, F. Idczak

ISSeP, Institut Scientifique de Service Public, rue du Chéra 200, 4000 Liège, Belgium
Corresponding author: I. V Dyakov, email: i.dyakov@issep.be

Key words: FTIR, multicomponent gas mixtures, industrial stack emission

This study is dedicated to the evaluation of the potential of broadening the data conventionally characterized by the Standard Reference Methods (SRM) to the Fourier Transform Infrared Spectroscopy (FTIR), that have a wide measuring range of organic and inorganic species. The method FTIR is under enhancement to be considered as a reference method by a European standardization working group CEN/TC264/WG36. The presented study has a link to the integrated efforts of that group since the organization of ISSeP is involved in environmental of industrial emission monitoring.

The purpose of this work is to elaborate a measuring routine for different industrial sectors, to study the influence among different components of the exhaust in accordance with the gas matrix specifics to the industry; to determine the limit of detection and measurement uncertainty which can be reasonability achieved.

The field measurements were carried out at the stack of the biomass power plant using as fuel wood pellets and a large scale wood pellets and chips production facility. Tests have also been performed in a certified laboratory VITO where gas mixtures of known compositions were generated to verify the performance of the instrument.

Gasmet DX4000 FTIR analysers with complementary equipment including pump, heated lines and a probe have been used in the study. Either Horiba PG-300 Portable Gas Analyser or rack mounted setup consisted of analysers X-Stream Emerson for $SO_2$, ABB AO2020 for CO and $CO_2$ connected in series and X-Stream Emerson for $NO_x$ connected in parallel were used as SRM.. A dry sample technique was applied in each case.

As every FTIR instrument is unique due to the optics features, the measurements of two analysers were compared in this work. FTIR1 of that list is the instrument of ISSeP.

Series of measurements were carried at each industrial site. The uncertainty of measurements are assessed from records applying the following formula recommended in ISO 20988:

$$u = \sqrt{\frac{1}{2N}\sum_{j=1}^{N}(y(1,j) - y(2,j))^2} \qquad (1)$$

where: N – number of measurements; y(1,j) – measurement of a reference instrument; y(2,j)– measurement of a certain instrument or an average value of measurements of several instruments compared to the reference.

The values of those uncertainties are represented in Table 1 as the maximum, minimum and average emission values for every component.

The present results reasonably agree with those of Larjava et all. (1997) and Jaakkola et al; (1998). The uncertainty values are in general similar at different levels of concentration. Obviously they are more perceptible at lower concentrations. Several factors could cause those uncertainties. The systematic nature of uncertainties of different instruments attribute to the intrinsic properties of the devices' mechanics and optics. Spectral cross-interferences of the gas mixture components are also important in case of FTIR (Larjava et all., 1997).

The comparison of FTIR measurements with exact concentrations generated during the laboratory tests indicating some interference of $H_2O$, $CO_2$, CO and $NO_x$ are shown in Table 2. The instrument's software includes several options to correct those interferences and eliminate the systematic errors, though this work demonstrates the data obtained using original libraries and parameters provided by the supplier. The results for $H_2O$ and $CO_2$, abundant in the flue gases, have the uncertainties of less than 1% of absolute concentration. Very high absorptivity of those components in the infrared region facilitates the quantitative measurements.

Uncertainties found for CO, $NO_x$ and $SO_2$ measurements by different instruments can depend on various factors. Expectedly, carbon monoxide variations in the stack are higher than other components. Being mostly below 10 ppm, concentrations of this component occasionally produce sharp peaks of considerable amplitude influencing the overall uncertainty values since the difference of the response time of measuring devices on the sharp concentration changes. The $NO_x$ concentrations are represented as a sum of NO and $NO_2$ measured by FTIR instruments and direct measurements by SRM. The detection of these components could depend on the water and carbon dioxide interferences due to the large overlap of the spectra, as seen from the Table2. The detection of nitrogen oxide, a major constituent of $NO_x$, is hampered by its lower absorption coefficient. At the same time $H_2O$ and $CO_2$ could influence on the chemiluminescent measurements used as SRM for NO, due to some quenching effect, decreasing the apparent concentrations of nitrogen oxide (Larjava et all., 1997). All data for sulfur dioxide are in good agreement, the majority of measured concentrations usually at the level below 10 ppm.

During the measurements the discrepancies of the time steps produced by the equipment and the software are unavoidable. There could also be some difference in the above mentioned response time of the instruments. The errors associated with these discrepancies can become quite noticeable at lower concentrations. The formula (1)

originally appropriate for the identical measurements could be used anticipating occurrence of those variations. As seen from the Table 2 the results can vary with interferometer conditioning, which can be flushed with pure nitrogen or ambient air. The importance of this parameter increases at lower measured concentrations approaching the detection limits since it could affect the zero concentration levels.

Table 1. Uncertainties of measurements of flue gas components performed at different industrial sites.

| Component | $H_2O$, % | $CO_2$, dry % | CO, dry ppm | $NO_x$, dry ppm | $SO_2$, dry ppm |
|---|---|---|---|---|---|
| Production facility of wood pellets and chips | | | | | |
| max value | 20.4 | 12.8 | 269.5 | 207.5 | 167.0 |
| min value | 16.3 | 10.4 | 1.3 | 130.2 | 64.5 |
| Average emission | 18.1 | 11.4 | 7.7 | 175.6 | 91.7 |
| u, FTIR,SRM | - | 0.5 | 9.8 | 30.4 | 11.7 |
| Biomass power plant | | | | | |
| max value | 10.7 | 13.2 | 204 | 69 | 3 |
| min value | 7.5 | 9.3 | 3 | 45 | 1 |
| Average emission | 9.2 | 11.8 | 10 | 60 | 2 |
| u, all instruments | 0.3* | 0.2 | 10 | 1 | 1 |
| u, FTIR,SRM | - | 0.2 | 10 | 1 | 1 |

* Measurements between two FTIR instruments are compared

Table 2. FTIR measurements of generated in the laboratory conditions gas concentrations

| Component | | $H_2O$, % | $CO_2$, % dry | CO, ppm dry | NO, ppm dry | $NO_2$, ppm dry | $SO_2$, ppm dry |
|---|---|---|---|---|---|---|---|
| Interferometer flushed with pure Nitrogen | | | | | | | |
| Matrix1 | Real | 10.2 | 12.0 | 15 | 54 | 5 | 3 |
| | FTIR | 10.4 | 12.3 | 15 | 50 | 4 | 10 |
| Matrix2 | Real | 18.9 | 10.6 | 3 | 70 | 0 | 3 |
| | FTIR | 19.1 | 10.9 | 2 | 59 | 0 | 8 |
| Matrix2' | Real | 0.0 | 10.6 | 3 | 70 | 0 | 3 |
| | FTIR | 0.0 | 10.5 | 3 | 75 | 0 | 2 |
| Interferometer flushed with ambient air | | | | | | | |
| Matrix1 | Real | 10.2 | 12.0 | 15 | 54 | 5 | 3 |
| | FTIR | 10.4 | 12.4 | 15 | 51 | 5 | 8 |
| Matrix2 | Real | 18.9 | 10.6 | 3 | 70 | 0 | 3 |
| | FTIR | 19.1 | 10.9 | 2 | 61 | 0 | 6 |
| Matrix2' | Real | 0.0 | 10.6 | 3 | 70 | 0 | 3 |
| | FTIR | 0.0 | 10.6 | 3 | 76 | 0 | 2 |

**Conclusions** Measurements using FTIR analysers in comparison with SRM were carried out at the industrial sites and in the laboratory. The uncertainties of measurements determined using the recommendations of ISO 20988 have systematic feature caused by different factors to be taken into account. At lower concentrations the uncertainties of measurements become comparable with the measured values. Flushing the interferometer with nitrogen improves the results of measurements. The influence of water present in the sample on measured concentrations is observed. The results are in reasonable agreement with literature data.

**Acknowledgements** This work is supported by the Walloon Government through the Moerman REFGAZ project. R. Caillet, P. Krugel, T. Alleleyn, V. Wuestenbergs, F. Fernandez, G. Lenaerds, R. Brabers, J. Mertens, P. Rogiers, J. Annendijck are appreciated for their assistance during the experiments.

**References**

European standardization working group CEN / TC264 / WG36 http://fairmode.jrc.ec.europa.eu/

Larjava, K.T., Tormonen, K.E., Jaakkola, P.T. and Roos, A.A., 1997. Field measurements of flue gases from combustion of miscellaneous fuels using a low-resolution FTIR gas analyser. Journal of the Air & Waste Management Association, 47(12), pp.1284-1290.

Jaakkola, P.T., Vahlman, T.A., Roos, A.A., Saarinen, P.E. and Kauppinen, J.K., 1998. On-line analysis of stack gas composition by a low resolution FT-IR gas analyser. Water, Air, and Soil Pollution, 101(1-4), pp.79-92.

ISO 20988 Air quality -- Guidelines for estimating measurement uncertainty. http://www.iso.org

Calcmet manual. http://www.gasmet.com

# Numerical modeling of multi-component viscous fuels combustion

A.H. Mahmoudi[*1], A.K. Pozarlik[1], E. van der Weide[2], S.R.A. Kersten[3], S. Luding[4], G. Brem[1]

[1] Laboratory of Thermal Engineering, University of Twente
[2] Engineering Fluid Dynamics, University of Twente
[3] Sustainable Process Technology, University of Twente
[4] Multi Scale Mechanics, University of Twente
[*]University of Twente, P.O.Box 217, 7500 AE, Enschede, The Netherlands
a.mahmoudi@utwente.nl,

## Introduction

The worldwide concern regarding global warming has increased the interest of using biomass as a renewable and $CO_2$ neutral source of energy. Pyrolysis oil (PO), as one of the most important product of biomass conversion, has the potential to be used as a fuel oil substitute in many applications for heat and electricity generation. However, pyrolysis oil properties and its behavior during combustion are considerably different from conventional fossil fuels. From a chemical point of view, PO contains large number of oxygenated compounds derived from the decomposition of biomass during thermal treatment. It has also considerable amount of water originated from both moisture content and the decomposition reactions. Water is homogeneously dissolved in the oil and cannot be eliminated with drying processes without losing volatile hydrocarbon compounds [1]. From the physical point of view, bio-oils are characterized by high viscosity and surface tension, low heating value and, due to multicomponent composition, a very wide boiling range [2]. Moreover, they are thermally unstable and when heated, undergo polymerization processes, leading to the formation of carbonaceous solid material (char) in the fuel supply line, at the nozzle tip and in the combustion chamber [1]. Van Rossum et al. [3] found that pyrolysis oil evaporation is always coupled with the formation of char.
Literature survey indicates that combustion behavior of pyrolysis oil is still unknown process. More investigations is required to understand PO spray formation, evaporation and combustion. Especially, the impact of char formation on the combustion characteristics, which has been not yet explored, needs detailed assessment. Knowledge and data about the specifics of the processes and phenomena which interact during combustion of PO will support efficiency increase and design of new generation of burners operating on this bio-fuel.
The objective of this work is to investigate pyrolysis oil combustion, taking into account mutual interactions between gaseous, liquid and solid fields. A numerical model that takes into account liquid fuel evaporation and gaseous and char combustion has been developed in OpenFOAM. The char is considered to be present in the fuel droplets and its oxidation is modeled after complete evaporation of liquid.

## Modeling

A new numerical model for combustion of multicomponent and multiphase fuels has been implemented into the open source CFD package OpenFOAM with the Eulerian-Lagrangian formulation, where the gas phase is a continuous phase but each particle/droplet is tracked with a Lagrangian approach. A two way data exchange is applied between particles and gas phase which makes a strong coupling between Eulerian and Lagrangian domain. Each particle consist of two phases (liquid and solid), while it interacts with surrounding gas phase by heat, mass and momentum transfer. Due to small particle/droplet size and low Biot number, the intra-particle gradient of temperature and species is neglected. The coupling model describes the interaction between particles and environment through heat and mass transfer. Energy and mass are transferred from gas to particles and/or particles to gas phase as heat and mass source, respectively. A uniform droplet size of 50μm was applied.
Van Rossum et al. [3] observed that some amount of solid char is always produced during the evaporation of pyrolysis oil (8% - 30% on carbon basis). The amount of char formation is dependent on heating rate, where higher heating rates produce less char. However, the process of char formation inside the droplet is not well known. In this study, since the droplet size is relatively small, it has been assumed that there is constant amount of char in the particles, i.e. 10 wt.%. Phenol and water (25 wt.%, on liquid weight basis) are used as representative for pyrolysis oil.

## Results

Figure 1 presents the species and temperature distribution in the burner as a result of spray combustion of pyrolysis oil. As can be seen in Fig. 1a and 1b, phenol and water in the particles evaporate and go to the gas phase, while char remains in the particle. The remaining char undergoes heterogeneous reaction with oxygen. High temperature and enhanced $CO_2$ concentration downstream in the domain indicate char combustion. Phenol in the gas phase reacts with $O_2$ and produces $H_2O$ and $CO_2$. It is consumed totally before the char combustion is accomplished.

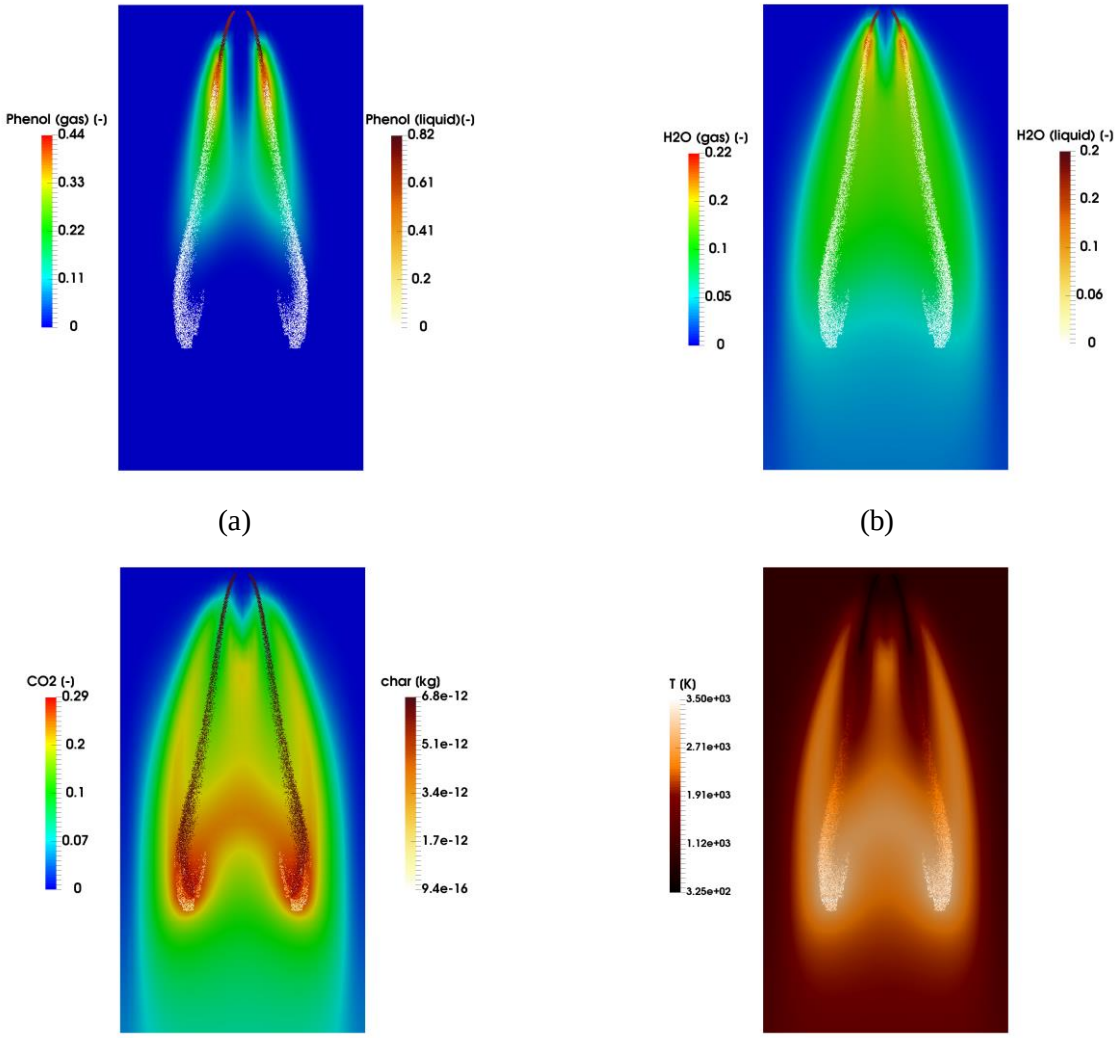


Figure1: Species and temperature distribution in spray combustion of phenol/water

## Conclusions

The research presents combustion of renewable multicomponent fuel. As a representative for pyrolysis oil droplets, a phenol/water blend containing 10 wt% of solid char was used. Further char formation inside the droplets, due to heat flux from the hot combustion environment was neglected. An Eulerian-Lagrangian transient simulation was performed in OpenFOAM code to study the effect of multicomponent fuel combustion on flame behavior. It was observed that presence of char in the fuel influences combustion process significantly. Char combustion downstream of the primary combustion region may result in combustion chamber fouling, walls overheating and combustion device life time reduction.

## Acknowledgement

The authors would like to thank the Science Based Engineering Institute of University of Twente for sponsoring this research.

## References

[1] J. D'Alessio, M. Lazzaro, P. Massoli, V. Moccia, Thermo-optical investigation of burning biomass pyrolysis oil droplets, Symposium (International) on Combustion 27 (1998) 1915–1922.
[2] C. Branca, C. D. Blasi, R. Elefante, Devolatilization and heterogeneous combustion of wood fast pyrolysis oils, Industrial and Engineering Chemistry Research 44 (2005) 799–810.
[3] G. van Rossum, B. M. Guell, R. P. B. Ramachandran, K. Seshan, L. Lefferts, W. P. M. V. Swaaij, S. R. A. Kersten, Evaporation of pyrolysis oil: Product distribution and residue char analysis, AIChE Journal 56 (2010) 2200–2210.

# Heat2Control

## Modeling of Split-injection Spray-A Case from ECN with FGM in OpenFOAM

B. Akkurt, L.M.T. Somers, N.G. Deen
Technische Universiteit Eindhoven
b.akkurt@tue.nl

**Abstract**

Diesel like combustion is mostly preferred for the internal combustion engines due to its efficiency. However, it has several drawbacks at which emissions are one of them. Reducing emissions down while keeping the efficiency high is a tough task to cope with. In this respect, multi-phase injection studies are performed in order to control the combustion since diesel combustion is mostly a mixing controlled process. In this project, nominal condition for the double injection Spray-A case from Engine Combustion Network (ECN) is modelled with Flamelet-Generated-Manifold (FGM) in OpenFOAM computational fluid dynamics (CFD) tool with Reynolds Averaged Navier-Stokes (RANS) turbulence model to validate the solver code that will be used for engine applications later on. FGM is an efficient chemistry reduction method, which holds good accuracy while keeping the computational power lower compared to the other reduction methods for chemical kinetics, shown in Figure 1. The solver code for OpenFOAM is from Lib-ICE library (Lucchini, 2013). FGM method is implemented into the OpenFOAM solver since the original solver utilizes Tabulation of Dynamic Adaptive Chemistry (TDAC) method for chemical kinetics. TDAC solves transport equations for chemical kinetics online; therefore it's limited to chemical reaction mechanisms with 50-species and 100-reactions whilst FGM method is suitable for larger reaction mechanisms since the chemistry is decoupled from the flow field.

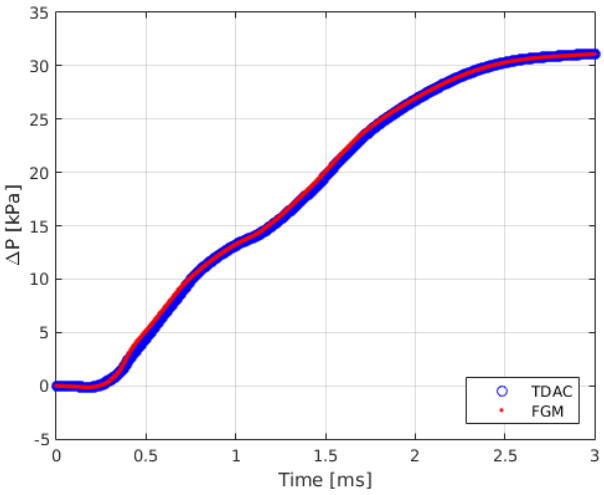


*Figure 1. Comparison of the rises in average pressure between TDAC and FGM chemistry reduction methods for double injection Spray-A case (Skeen, 2015) from ECN*

FGM look-up table stores sources terms for transport equations and thermophysical variables that are required for transport equations with respect to user-defined controlling variables. Besides, selected species can be stored in the look-up table to be retrieved with respect to the controlling variables. Furthermore, thermophysical properties are updated with the virtual-fuel approach. In this respect, a linear system is solved to evaluate virtual species mass fractions by satisfying the conservation of energy, mixture properties, and elemental masses, as shown in Figure 2.

This approach improves the computational time significantly, 30 times faster for each CFD simulation of 3 [ms], compared to the original OpenFOAM solver code with TDAC and provides comparable results.

$$[A] = \begin{bmatrix} \frac{h_1}{H_{tot}} & \frac{h_2}{H_{tot}} & \frac{h_3}{H_{tot}} & \frac{h_4}{H_{tot}} & \frac{h_5}{H_{tot}} & \frac{h_6}{H_{tot}} & \frac{h_7}{H_{tot}} \\ \frac{c_{p,1}}{C_p} & \frac{c_{p,2}}{C_p} & \frac{c_{p,3}}{C_p} & \frac{c_{p,4}}{C_p} & \frac{c_{p,5}}{C_p} & \frac{c_{p,6}}{C_p} & \frac{c_{p,7}}{C_p} \\ \frac{R_{g,1}}{C_p} & \frac{R_{g,2}}{C_p} & \frac{R_{g,3}}{C_p} & \frac{R_{g,4}}{C_p} & \frac{R_{g,5}}{C_p} & \frac{R_{g,6}}{C_p} & \frac{R_{g,7}}{C_p} \\ C_1 & C_2 & C_3 & C_4 & C_5 & C_6 & C_7 \\ H_1 & H_2 & H_3 & H_4 & H_5 & H_6 & H_7 \\ O_1 & O_2 & O_3 & O_4 & O_5 & O_6 & O_7 \\ N_1 & N_2 & N_3 & N_4 & N_5 & N_6 & N_7 \end{bmatrix} \quad x = \begin{bmatrix} C_{12}H_{26} \\ CO_2 \\ H_2O \\ O_2 \\ N_2 \\ CO \\ H_2 \end{bmatrix} \quad b = \begin{bmatrix} 1 \\ 1 \\ \frac{R_{g,tot}}{C_p} \\ C_{tot} \\ H_{tot} \\ O_{tot} \\ N_{tot} \end{bmatrix}$$

*Figure 2. Linear system that is solved to evaluate the virtual species mass fractions*

Figure 3 shows the chemistry effects on ignition and lift-off length for both injections that are computed in CFD simulations with respect to the different chemical reaction mechanism, which are for n-dodecane surrogate fuel. The smallest mechanism (Yao, 2015) in terms of the number of species gives comparable results for ignition delays and lift-off lengths with respect to the experimental results, (Skeen, 2015).

| | Narayanaswamy | Luo | OH-star | Yao | Experiment | |
|---|---|---|---|---|---|---|
| **Species [-]** | 369 | 106 | 257 | 54 | - | |
| **Liquid Length 1 [mm]** | 10.7/9.4 | 10.9/9.5 | 10.7/9.4 | 10.9/9.6 | - | **max/mean** |
| **Liquid Length 2 [mm]** | 12.2/9.7 | 14.0/9.9 | 11.1/9.7 | 13.8/10.1 | ~10 | **max/mean** |
| **Ignition Delay 1st [ms]** | 0.730 | 0.684 | 0.741 | 0.343 | 0.33 ± 0.03 | **dP = 3 kPA** |
| **Ignition Delay 1st [ms]** | 0.744 | 0.713 | 0.727 | 0.405 | - | **OH_max = 2%** |
| **Ignition Delay 2nd [ms]** | 0.378 | 0.411 | 0.366 | 0.138 | 0.17 ± 0.01 | **aROHR = 20%** |
| **LOL 1 [mm]** | 27.66 | 27.23 | 26.81 | 15.82 | ~15 | |
| **LOL 2 [mm]** | 26.81 | 26.81 | 26.40 | 12.19 | ~13 | |

*Figure 3. Comparison of the CFD results for different reaction mechanisms for split injection of 0.5ms / 0.5ms dwell / 0.5ms profile*

**References**


Lucchini, T., D'Errico, G. (2013). Diesel spray simulations using OpenFOAM and Lib-ICE. *Politecnico di Milano, Department of Energy, Internal Combustion Engine Group.*

Skeen, S., Manin, J., and Pickett, L. (2015). Visualization of Ignition Processes in High-Pressure Sprays with Multiple Injections of n-Dodecane. *SAE Int. J. Engines 8*(2):696-715, 2015, doi: 10.4271/2015-01-0799

Yao, T., Pei, Y., Zhong, B-J., Som, S., Lu, T. (2015). A hybrid mechanism for n-dodecane combustion with optimized low-temperature chemistry. *9th U.S. National Combustion Meeting, May 17-20, 2015*, Cincinnati, Ohio.

# Numerical Study on Diesel Spray Combustion Characteristics: LES of Spray-A using Flamelet Generated Manifold

H.Y. Akargun*, L.M.T. Somers, N.G. Deen
*Corresponding author: h.y.akargun@tue.nl

Improving the efficiency of Diesel engine while meeting low-emission regulations is one of the biggest challenge of the engine manufacturers. In that aspect, Computational Fluid Dynamics (CFD) modeling for the modern compression ignition engine conditions is of great interest due to its ability to provide information about combustion that cannot be obtained by even the most advanced experimental techniques. Solving Reynolds-averaged Navier-Stokes (RANS) equations is one of the approaches to simulate these conditions. While it is extensively used for engine optimization and provides averaged field data with low computational cost; it has lower accuracy, especially for emissions, compared to more advanced Large-Eddy Simulation (LES).

In this study, LES in conjunction with a chemistry tabulation method used to understand two-phase turbulent combustion characteristics by focusing on the so-called spray A conditions [1]. Chemistry tabulation method used in this study is the Flamelet Generated Manifold (FGM), which is developed by van Oijen [2]. Numerical framework of the LES-FGM approach is shown in Figure.1. In this framework, detailed simulations of the representative 1D flames are performed and then the combustion information is tabulated as a function of controlling variables which are mainly mixture fraction and progress of the combustion. As a result; in the CFD part, rather than solving detailed chemistry equations, only the controlling variables are transported in addition to the flow equations.

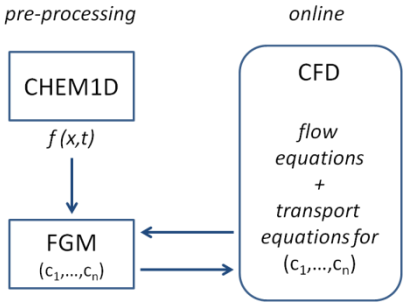


Figure.1 - CFD-FGM interaction

The discussion includes an evaluation of the performance of the models to predict the most relevant reacting spray macro-parameters, which are the ignition delay and lift-off length (Figure.2). This is followed by the description of the temporal evolution and localization of key species during auto-ignition and flame stabilization in spatial coordinates (Figure.3) and in the mixture fraction-progress variable space.

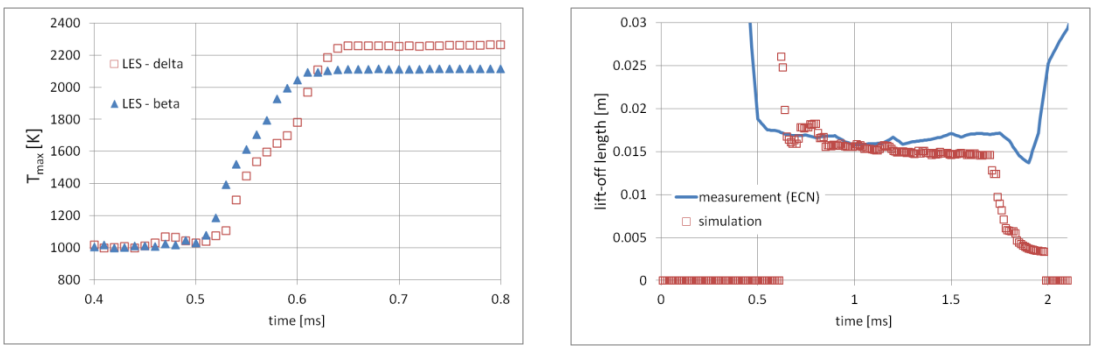


Figure.2 - Maximum temperature (left) and lift-off length (right) as function of time

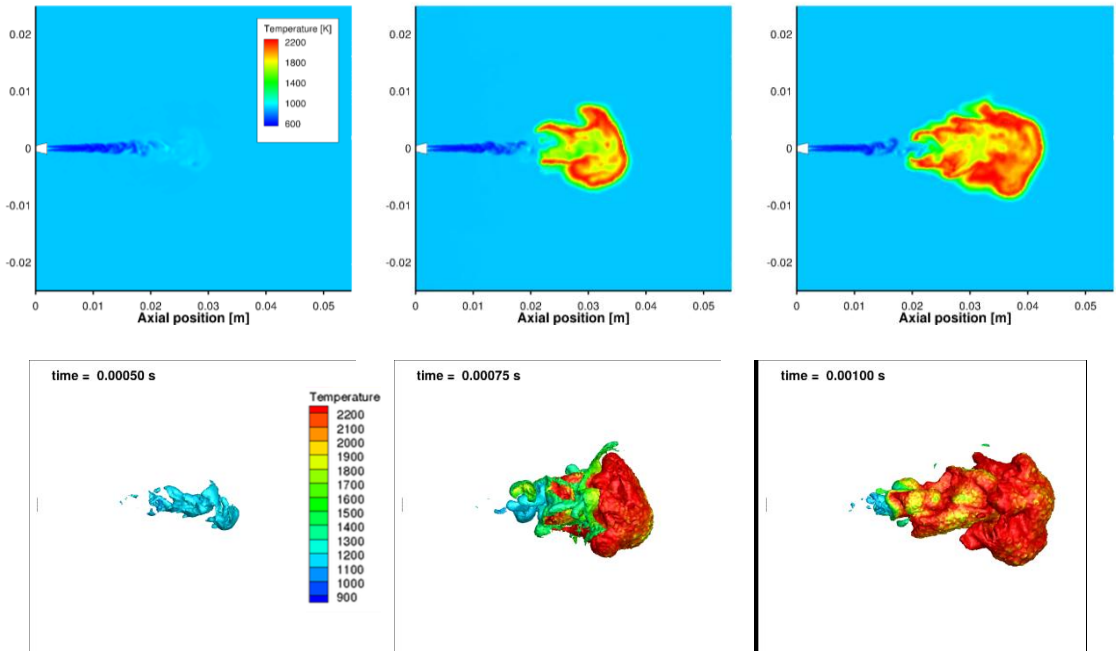


Figure.3 - Contour slice of temperature (top) and isosurface of carbon monoxide at 10% of its maximum mass fraction colored by temperature (bottom) at different times (left to right: 0.5, 0.75, 1.0 ms)

## References

[1] Engine Combustion Network (ECN). "Spray A" Operating Condition, September 2016. URL http://www.sandia.gov/ecn/cvdata/targetCondition/sprayA.php

[2] van Oijen, J.A., de Goey, L.P.H. (2000) "Modelling of Premixed Laminar Flames using Flamelet-Generated Manifolds". Combustion Science and Technology, 161(1):113–137

# Validation of Standard and Extended Eddy Dissipation Concept Model for the Delft Jet-in Hot Coflow (DJHC) Flame

H. Bao*, X. Huang, D.J.E.M. Roekaerts

*Department of Process and Energy, Delft University of Technology, The Netherlands*

*H.Bao@student.tudelft.nl

The Delft Jet-in Hot Coflow (DJHC) burner is used to investigate flameless combustion by imitating the recirculation flow characteristics appearing in a real complex furnace via a hot diluted coflow[1]. A well-defined stream of high temperature, low oxygen concentration combustion products is injected around the fuel jet as oxidizer in order to obtain 'Moderate and Intense Low-oxygen Dilution (MILD)' combustion conditions. For a range of jet and coflow conditions detailed experiments were made [2] and also several numerical validation studies, see e.g. [4,5]. The Eddy Dissipation Concept (EDC) model for turbulence chemistry interaction modeling has been widely used for modeling MILD combustion. EDC is providing a closure for the mean chemical source term based on a proposed microstructure of the reacting flow following from energy cascade concepts. It assumes that chemical reactions can only happen in the smallest eddies, whose size are of the same order of magnitude as the Kolmogorov scales, the so-called fine structures. Thus, the fraction of fine structure $\gamma^*$ and mean residence time $\tau^*$ (the reciprocal of it denotes the mass exchange between reactants inside fine structure and the surrounding) are necessary for EDC simulation. They are related to turbulent kinetic energy $k$ and eddy dissipation rate $\varepsilon$ (which are calculated from turbulent models) via two constants $C_{D1}$ and $C_{D2}$. It has been confirmed that $\varepsilon = 2C_{D1}u^{*3}/L^* = 4C_{D2}u^{*2}/3L^{*2}$.

It has been found that the standard EDC model tends to predict too early ignition and too high peak temperature for the JHC systems [3,4]. But by a global change of a model constant ('residence time scale' $C_\tau$) from its original value 2.1377 to the value 3 too early ignition can be avoided [5-7] and better predictions were obtained. Recently, Parente et al. [8] published an extension of the EDC model containing position dependent values of model constants, depending on a turbulent Reynolds number and a Damköhler number. In standard EDC, Kolmogorov scales are used as fine structure characteristics. However, due to "distributed" reaction zone and thus reduced temperature and species gradients in MILD conditions, the relevant characteristics $\gamma^*$ and $\tau^*$ can be different. In the extended EDC model the assumption of reaction zones as small scale eddies of the Kolmogorov length scale $\eta = (\nu^3/\varepsilon)^{1/4}$ is kept. But the velocity scale is replaced by the turbulent flame speed $S_T = S_L\sqrt{Re_T + 1}$, where $S_L$ is the laminar flame speed and the Reynolds number $Re_T$ is only related to fluid motion properties ($Re_T = k^2/\nu\varepsilon$). Defining the chemical time scale as the time needed to traverse the fine structure with the laminar flame speed $S_L$, a Damköhler number based on the fine structure time scale and the chemical time scale can be defined and after some derivation two adjusted fluid motion based model constants are obtained:

$$C_\tau = \frac{1}{2}\frac{1}{\sqrt{Re_T+1}Da} \quad (1)$$

$$C_\gamma = [\frac{3}{2}(Re_T + 1)]^{1/2}Da^{3/4} \quad (2)$$

where $C_\tau$ and $C_\gamma$ denote residence time constant and fine structure volume constant, respectively. Compared to Parente et al. [8] the exponent of *Da* has increased from ½ to ¾ by taking into account that the time scale needed to cross the small scale structure is not identical to the time scale needed to traverse the laminar flame thickness. In the EDC model the fine scale structures react as plug flow reactor over the Kolmogorov time and the mixing with the surroundings is controlled by the large scale turbulence time. The chemical time scale used in *Da* is derived from a one step mechanism [9]. A comparison of standard EDC, global modified EDC constants based on experimental data and extended EDC model are shown below. The new extended EDC model shows better agreement with the experimental data.

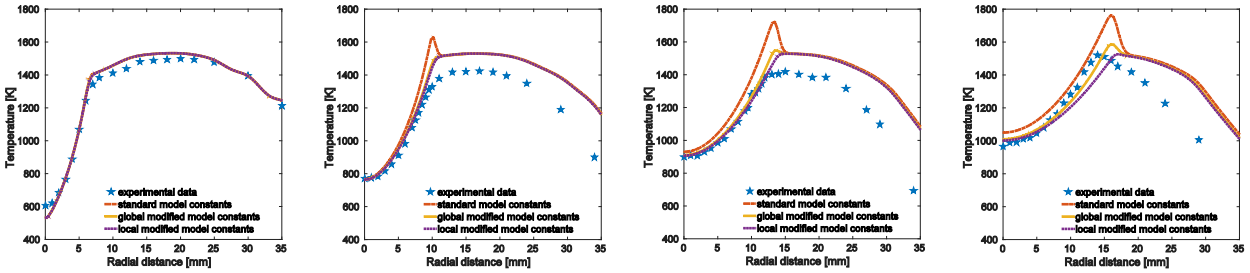


(a) Height 30 mm (b) Height 60 mm (c) Height 90 mm (d) Height 120 mm

Fig. 1. Measurements and EDC model predictions of mean temperature at different heights

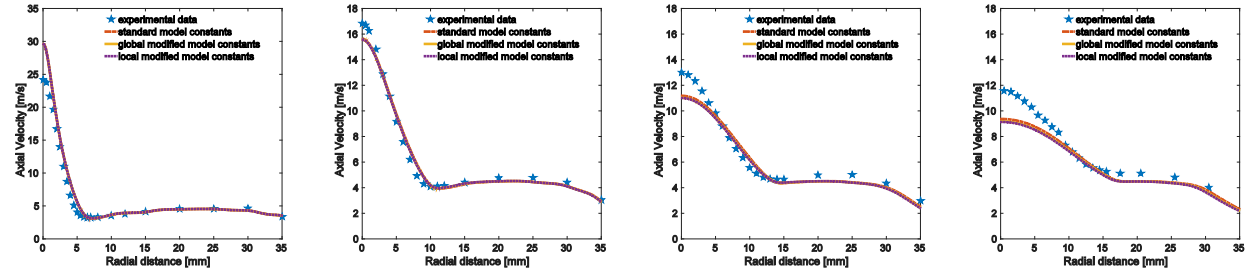


(a) Height 30 mm (b) Height 60 mm (c) Height 90 mm (d) Height 120 mm

Fig. 2. Measurements and EDC model predictions of mean axial velocity at different heights

The overestimation of peak temperature is reduced significantly in the case of the extended EDC model, especially for further downstream area. The temperature on the axis is also in better agreement with experiment. It should be pointed out that different EDC models do not change the fluid field a lot, which respects to the concept that fluid motion dominates the reaction zones, only standard EDC model shows slightly difference.

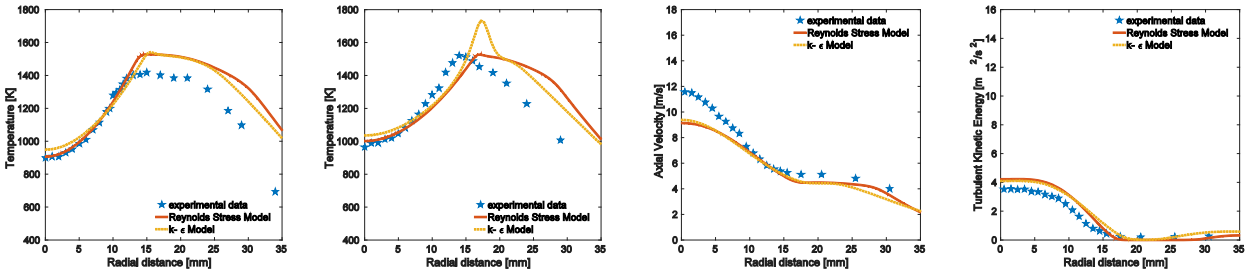


(a) Height 90 mm (b) Height 120 mm (c) Height 120 mm (d) Height 120 mm

Fig. 3. Turbulence model effect

The effect of turbulence model has also been investigated. It has been found that using the standard $k-\varepsilon$ model the temperature peak is more overpredicted than using the Reynolds Stress Model (RSM). The prediction of the flow field (mixing) around the momentum shear layer is sensitive to the choice of turbulence model.

**References**

[1] Oldenhof E, Tummers M J, Van Veen E H, et al. Combustion and Flame, 2011, 158(8): 1553-1563.
[2] Oldenhof E, Tummers M J, Van Veen E H, et al. Combustion and Flame, 2010, 157(6): 1167-1178.
[3] Aminian J, Galletti C, Shahhosseini S, et al. Applied Thermal Engineering, 2011, 31(16): 3287-3300.
[4] Sarras G, Mahmoudi Y, Arteaga Mendez LD et al. Turbulence and Combustion, 2014, 93(4): 607-635.
[5] De A, Oldenhof E, Sathiah P, et al. Flow, Turbulence and Combustion, 2011, 87(4): 537-567.
[6] Evans M J, Medwell P R, Tian Z F. Combustion Science and Technology, 2015, 187(7): 1093-1109.
[7] Wang F, Li P, Mi J, et al. International journal of hydrogen energy, 2015, 40(46): 16634-16648.
[8] Parente A, Malik M R, Contino F, et al. Fuel, 2016, 163: 98-111.
[9] Westbrook C K, Dryer F L. Progress in Energy and Combustion Science, 1984, 10(1): 1-57.

# Investigating the effects of a heat exchanger on the thermoacoustics in a Rijke tube

Naseh Hosseini[1,2,*], Viktor Kornilov[1], O.J. Teerling[2], Ines Lopez Arteaga[1,3] and L. P. H. de Goey[1]

[1] Eindhoven University of Technology, Mechanical Engineering Department, Eindhoven, the Netherlands.
[2] Bekaert Combustion Technology B.V., Assen, the Netherlands.
[3] KTH Royal Institute of Technology, Department of Aeronautical and Vehicle Engineering, Stockholm, Sweden
[*] E-mail: n.hosseini@tue.nl

**Abstract**
The goal of the present work is to investigate the effects of a heat exchanger on the instabilities in a Rijke tube. The motivation is the experimentally observed fact that the presence of the heat exchanger in a practical boiler changes the acoustics of the system. While the interactions between acoustic waves and premixed flames have been well studied in the literature, the thermoacoustic effects of the heat exchanger as a heat sink has mainly been ignored. In this study, we strive to reveal these effects on the stability of the system. This is achieved using a Helmholtz solver for modeling thermoacoustics in a Rijke tube including a heat source and a heat sink. We perform a parametric study on the interaction indices and time delays of the elements. The chosen values are then refined based on previous CFD calculations for a more detailed analysis. The results demonstrate that the heat sink can enhance as well as suppress the instabilities. Therefore, it is of utmost importance to study the thermoacoustics of both elements together to have a correct prediction of the system stability.

**Introduction**
Many researchers have investigated the thermoacoustic instabilities in lean premixed systems focusing on characterizing flame transfer functions for various types of flames [1-4]. While the interactions between acoustic waves and premixed flames have been well studied in the literature, the thermoacoustic effects of the heat exchanger as a heat sink has mainly been ignored. In this study, we strive to reveal these effects on the stability of the system. This is achieved using a Helmholtz solver for modeling thermoacoustics in a Rijke tube including a heat source and a heat sink. The chosen values for thermoacoustic properties of the elements are based on previous CFD calculations of a simplified setup comprising of wedge shaped (2D) premixed flames with cylindrical heat exchanger tubes placed downstream the flames [5]. This configuration is practically relevant as it is representative for the design of a majority of boilers and is composed of relatively simple elements that have been intensively studied separately [6-8].

**Rijke Tube Model**
An illustration of the Rijke tube with its dimensions is shown in Figure 1. The tube length is 1m and the heat source and sink are located at X=0.25 and 0.75m, respectively.

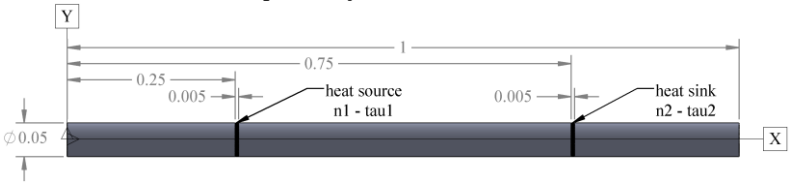


Figure 1. The Rijke tube model.

The Helmholtz solver COMSOL was used to calculate the eigenfrequencies and corresponding growth rates of the system. The heat source and sink were modeled by an interaction index, n, and a time delay, $\tau$, using the methodology described in [9]. We use subscripts 1 and 2 for the properties of the heat source and sink, respectively. The parametric study was performed for $0 \leq n \leq 1$ and $0 \leq \tau \leq 3$ms for both elements. The effects of the mean flow and temperature variations are neglected in order to make the analysis simpler and isolate the effects of other parameters.

**Results and Discussion**
Figure 2 shows the eigenfrequencies and corresponding growth rates for varying $\tau_1$ and $\tau_2$ between 0 and 3ms when $n_1=n_2=1$. The eigenfrequency predominantly decreases with an increase in any of the time delays. For $\tau_1<2$ms, maximum growth rate occurs for $\tau_2=0.5$ms, with a large deviation from $\tau_2=0$ms. This is specifically interesting because previous CFD simulations have revealed that the interaction index and time delay of a tube heat exchanger is much smaller than that of flames [5]. It can be seen in Figure 2 that smaller values of $\tau_2$ are even more critical than larger ones. Therefore, further analysis was made for $0 \leq \tau_2 \leq 0.5$ms and the results are plotted in Figure 3.

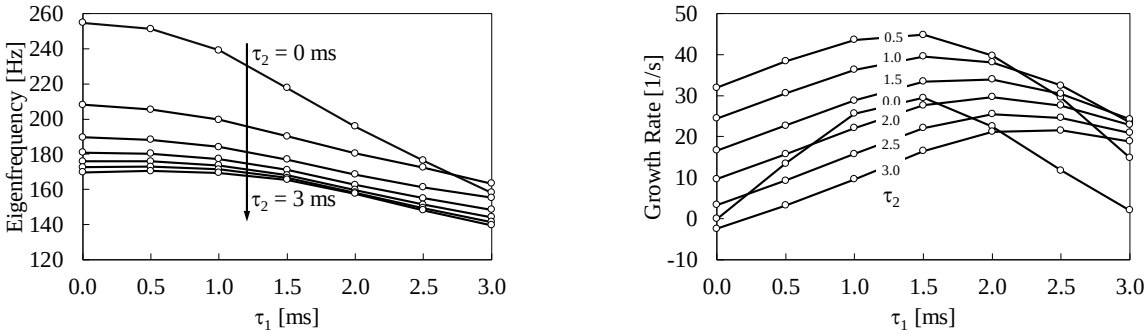


Figure 2. Eigenfrequencies and corresponding growth rates for $0 \leq \tau_1 \leq 3$ms and $0 \leq \tau_2 \leq$ms when $n_1=n_2=1$.

Figure 3 illustrates the eigenfrequencies and corresponding growth rates for $0 \leq n_2 \leq 1$ and $0 \leq \tau_2 \leq 0.5$ms when $n_1=1$ and $t_1=1$ms. The results show that as long as $n_2$ is not zero, any increase in the time delay of the heat sink (in the specified limits), increases the system instability. The same analysis for other values of $\tau_1$, or further increase in $\tau_2$ will result in local maxima which should be investigated per case and are beyond the scope this short communication. However, more detailed results will be orally presented.

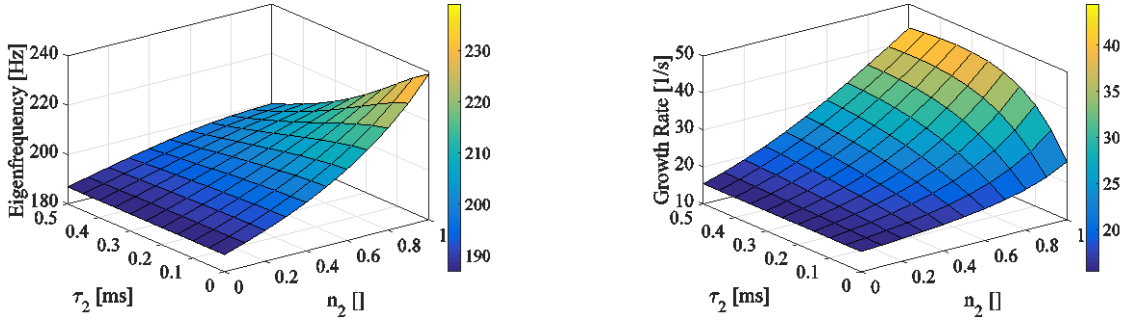


Figure 3. Eigenfrequencies and corresponding growth rates for $0 \leq n_2 \leq 1$ and $0 \leq \tau_2 \leq 0.5$ms when $n_1=1$ and $\tau_1=1$ms.

These results demonstrate that the heat sink can enhance as well as suppress the instabilities. Therefore, it is of utmost importance to study the thermoacoustics of both elements together to have a correct prediction of the system stability.

**Acknowledgement**

The presented work is part of the Marie Curie Initial Training Network, Thermo-acoustic and Aero-acoustic Nonlinearities in Green combustors with Orifice structures (TANGO). We gratefully acknowledge the financial support from the European Commission under call FP7-PEOPLE-ITN-2012.

**References**

[1] Kornilov, V., Experimental research of acoustically perturbed Bunsen flames, Doctor of Philosophy Thesis, Eindhoven University of Technology, (2006).

[2] de Goey, L. P. H., ten Thije Boonkkamp, J. H. M. and Kornilov, V., Premixed laminar flame modeling for thermo-acoustics, Advances in aero-acoustics and thermo-acoustics - Von Karman Institute lecture notes, 1, (2001).

[3] Jaensch, S., Emmert, T., Silva, C. F. and Polifke, W., A Grey-box identification approach for thermoacoustic network models, Proceedings of the ASME Turbo Expo, Düsseldorf, Germany, (2014).

[4] Sattelmayer, T. and Polifke, W., A novel method for the computation of the linear stability of combustors, Combustion Science and Technology, 175(3), 477–497, (2003).

[5] Hosseini, N., Kornilov, V., Teerling, O. J., Lopez Arteaga, I. and de Goey, L. P. H., Transfer function calculations of segregated elements in a simplified slit burner with heat exchanger, Proceedings of the 22nd International Congress on Sound and Vibration, Florence, Italy, (2015).

[6] T. C. Lieuwen, Modeling premixed combustion-acoustic wave interactions: a review, Journal of Propulsion and Power, 19(5), 765–781, (2003).

[7] V. Kornilov, R. Rook, J. ten Thije Boonkkamp, and L. P. H. de Goey, Experimental and numerical investigation of the acoustic response of multi-slit Bunsen burners, Combustion and Flame, 156(10), 1957–1970, (2009).

[8] F. Selimefendigil, S. Föller, and W. Polifke, Nonlinear identification of unsteady heat transfer of a cylinder in pulsating cross flow, Computers and Fluids, 53, 1–14, (2012).

[9] Hoeijmakers, P. G. M., Flame-acoustic coupling in combustion instabilities, Doctor of Philosophy Thesis, Eindhoven University of Technology, (2014).

# Comparative study of RANS-EDC, LES-CSE and LES-FGM simulations of Delft jet-in-hot-coflow (DJHC) natural gas flames

D.J.E.M. Roekaerts[1,2,*], H. Bao[1], X. Huang[1], A. Vasavan[2], J.A. van Oijen[2], J. Labahn[3], C. Devaud[3]

*1. Department of Process and Energy, Delft University of Technology, The Netherlands*

*2. Multiphase and Reacting Flows, Eindhoven University of Technology, The Netherlands*

*3. Department of Mechanical and Mechatronics Engineering, University of Waterloo, Canada*

*D.J.E.M.Roekaerts@tudelft.nl

We report on a comparative study of model predictions of jet-in-hot-coflow flames. The Delft Jet-in-Hot-Coflow (DJHC) burner was built to mimic the important characteristics of flameless combustion without the complications of a real furnace [1,2]. The DJHC burner has been used to create a turbulent diffusion flame of Dutch Natural Gas in a coflowing oxidizer stream of high temperature with low oxygen concentration. The experimental database contains the results of high speed chemiluminescence imaging, velocity statistics from LDA measurements and temperature statistics from CARS_measurements. In recent years several computational studies have been made using the DJHC burner as validation database [3-9]. It has been shown before that predictions are sensitive to the coflow radial profiles of temperature and oxygen concentration, to the representation of effects of entrained air, and to turbulence-chemistry interaction and this is also the focus of the present study. Table 1 gives a summary of the models used.

Table 1: Overview of submodels and boundary conditions

| | RANS-EDC | RANS-CSE [8] | LES-CSE [9] | LES-FGM |
|---|---|---|---|---|
| Domain (mm)<br>Axial-radial | 2D<br>225 x 80 | 2D<br>225 x 80 | 3D cylindrical<br>225 x 80 | 3D Cartesian<br>250x43x43 |
| Grid size (#) | 27175 | 31250 | $1.5\ 10^6$ | $7.5\ 10^6$ |
| Platform | ANSYS | OpenFOAM | OpenFOAM | In-house |
| Turbulence | RANS | RANS | LES | LES |
| Closure model | RSM | Realisable k-$\boldsymbol{\varepsilon}$ | Smagorinsky | Vreman (2009) |
| Kinetic scheme | GRI 1.2 | GRI 2.11 | GRI 2.11 | GRI 3.0 |
| Reduction | DRM19 | TGLDM | TGDLM | FGM: Igniting mixing layer Le=1 flamelets |
| Turb-chem-interaction | EDC<br>$C_\tau$**=3** | Multistream CSE (two mixture fractions, **β**-pdf) | Multistream CSE (two mixture fractions, **β**-pdf)) | SGS fluctuations neglected |
| Scalar equations | Mean of species<br>Mean of enthalpy | Mean and variance of two mixture fractions | Resolved mixture fractions and SGS variances<br>Resolved enthalpy | Resolved mixture fraction and resolved progress variable<br>Resolved enthalpy |
| Radiation | Not included | Not included | Optically thin.<br>TRI not included. | Not included |
| Scalar BC<br>Coflow mean T<br>Coflow Trms<br>Coflow $O_2$ mass %<br><br>Surrounding'Air' | <br>From expt.<br>Set to 0<br>Mean 7,6%<br>Profile from expt.<br>Air 300K | <br>From expt.<br>Set to 0<br>Mean 7.6%<br>Coupled to mean T<br>Air 300K | <br>From expt.<br>Set to 0<br>Mean 7.6%<br>Coupled to mean T<br>Air 300K | <br>From expt.<br>Set to 0<br>Mean 9.5%<br>Flat profile<br>Coflow comp. at 300K |

In the EDC model a model constant was changed from its default value to obtain the correct lift-off height. The CSE model [8,9] uses a double conditioned conditional source term estimation (CSE) formulation of turbulence chemistry interaction including two mixture fractions. The FGM model is based on flamelets computed using one-dimensional igniting mixing layers with constant unity Le. The progress variable is based on $CO_2$, $H_2O$ and $H_2$. In the FGM model, the SGS-variance of mixture fraction and progress variable are obtained from algebraic equations, but this information has not been used in calculation of subgrid scale influences on resolved properties (density, resolved temperature).

Representation of the non-uniform radial profile of scalar properties at the inflow boundary is an issue for the mixture fraction based approaches. In the LES-CSE a second mixture fraction is used to represent temperature variation and oxygen variation is coupled to the same mixture fraction. In the LES-FGM temperature variation is included via the enthalpy equation and considering flamelets with heat loss at the oxidizer side. The oxygen variation is not taken into account. This simplification is based on a separate study showing that ignition delay is much more sensitive to temperature variation than to oxygen concentration variation. Figure 1 shows snapshots of scalar fields from LES-FGM. The poster presents comparisons of predicted velocity and scalar statistics, also compared to experiments, at the heights 15, 30, 60 and 90 mm above the burner exit. Figure 2 shows the good agreement obtained for mean temperature at 30 mm but for large axial distance significant differences are observed. Overall best results are obtained with the LES-CSE model of [9]. Additional results on the case studied here are presented at this meeting in the presentation by A. Vasavan and J.A. van Oijen and the poster by H. Bao et al..

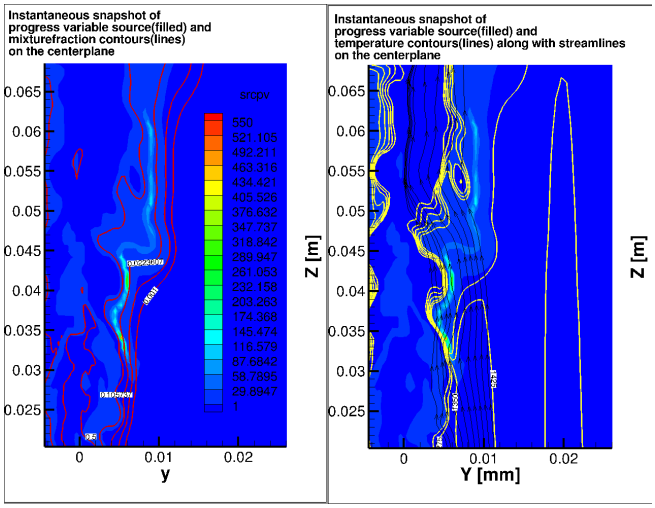


Figure 1

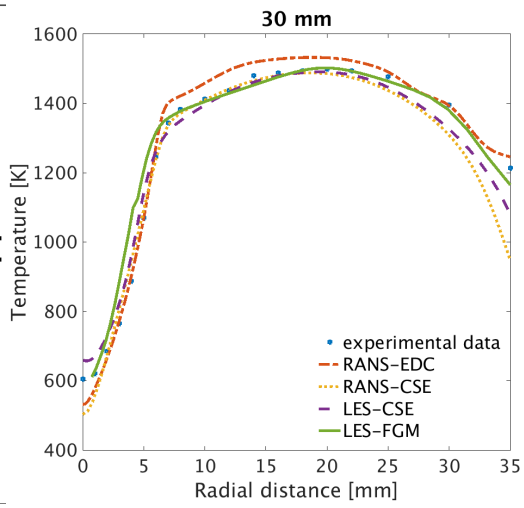


Figure 2

**References**


[1] E. Oldenhof et al., Combustion and Flame, 2010, 157 (6), 1167 -1178.
[2] E. Oldenhof et al., Combustion and Flame, 2011, 158 (8), 1553-1563
[3] A. De et al., Flow, Turbulence and Combustion, 2011, 87 (4), 537-567
[4] R.M. Kulkarni and W. Polifke, Fuel processing technology, 2013, 107, 138-136
[5] Rohit Bhaya et al., Combustion Science and Technology, 2014, 186 (9), 1138-1165
[6] Ashoke De and Akshay Dongre, Flow Turbulence Combustion, 2015, 94, 439–478
[7] G. Sarras et al., Flow, Turbulence and Combustion, 2014, 93, 607-635
[8] J.W. Labahn, D. Dovizio, C.B. Devaud, Proc. Combust. Inst., 2015, 35, 3547-3555
[9] J. Labahn and C. Devaud, Combustion and Flame, 2016, 164, 68–84

# FGM with additional chemically reactive dimensions

*D.V. Efimov, J.A. van Oijen*
*Multiphase & Reactive Flows, Eindhoven University of Technology, The Netherlands.*
*E-mail: D.V.Efimov@tue.nl*

In this work, we propose an innovative approach intended to improve the general accuracy of the Flamelet Generated Manifolds chemistry reduction method. It is based on increasing the dimensionality of the FGM by allowing for an additional degree of freedom. This extra dimension of the manifold accounts for chemical kinetics, describing conversion of one species into others. We follow the ideas of ILDM to perform a time scale analysis of chemical source term. It is done locally in each grid point of the FGM, yielding the local chemical time scales and the directions in composition space of their corresponding reaction groups. The assumption is that the chemistry evolution quickly vanishes in the directions of the fast reaction groups. This means that the reaction process develops only along the few "slowest" directions. Then the FGM is extended locally by the directions of the slow chemistry. Still, the movement in the direction of the extension is bound to the narrow vicinity of the original manifold. An additional transport equation needs to be solved for the secondary reactive control variable used to parametrize the movement in the direction of the extension. The movement on the manifold along the 1D FGM is still parametrized by the reaction progress variable, which is the main reactive control variable. This approach is not restricted to just one additional dimension. On the contrary, an arbitrary number of chemically reactive dimensions can be included.

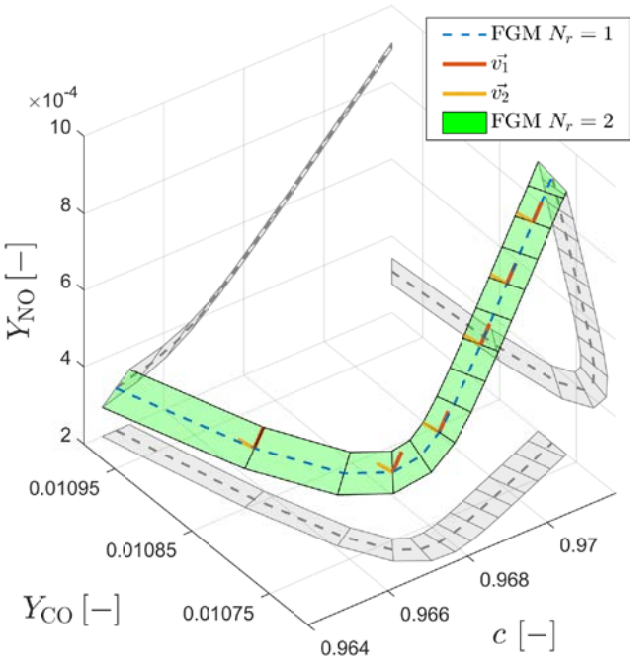


*Figure 1: FGM with two reactive dimensions, $N_r$=2. FGM with one reactive dimensions is shown by the blue line. Directions of the two slowest reaction groups, $\vec{v}_1$ and $\vec{v}_2$, locally span the 2D manifold. Coordinate axes represent the scaled progress variable c and the mass fractions of CO and NO. To aid the visualization, the projections on the coordinate planes are shown in grey.*

The performance of the new developed model is examined in one-dimensional test configurations, which simulate the process of expansion of a mixture of burnt gases. The purpose of this theoretical exercise is to obtain conditions severe enough for the thermochemistry to go off the FGM with one chemical degree of freedom, in the direction of the secondary reactive dimension. In the utilized test cases, this is achieved by the high rate at which the expansion happens. These fast time scales of the change of the thermodynamic variables can interact with the post flame chemistry, for example altering the concentration of the pollutants. The idea of expansion or compression of burnt gases can be related to several applications. Often, expansion of burnt gases is used to convert the released heat into work. Here, we adopt a somewhat idealized test case setup that resembles the idea of the gas turbine stators, also called the nozzle guide vanes (NGV). There, the burnt gases, formed in the combustor, are led through a decreasing area duct. Accompanied by the decrease of temperature and pressure, the velocity

increases almost up to the speed of sound. Due to the high velocity, the residence time inside the NGV is small, resulting in a high rate of cooling and expansion.

The results of the test problems show that the FGM method with one additional reactive dimension yielded a better agreement with the detailed chemistry simulations. Improvements are observed for the source terms of the reactive control variables and for the species composition. Also, the accuracy of the CO and $NO_x$ predictions increased by an order of magnitude.

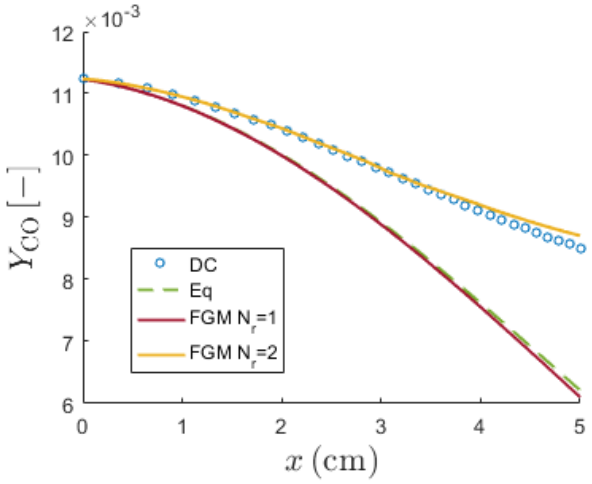


*Figure 2: NGV simulation results for the mass fraction of CO. The relative performance of the manifolds with one and two reactive dimensions ($N_r$=1 and $N_r$=2) is compared. Detailed chemistry (DC) predictions are used as reference for the FGM results. FGM with two reactive dimensions shows a good agreement with DC, in counterpart to the FGM $N_r$=1, which yields qualitatively incorrect predictions.*

COMBURA 2016
Kontakt der Kontinenten, Soesterberg
05 – 06 October 2016

# Angle-dependent light scattering study of soot aggregate growth in 1-D premixed rich ethylene/air flames

*P.N. Langenkamp*[1], *H.B. Levinsky*[1,2], *A.V. Mokhov*[1]

[1]*Combustion Technology, Energy and Sustainability Research Institute, University of Groningen, Nijenborgh 4, 9747 AG Groningen, The Netherlands*
[2]*DNV GL - Oil & Gas, Nederland B. V. – P.O. Box 2029, 9704 CA Groningen, The Netherlands*

Combustion generated particles such as soot can have a significant impact on the environment and human health; an impact that is strongly linked to their size and structure. Primary soot particles generated in the incomplete combustion of hydrocarbons coalesces together into particles which subsequently form even larger aggregates of various shapes and sizes. Despite much research into this topic, modeling and predicting soot formation and growth in flames remains challenging. Experimental studies of the formation and growth of soot are indispensable to gain a better understanding of relevant processes. To investigate aggregate growth in premixed $C_2H_4$/air flames as a function of residence time, we used angle-dependent light scattering – which does not rely on detailed knowledge of the soot's optical properties – as a quicker and less invasive alternative to ex-situ methods such as TEM.

The flame temperature in these experiments is controlled by changing the exit velocity of the gas mixture and determined by solving the governing equations with Cantera suite code using the chemical-kinetic San Diego Mechanism. In addition, at least up to an equivalence ratio $\phi$ of 2.1 we are able to measure the flame temperature through spontaneous Raman spectroscopy. The flame temperature was determined by fitting recorded spectra, using the same experimental setup and procedure as described by Sepman et al. [1]. In richer flames it becomes increasingly hard to recover the Raman signal from the high soot black-body background.

The experimental setup used for the angle-dependent scattering measurements (Fig. 2) was used before for measurements of silica particles [2]. In short, a 532 nm laser is directed through the flame and the scattered light is measured simultaneously by photomultipliers placed at four distinct angles (42°-133°). The angle dependence of the scattered signal can be used to determine the mass-averaged root-mean-square radius (radius of gyration) $R_g$ of the aggregates. One of the main challenges of this technique lies in the very weak angle dependence of the

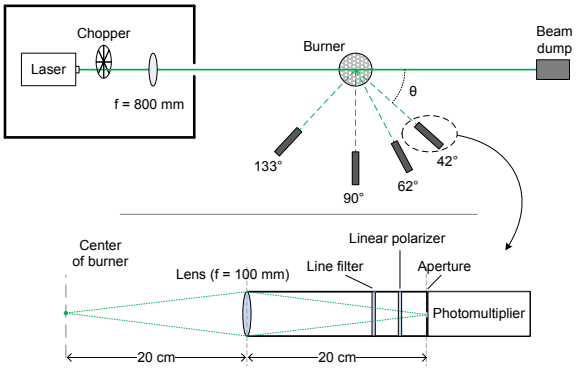


Fig. 1. Schematic of the light scattering setup. The angular orientations of the collection systems are stated with respect to the forward direction of the laser beam.

scattering signal for small particles. This necessitates effective suppression of any background light (including black body emissions of soot) and accurate calibration of the measured signals, which we attain by using Rayleigh scattering from $SF_6$.

Some preliminary results are presented in the figures below. Fig. 2 shows the spontaneous Raman spectrum measured in a rich ($\phi$ = 2.1) ethylene flame; fitting this spectrum gives a flame temperature of 1600 K. Fig. 3. shows scattering data obtained in this flame for multiple heights above the burner (HAB), as function of $q^2$, where $q$ is the scattering wave vector (a function of the scattering angle). The soot particles' $R_g$ is provided by linear fits of the data; results show that particle size increases with increasing HAB, which is in line with expectations. The apparent bend in the data warrants some more attention, but is likely an experimental artifact resulting from the very small relative changes in signal and slightly imperfect calibration.

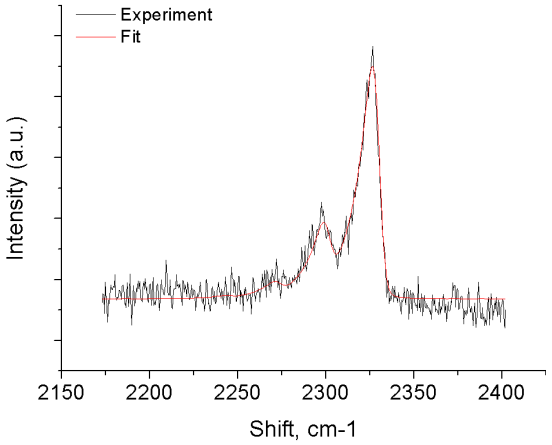


Fig. 3. Spontaneous Raman spectrum of Nitrogen in a rich ($\phi$ = 2.1) ethylene flame. From fitting we find a temperature of 1600 K.

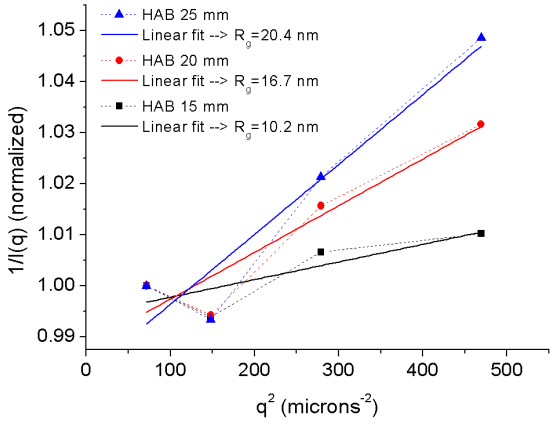


Fig. 2. Normalized scattering data for a 1600 K rich ($\phi$ = 2.1) flame at multiple heights above the burner (HAB). Linear fits provide the particles' radius of gyration $R_g$: 10.2, 16.7 and 20.4 nm at HAB 15, 20 and 25 mm respectively.


[1] A. V. Sepman, V. V. Toro, A. V. Mokhov and H. B. Levinsky, Appl. Phys. B (2013) 112:35-47

[2] P. N. Langenkamp, A. V. Mokhov and H. B. Levinsky, Combust. Sci. Tech. http://dx.doi.org/10.1080/00102202.2016.1193500 (accepted)

# The Three Power Crossover (3PX) concept

## Utilizing a plug-in hybrid electric car as a micro-CHP

*B.F.W. Vermeltfoort*
*Department of Mechanical Engineering, Eindhoven University of Technology, The Netherlands.*
*B.f.w.vermeltfoort@tue.nl*

In order to decrease the amount of $CO_2$ that a household produces when using energy, a new concept is currently being tested. The heart of the new concept, baptized 3PX for Three Power Crossover, is a generator driven by an internal combustion engine, normally used as a range extender in a plug-in hybrid car. In this concept the hybrid car will use natural gas as a fuel to provide the household with heat, electricity and mobility. It is therefore a "bridge" between the three biggest household energy needs (see *Figure 1*). The concept can be operated in such a way that it becomes an important addition in the energy transition and a building block of smart grids.

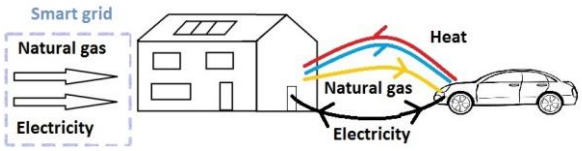


*Figure 1: Schematic overview of the 3PX concept.*

## Benefits

Model calculations show that by utilizing a plug-in hybrid electric vehicle as a micro-CHP, there is potential to decrease greenhouse gas emissions and energy costs with relatively low investment. The calculations demonstrated that this combination is energetically, economically and environmentally positive. Financially, a Dutch household with an relatively well-insulated house will almost half the yearly energy costs, going from around 1200 euro to around 700 euro. Calculations indicate that the total $CO_2$ emission of a household, including emission directly traceable to energy usage such as: emission from power plants, central boiler system and tailpipe emissions, but excluding material mining and production, can decrease from 9000 kg to 5000 kg. From the 4000 kg yearly decrease roughly half comes from the household heating and the other half comes from switching from a petrol powered car to a CNG-electric-hybrid powered car.

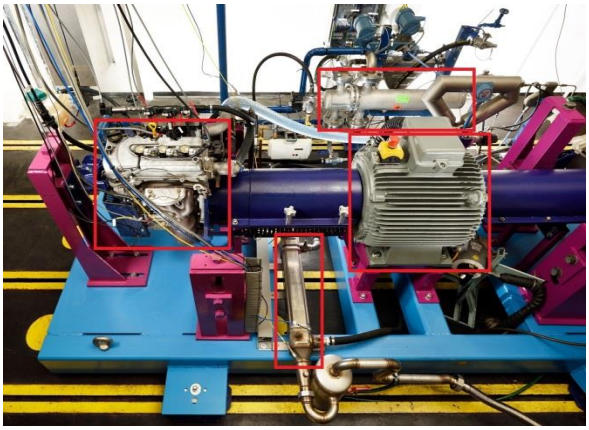

*Figure 2: The test bench setup with the internal combustion engine and generator.*

Additional benefits include the extra energy flexibility that this concept delivers, which can potentially increase the availability of intermittent renewable energy sources. With an increasing amount of photovoltaic energy, the difference in availability of energy during summer and winter (which is intensified by utilizing heatpumps), can be mitigated by using the concept. Both additional benefits are also noticeable with most other types of (micro-)CHP installations.

## Experimental results

A setup is build (*Figure 2*), which can replicate the operation modes of a range-extender. It consists of a Suzuki 1.0 liter engine (left) running on natural gas, which drives a generator (right). The electricity that is produced is fed into the grid. The coolant passes the exhaust gas cooler (bottom), the engine block and the heat exchanger (right top, behind the generator). The heat exchanger simulates the heat use of a household and cools down the coolant. In *Figure 3* a preliminairy result is shown in which the

electrical as well as the thermal efficiencies are shown as a function of ignition timing. It can be seens that the maximum combined efficiency, at ignition at 24 degrees before top dead center, is around 82%. The maximum electrical efficiency is 29.5%. This might seem low, however because of material constrains in the exhaust, the maximum intake pressure was 84 kPa at 1600 rpm, whereas the maximum efficiency of this engine is expected to be at 3000 rpm and an even higher intake pressure.

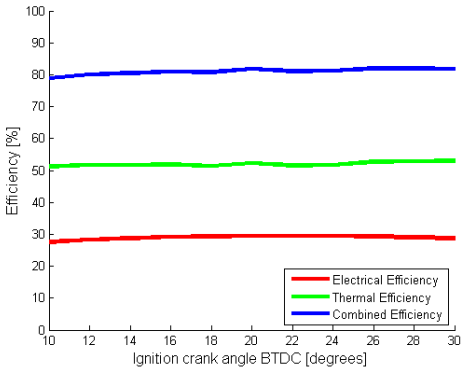


*Figure 3: (Preliminary) efficiencies of the setup as a function of ignition timing. The red line is the electrical efficiency, the green line is the thermal efficiency and the blue line is the sum of the green and red line.*

## Future work

The setup will be upgraded with an additional exhaust gas cooler in order to test higher engine loads. It is predicted that this will give higher efficiencies and more insight in the optimal engine parameters. In the near future different types of natural gas (such as green gas and Bio-LNG) will be tested. This will make sure the concept is futureproof and can be fully sustainable without major obstacles. Furthermore, research will continue to experimentally prove the concept both in laboratory as well as in realistic circumstances. To test the concept in a realistic environment a second setup will be build inside a Nissan Leaf (*Figure 4*). This electric car will then become a CNG-hybrid that will be connected to a household, in order to gain further insight in the feasibility of the concept and the effects on local (smart) energy grids.

*Figure 4: A Nissan Leaf will be used to further test the concept.*

# Plasma Assisted Combustion: Interaction of a Flat Flame with a Nanosecond Dielectric Barrier Discharge Plasma

Ahmed Elkholy, Jeroen van Oijen, Philip de Goey

† Mechanical Engineering Department, Eindhoven University of Technology

Contact: A.Elkholy@tue.nl

## 1. Introduction

Using of non-equilibrium Plasma-assisted for ignition, combustion and high speed flow applications are rapidly developing in the last decades due to its ability to produce a large amount of radicals and excited species. Which has a great potential in flame stabilization and emission control.

Although many studies have demonstrated the effectiveness of plasma to enhance combustion properties, the detailed enhancement mechanism is still highly unknown. Toward a better understanding of the flame behavior under plasma effect, a one dimensional flame structure setup integrated with a non-thermal plasma source has been designed.

## 2. Experimental setup

Fig. 1 shows schematically of the burner setup. The main parts of the setup are the plasma reactor which is the source of the non-equilibrium plasma. This reactor uses the DBD (Dielectric barrier discharge) for non-equilibrium plasma generation. The reactor consisting of four layers of electrodes separated by three layers of dielectric material as shown in the detailed view. The 1mm think perforated burner plate has holes of 0.5mm diameter with 1.0 mm pitch drilled in hexagonal pattern. The upper and lower copper layers works as (cathode) grounded electrodes, while the inner electrodes are the (anode) high voltage side. This design allows the flow to interact with the plasma by pass through the plasma micro holes meanwhile it works as a burner plate.

A non-thermal plasma is produced by a semiconductor based generator model (NPG-6/15k). An electric positive polarity pulses of 3.5 kV in amplitude, 10 ns in duration and 3ns rise time is created at a repetitive frequency of up to 20 kHz (Fig. 3). The generator is externally triggered by frequency generator model (FY22S). The voltage and the current are simultaneously monitored by data oscilloscope. The High voltage is recorded using a high-voltage probe model (HVP-18HF - 150MHz), and the current through the electrodes is measured using measured with a Pearson Coil (Model 2877)

A nanosecond repetitively pulsed plasma (NRPP) has been used to stabilize and improve the efficiency of a lean laminar premixed Methane/air flame at atmospheric pressure. We show that, the plasma produces a radical pool as well as heat that helps the flame for stabilization. Optical emission spectroscopy measurements is used to determine the concentration of the active species produced by the

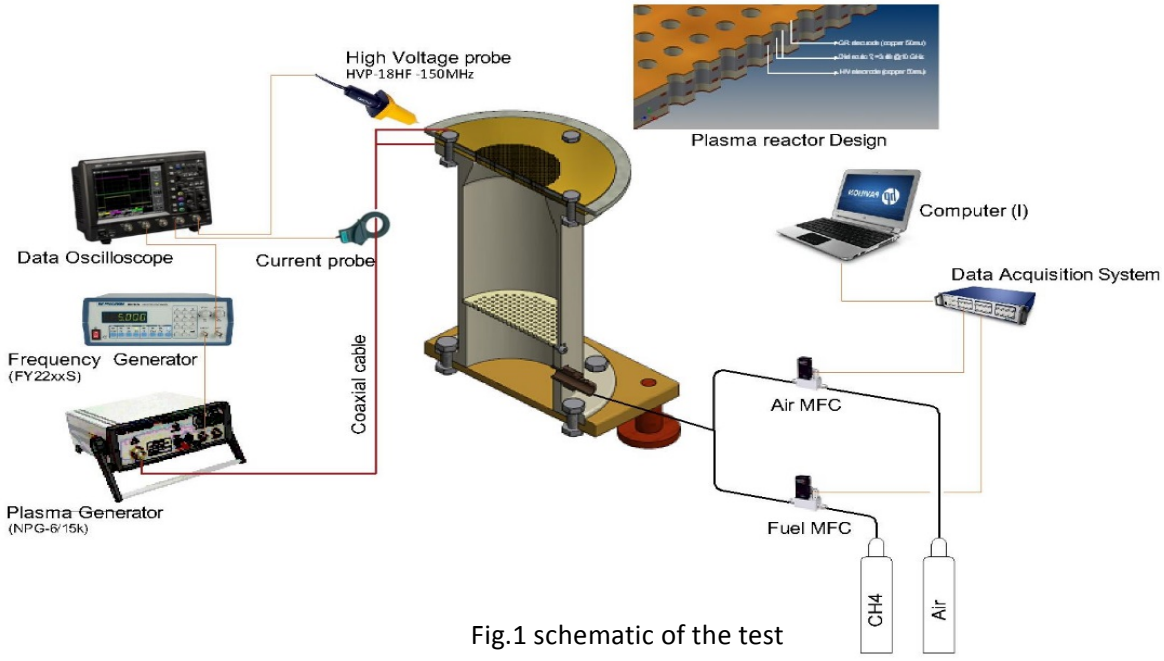


Fig.1 schematic of the test

plasma discharge.

## 3. Experimental results

Emission spectra of the plasma:

In this study, spectra of the free radicals for the plasma were recoded using spectrograph (Acton sp300) and CCD (model PI-MAX III), the spectrometer lens is focused just above the plasma reactor. Example of such spectra are presented at different air flow rates in fig. 2. The signal is average over 1000 Pulses.

It is highly noticeable that the plasma discharge of air in atmospheric pressure is very rich of excited radicals

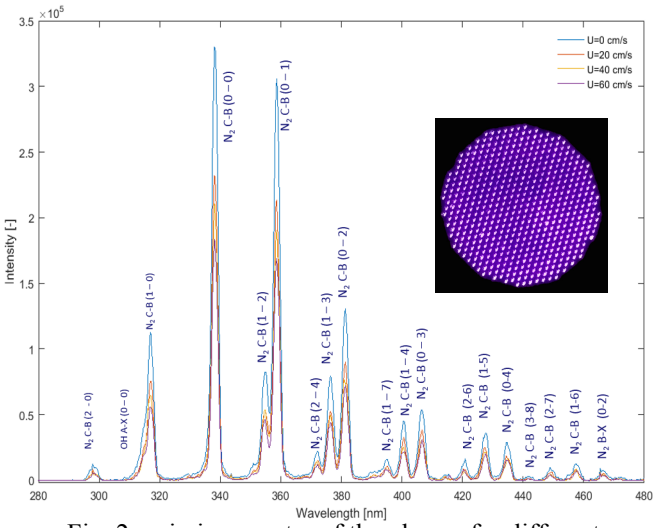


Fig. 2 emission spectra of the plasma for different flow velocity at atmospheric pressure.

Lean flammability limit:

Fig. 3 shows the effect of plasma at different frequencies on the lean blow-off equivalence ratio

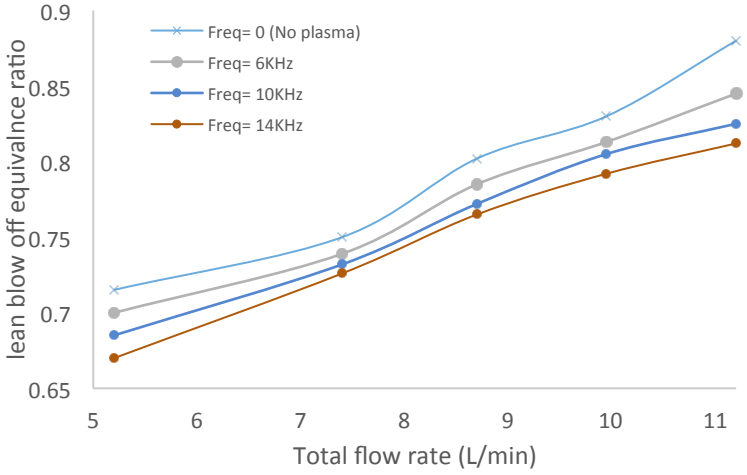


of the methane /air flame.

Fig. 3 lean blow-off equivalence ratio as a function of plasma frequency

Flame standoff height

Fig.4 shows that plasma has been successfully reduced the stand-off height of the methane/air flame as a result of the thermal and chemical effect of the non-thermal plasma.

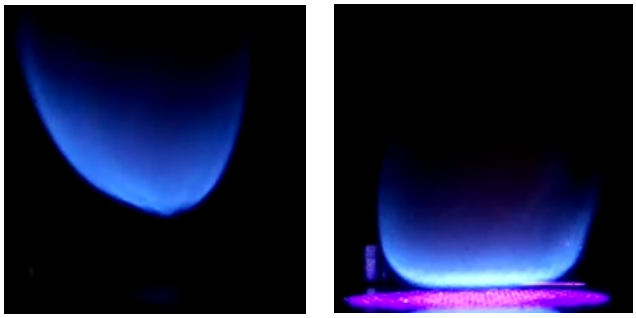

Fig.4. direct image shows the comparison of the flame standoff height at the same flow conditions with (right) and without plasma (lift).


## 4. Acknowledgements

This research project is supported by Egyptian ministry of education.


## 5. References:


[1] G. Pilla, D. Galley, D.A. Lacoste, F. Lacas, D. Veynante, C.O. Laux IEEE Trans. Plasma Sci., 34 (2006), pp. 2471–2477

[2] A. Bao, Y.G. Utkin, S. Keshav, G. Lou, I.V. Adamovich , IEEE Trans. Plasma Sci., 35 (2007), pp. 1628–1638

[3] S.V. Pancheshnyi, D.A. Lacoste, A. Bourdon, C.O. Laux, IEEE Trans. Plasma Sci., 34 (2006), pp. 2478–2487

[4] M. Uddi, N. Jiang, I.V. Adamovich, W.R. Lempert, J. Phys. D, 42 (2009), p. 075205

[5] N.L. Aleksandrov, S.V. Kindysheva, E.N. Kukaev, S.M. Starikovskaya, A.Y. Starikovskii
Plasma Phys. Rep., 35 (2009), pp. 867–882

# A study of flame stabilization and blow-off phenomenon for laminar premixed methane flames with hydrogen addition

F.H. Vance, Y. Shoshyn, J.A. van Oijen, L.P.H. de Goey

University of Technology, Eindhoven

f.h.vance@tue.nl

**Keywords**: Laminar Bluff body flame, preferential diffusion, flame stabilization, blow-off

## Abstract

In the near future hydrogen will be added to the natural gas supply in the Netherlands. Addition of hydrogen in the natural gas leads to lean combustion, which in turn leads to low emissions. However, the stability of flames with hydrogen addition poses a problem with respect to blow-off. Bluff body flames present an interesting case study for examining the effects of the hydrogen addition, both experimentally and numerically.

In the current work, a numerical study of such flames is carried out using Ansys Fluent software for a number of cases with and without hydrogen addition into methane gas. Experimental studies are also performed using the setup shown in figure 1. A uniform flow profile is generated using perforated plates upstream of the bluff body. Bluff body is made from brass and is enclosed in a glass tube. Figure 2 shows the CH concentration contour obtained from the experimental results for a case with hydrogen addition. A similar numerical setup is modelled with the conjugate heat transfer. By varying the inlet flow velocity and the fuel equivalence ratio, flame stabilization, effects of preferential diffusion and blow-off phenomenon will be studied in detail.

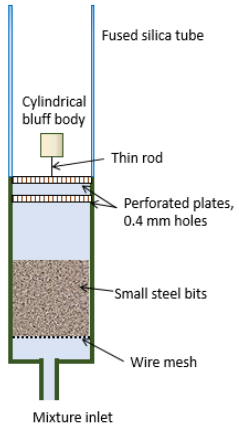


*Figure 1 Experimental setup for bluff body flame*

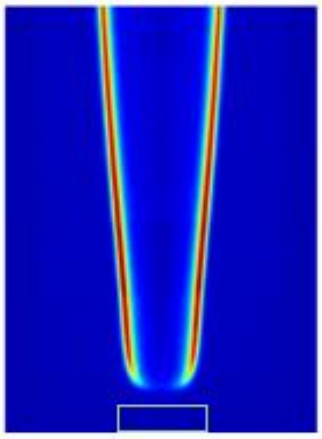

*Figure 2 Experimental CH concentration contours for inlet velocity =1 m/s and fuel equivalence ratio = 0.55 (fuel: 20%H2+80%CH4)*

Temperature contours for different fuel equivalence ratios (phi) are shown in figure 3 and figure 4 for inlet flow velocity of 1 m/s and 0.5 m/s respectively. The effect of flow velocity is evident from the difference in the flame shape and the curvature. Steady simulations have been performed for near lean blow-off limit. Analysis of the flame stretch rate, local equivalence ratio and heat transfer will reveal further knowledge about the stability of these flames.

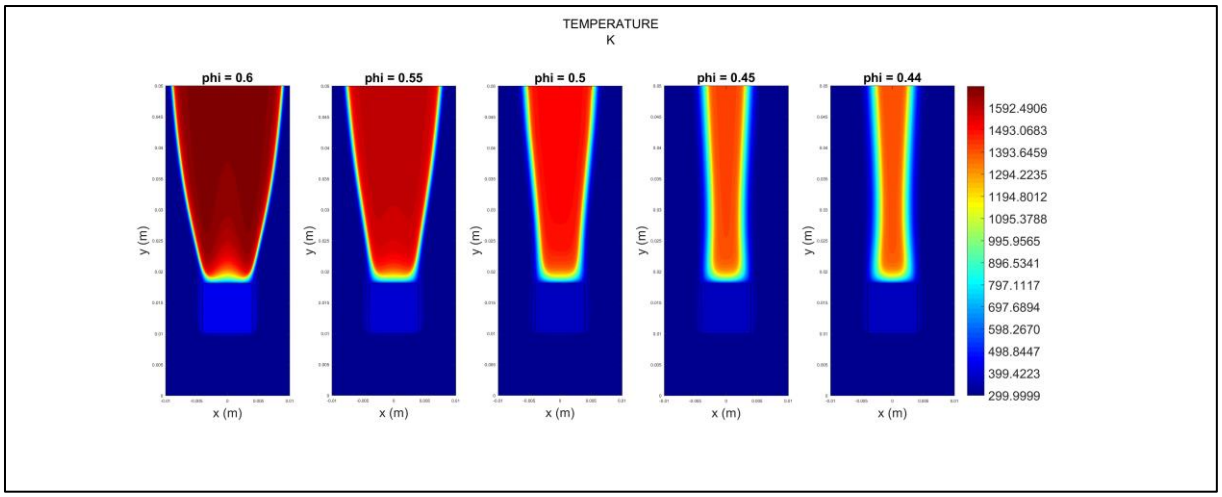


*Figure 3 Temperature contours (in Kelvin) for 20% Hydrogen and 80 % Methane with inlet velocity of 1 m/s*

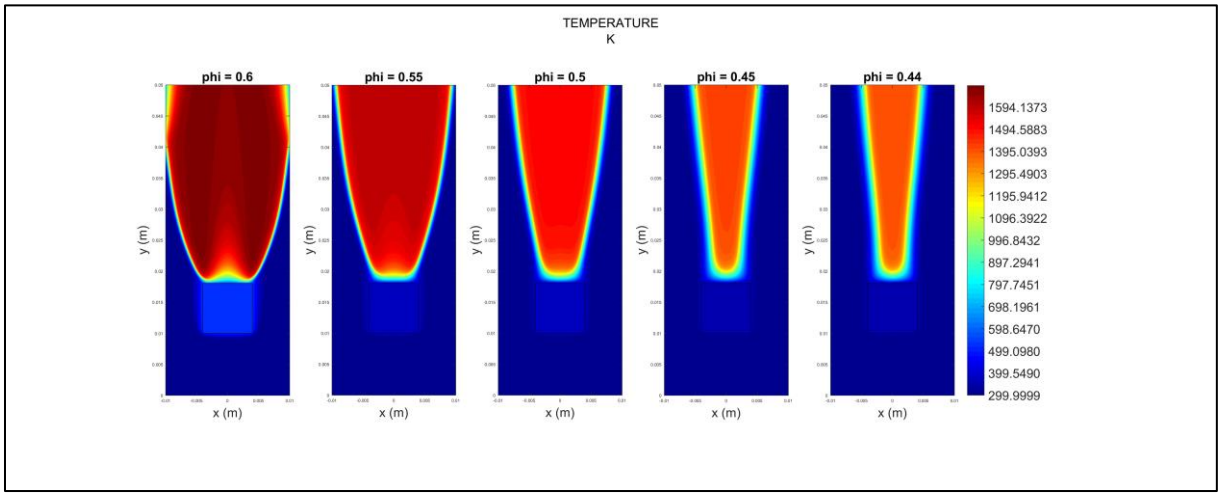


*Figure 4 Temperature contours (in Kelvin) for 20% Hydrogen and 80 % Methane with inlet velocity of 0.5 m/s*